Increased striatal glutamate and dopamine transmission in young VPS35 D620N knock-in mouse model of Parkinson's disease precedes reduced neurotransmission in old age

by

Anusha Kamesh

Integrated Program in Neuroscience

Montreal Neurological Institute

McGill University

December 2023

A thesis submitted to McGill University in partial fulfillment of the requirements of the degree of

Doctor of Philosophy

Table of Contents

Abstract (English) 6

Abstrait (français) 8

Acknowledgements 10

Contribution to original knowledge 12

Contribution of authors 13

List of figures 15

List of abbreviations 17

Chapter 1: Introduction 19

Background 20

What is PD? 20

Monogenic PD 21

Striatal function and dysfunction in PD 22

What is VPS35 and why is it linked to PD? 24

D620N mutation in VPS35 30

Rationale for this study 34

Hypothesis 35

Specific objectives 35

Materials and Methods 36

Animals 36

Genotyping 36

Surgery 37

Construct specific injection details 38

Preparation of acute brain slices 39

Whole-cell patch-clamp electrophysiology 39

iGluSnFR and dLight imaging 41

Acute LRRK2 kinase inhibition 43

Statistical analysis 43

Chapter 2: Investigating striatal glutamate transmission in VKI mice 44

Effects of VPS35 D620N mutation on striatal glutamate transmission in young adult mice 44

2.1 Membrane properties of dorsolateral striatal medium spiny neurons are transiently altered in VKI mice 44

2.2 Spontaneous glutamate transmission in the dorsolateral STR is increased in VKI MSNs by 6 months 46

2.3 Evoked corticostriatal glutamate transmission is increased in VKIs by 6 months 48

2.4 Corticostriatal glutamate transmission through AMPA and NMDA receptors are significantly increased in VKIs by 6 months 50

2.5 Electrically-evoked glutamate release onto dorsolateral STR MSNs is altered in VKI mice by 6 months 52

Effects of acute LRRK2 kinase inhibition on striatal glutamate transmission in young adult mice 54

2.6 Acute inhibition of LRRK2 kinase activity does not alter STR glutamatergic transmission in 6-month-old mice 54

2.7 Captisol® vehicle treatment differentially alters striatal glutamate transmission and membrane properties in VKI and WT MSNs 56

Effects of VPS35 D620N mutation +/- acute LRRK2 kinase inhibition on striatal glutamate release in aged mice 58

2.8 STR glutamate release is reduced in 25-month-old VKI mice and does not respond to acute LRRK2 kinase inhibition 58

Chapter 3: Investigating striatal dopamine release in VKI mice 61

Effects of VPS35 D620N mutation on striatal dopamine release in young adult mice 61

3.1 STR dopamine release is not significantly different between WT and VKI mice at 3 months 61

3.2 STR dopamine release evoked with paired electrical stimulation is significantly higher in 6-month VKI mice 64

3.3 STR dopamine release from high frequency electrical stimulation is significantly increased in 6-month-old VKI mice and is not responsive to MLi-2 treatment 66

Effects of VPS35 D620N mutation +/- acute LRRK2 kinase inhibition on striatal dopamine release in aged mice 68

3.4 STR dopamine release is reduced in aged VKI mice and is partially responsive to LRRK2 kinase inhibition 68

Chapter 4: Discussion 70

Glutamate transmission is altered in the dorsolateral STR of VKI mice 70

Spontaneous striatal glutamatergic transmission is increased in young adult VKI mice 70

Corticostriatal glutamatergic transmission is increased in young adult VKI mice 73

Striatal glutamate release is increased in young adult VKI mice 74

Clearance of glutamate is transiently altered in young adult VKI mice 75

Subunit composition of AMPA receptors is not altered in young adult VKIs 76

Passive membrane properties are transiently altered in young adult VKI mice 77

Striatal glutamate release is reduced in aged VKI mice 78

Other caveats and limitations 79

Conclusion 83

Dopamine transmission is altered in the dorsolateral STR of VKI mice 84

Striatal dopamine release is increased in young adult VKI mice 84

Striatal dopamine release is reduced in aged VKI mice 86

Clearance of striatal dopamine is slowed in young adult VKI mice 87

Other caveats and limitations 88

Conclusion 91

Acute LRRK2 kinase inhibition does not alter glutamatergic or dopaminergic striatal neurotransmission. 92

Acute LRRK2 kinase inhibition does not alter striatal glutamatergic transmission 93

Acute LRRK2 kinase inhibition does not alter striatal dopamine release 95

Other caveats and limitations 98
Conclusion 100
The bigger picture 101
VPS35 D620N may globally increase neurotransmitter release 101
VPS35 D620N may alter presynaptic release through impaired synaptic vesicle recycling 101
VPS35 D620N may impair retromer interactions 102
VPS35 D620N may increase lysosomal stress while reducing lysosomal function 103
VPS35 D620N may increase mitochondrial stress while reducing mitochondrial turnover 104
VPS35 D620N may lead to PD through changes to neuronal development, maturation, and aging 106
Towards a better understanding of PD 106
Bibliography 109
Appendix 129
Vehicle effects in WT and VKI mice 129
Striatal neurotransmitter release in aged animals by sex 136

Abstract (English)

The autosomal dominant D620N mutation in vacuolar protein sorting 35 (VPS35) causes a clinically-typical form of late-onset Parkinson's disease. Canonically, VPS35 functions as a core subunit of the retromer complex that recycles transmembrane cargo from sorting endosomes. Although some of these cargoes are involved in synaptic transmission, the neuronal function of VPS35 is not well known. To better understand the role that VPS35 D620N mutations play in Parkinson's disease, neurotransmission was assessed in the disease-relevant dorsolateral striatal brain region of young and aged VPS35 D620N knock-in (VKI) mice. Glutamatergic neurotransmission in the striatum was assessed using patch-clamp electrophysiology and with fluorescent reporter, iGluSnFR. By 6 months, spontaneous and evoked glutamatergic transmission in the dorsolateral striatum is increased in VKI mice. Contrastingly, by 25 months old, striatal glutamate release in VKI mice is reduced compared to wild-type littermates. Assessment of dopamine release using the fluorescent reporter dLight revealed that evoked striatal dopamine release is also elevated in 6-month-old VKI mice. Similar to changes in glutamatergic release, striatal dopamine release is reduced in 25-month-old VKI mice.

In addition, mutations in leucine-rich repeat kinase 2 (LRRK2) that increase LRRK2 activity pose the highest genetic risk for Parkinson's disease. LRRK2 & VPS35 coimmunoprecipitate, and VKI mice show elevated phosphorylation of several LRRK2 substrates. This suggests a mechanistic synergy between LRRK2 and VPS35 Parkinsonism, centred on increased LRRK2 kinase activity. However, it is unclear if hyperphosphorylation of LRRK2 substrates is causal or even correlated with neuronal dysfunction in VPS35 mutant mice. Involvement of LRRK2 was investigated using the LRRK2 kinase inhibitor MLi-2. Neither striatal

glutamate nor dopamine neurotransmission in young VKI mice is significantly altered by MLi-2 treatment. Reduced glutamate and dopamine release in the striatum of VKI mice are largely unaltered by MLi-2. As such, LRRK2 kinase activity does not appear to have an immediate role in the dysfunction of neurotransmission observed in VKI mice.

Together, early elevations of glutamate and dopamine transmission observed in VKI mice precede later loss of neurotransmission in aged animals. Thus, VPS35 seems to play a regulatory role in striatal neurotransmission that is altered by the D620N mutation. Changes to striatal neurotransmission observed in VKI mice is, at least acutely, not a result of ongoing LRRK2 kinase activity. A better understanding of the mechanism underlying early neuronal dysfunction in the striatum of Parkinson's disease-mutant knock-in mice may reveal new, potentially disease-modifying, therapeutic targets. Our hope is that in targeting early neuronal dysfunction, we can prevent the onset of Parkinson's disease altogether.

Abstrait (français)

La mutation autosomique dominante D620N de la protéine vacuolar protein sorting 35 (VPS35) est à l'origine d'une forme cliniquement typique de la maladie de Parkinson à déclenchement tardif. Classiquement, VPS35 fonctionne comme une sous-unité centrale du complexe retromer qui recycle les cargaisons transmembranaires des endosomes de tri. Bien que certaines de ces cargaisons soient impliquées dans la transmission synaptique, la fonction neuronale de VPS35 n'est pas bien connue. Pour mieux comprendre le rôle de la mutation VPS35 D620N dans la maladie de Parkinson, nous avons mesuré la neurotransmission dans le striatum dorsolatérale (impliquée dans la maladie), chez des souris knock-in VPS35 D620N (VKI) jeunes et âgées. La neurotransmission glutamatergique dans le striatum a été mesurée à l'aide de l'électrophysiologie par patch-clamp et du rapporteur fluorescent iGluSnFR. Dès l'âge de 6 mois, la transmission glutamatergique spontanée et évoquée dans le striatum dorsolatéral est augmentée chez les souris VKI. En revanche, à l'âge de 25 mois, la libération de glutamate dans le striatum est réduite chez les souris VKI par rapport aux souris de type sauvage. De même, l'évaluation de la libération de dopamine à l'aide du senseur fluorescent dLight a révélé que la libération de dopamine striatale évoquée est également élevée chez les souris VKI âgées de 6 mois puis diminue à l'âge de 25 mois comme pour la libération de glutamate.

En outre, les mutations affectant le gène *lrrk2* (leucine-rich repeat kinase 2) représentent le risque génétique le plus élevé pour la maladie de Parkinson. Ces mutations conduisent la plupart du temps à une activité augmentée de la kinase LRKK2. LRRK2 et VPS35 coimmunoprécipitent, et il a été démontré que les souris VKI présentent une phosphorylation accrue de plusieurs substrats de LRRK2. Cela suggère une synergie fonctionelle entre LRRK2 et le parkinsonisme associé à

VPS35, centrée sur l'augmentation de l'activité kinase de LRRK2. Cependant, on ne sait pas si l'hyperphosphorylation des substrats de LRRK2 est causale ou même corrélée avec le dysfonctionnement neuronal chez les souris mutantes VPS35. Nous avons étudié l'implication de LRRK2 en utilisant l'inhibiteur de la kinase LRRK2 MLi-2. Le traitement par MLi-2 ne modifie pas de manière significative la neurotransmission striatale du glutamate et de la dopamine chez les jeunes souris VKI, ni la plupart des mesures de la neurotransmission striatale réduite chez les souris VKI âgées. Ainsi, l'activité de la kinase LRRK2 ne semble pas jouer un rôle déterminant dans le dysfonctionnement de la neurotransmission observé chez les souris VKI.

Globalement, les élévations précoces de la transmission du glutamate et de la dopamine observées chez les souris VKI précèdent la perte ultérieure de la neurotransmission chez les animaux âgés. Ainsi, VPS35 semble jouer un rôle régulateur dans la neurotransmission striatale qui est altérée par la mutation D620N. Enfin, les modifications de la neurotransmission striatale observées chez les souris VKI ne résultent pas, du moins dans un premier temps, d'une activité exagérée de la kinase LRRK2. Cependant, une meilleure compréhension du mécanisme qui sous-tend le dysfonctionnement neuronal précoce dans le striatum des souris knock-in mutantes pour la maladie de Parkinson permettrait d’identifier de nouvelles cibles thérapeutiques susceptibles de modifier la maladie. Nous espérons qu'en ciblant le dysfonctionnement neuronal précoce, nous pourrons à terme prévenir l'apparition de la maladie de Parkinson.

Acknowledgements

It feels like the time encompassing my PhD contains several lifetimes worth of friendships, relationships, politics, and global crises. Whether despite, or because of, these experiences (I'm not even sure the distinction matters), I have arrived at the end of this chapter of my life a happier, healthier, and wiser person. I am forever grateful for the support and kindness shown by the friends and family I was surrounded by throughout my PhD and in all the moments that led up it.

To my parents, with everything I do with my life, I want to make you proud. I am incredibly lucky to have such generous, kind, funny, and loving people to look up to and learn from. I am even luckier to get to spend so much time with you in this chapter of my life. Seeing you through the eyes of an adult has made me appreciate you both in an entirely different and profound way. Thank you also for accommodating me getting a pet. Our cat is the sweetest, smartest, softest, and best addition to our family since I was born. If only he could read English, he would see how much joy he has brought to my life. Because he can't read, I would like to take this opportunity to blame any errors in this dissertation on his walking on my keyboard.

To Austen, yet another testament to how lucky I am. It only took 2 weeks from me reaching out to you to joining your lab, but you welcomed me with open arms even in -25°C weather. There's a reason the school year doesn't start in January in Canada. It may be too soon to tell, but I believe your unwavering support, wisdom, love of science, openness, and sense of humour have changed the course of my life for the better. Thank you for giving me the space and opportunity to grow in your lab. You've renewed my sense of purpose and strengthened my resolve to (incrementally, and perhaps naively) shift the academic system towards a more equitable place. Thank you most of all for bringing together the most incredible people.

To Naila, Chelsie, Anouar, Thaiany, Yuting, Bruno, Camila, Malak, Alessia, and Sean (dear God, I hope I haven't forgotten anyone!), you somehow managed to make working at a hospital as a grad student, fun. I never once dreaded coming into the lab knowing I'd be surrounded by you all. You truly saved my sanity during lockdown and I have so many treasured memories of the fun we've had both in and out of the lab. Additional thanks to Chelsie, you took me under your wing when I didn't even know what VPS35 was. You have inspired me academically, personally, and with your excellent taste in music, and I am so glad the world and academia gets to continue to benefit from your beautiful mind!

Additional thanks also to Naila, you've become one of my closest friends and introduced me into the world that exists at the intersection of two things I love very, very much – science and music. Your vision also created one of the most rewarding experiences I've had, working with Piece of Mind. Thank you for bringing together such an eclectic, talented, beautiful, humble, and kind group of people. Every single person that joined the collective is an incredible human being, and I don't think that's a coincidence. A special shout to Anne, Naomi, and Greg– I'm so happy to see you as often as I do, but frankly could stand to see you all more often. I'm grateful to call you all friends and for you to enrich my life with your creativity, joy, enthusiasm, and wisdom.

I'd also like to acknowledge Al and the Ferguson lab, Matt and the Parsons lab, and all my collaborators and peers. Know that your wisdom, support, and joy have laid the foundation from which my love of science continues to grow. Thank you for showing me that being a career nerd is an entirely plausible outcome.

Thank you to my friends outside the lab: Natasha, Christina, Emma, Laura, Emily, Megan, Sam, Mandy, Tom, Becky, Élodie, and Sarah, to name a few. And to those whom I've spend transformative minutes, hours, and days with. You've all helped me come into my own and made me feel like I am something and someone worth investing into. You've supported me through the tough times and the losses, but also have been there to lift me to new heights. Most of all, you're all just a downright pleasure to be around and can always put a smile on my face. I don't think I am myself without you. Thank you.

Finally, I'd like to express my gratitude to the mice whose lives contributed to my research. At times its hard to grapple with the sacrifices required, but that's made a little bit easier knowing the care, compassion, and respect shown towards these animals by all the staff and students that interact with them. I am forever indebted to your tiny little brains.

Contribution to original knowledge

Previously, we knew that VPS35 and VPS35 D620N modulates cortical glutamate transmission *in vitro*[1–3], but did not know whether the PD-linked D620N mutation alters glutamatergic transmission in the brain region central to PD, the striatum. This dissertation presents novel evidence of the role of VPS35 as a modulator of striatal glutamatergic transmission. We report for the first time, that striatal glutamatergic neurotransmission, and more specifically, striatal glutamate release is increased by 6 months in VPS35 D620N heterozygous knock-in mice. We also find that glutamate release is reduced in aged knock-in animals.

This shift from hyper- to hypo-activity is also observed in our measures of striatal dopamine release. Previous findings from the Milnerwood lab identified that dopamine release is

increased in the striatum of knock-in animals at 3 months by fast-scan cyclic voltammetry[4]. This dissertation presents evidence of dopaminergic alterations beyond, at 6 and ~25 months. Our study is also novel in its use of fluorescent reporters to assay dopamine and glutamate release in the VPS35 D620N knock-in model of PD, and the first to study neurotransmission in knock-in animals aged up to 27 months.

Furthermore, we do not observe any robust changes to striatal neurotransmission with LRRK2 kinase inhibition, which suggests that LRRK2 kinase may not be a direct interactor of VPS35 D620N, and/or that it does not contribute acutely to striatal glutamate or dopamine release. This is in contrast to previous literature, suggesting VPS35 D620N over-activates LRRK2 kinase and that this may contribute to PD-pathology[5].

Altogether, the findings presented in this dissertation demonstrate novelty, both in insight and in methodology, and uncovers a potential pathway towards Parkinsonism characterized by a period of dysregulated synaptic transmission prior to the expected reduction in striatal neurotransmitter release.

Contribution of authors

Chapters 2-3: I conceptualized and performed the research presented in this dissertation under the direct guidance of Dr. Austen Milnerwood. Additional training on imaging and analyzing iGluSnFR responses was provided by Dr. Matthew Parsons at Memorial University.

Genotyping of mice was performed by me, with the occasional help of Alessia Pietrantonio. I performed all stereotaxic injections for the LRRK2 kinase experiments and provided post-operative care for young mice. Aged mice were cared for and experimented on by Bruno Vieira,

whom I trained to carry out slice preparations and ensuing iGluSnFR and dLight recordings in aged animals. All data presented in this dissertation were entirely analyzed by me.

Chapter 2: All slice preparations for electrophysiological experiments were performed by me. Electrophysiology and iGluSnFR recordings from 1- to 6-month-old mice were obtained by me. iGluSnFR recordings from 6-month-old mice were obtained in collaboration with Emily Hurley during my training at Memorial University. Stereotaxic injections required for assessment of corticostriatal glutamate transmission were performed by Naila Kuhlmann and me. Injections for all other experiments were performed by me, apart from one animal that was injected and cared for by Jessica Barron at Memorial University. Experiments on this animal were carried out by Emily Hurley at Memorial University.

Post-operative care following surgeries on aged animals was done by Bruno Vieira. Bruno also collected data pertaining to iGluSnFR responses in aged mice (~25-month-olds). Sean Coady, whom I trained to record iGluSnFR responses, collected data pertaining to glutamate release in 3-month-old mice.

Chapter 3: All slice preparations for dLight recordings, as well as the recordings themselves, in 3- to 6-month-old mice were performed by me. I performed all stereotaxic injections required for dLight experiments and provided the post-operative care for mice aged 3- to 6- months. Slice preparations, post-operative care, and dLight recordings from aged animals were performed by Bruno Vieira.

List of figures

Figure 1 Membrane properties of dorsolateral striatum medium spiny neurons are modestly altered in VKI vs WT mice in an age-dependent manner 46

Figure 2 Spontaneous glutamate transmission is increased in VKI MSNs by 6 months 48

Figure 3 Corticostriatal glutamate transmission is increased in VKI MSNs by 6 months 49

Figure 4 AMPAR and NMDAR-mediated ChR2-PSCs are significantly higher in VKI MSNs by 6 months 51

Figure 5 Glutamate release in the dorsolateral STR is increased in VKI mice by 6 months 53

Figure 6 At 6 months, striatal glutamate transmission in WT but not VKI mice is sensitive to acute LRRK2 kinase inhibition with MLi-2 55

Figure 7 Evoked glutamate release in aged mice is reduced in VKI striata when compared to WT responses and is not altered with acute MLi-2 treatment 60

Figure 8 Electrically-evoked striatal dopamine release is not significantly different between WT and VKI mice at 3 months 63

Figure 9 Dorsolateral STR dopamine release at 6 months is altered in VKI brain slices and is not responsive to acute MLi-2 treatment 65

Figure 10 Striatal dopamine release is more exhaustive in VKI vs WT dorsolateral STR at 6 months and is not sensitive to acute LRRK2 kinase inhibition 67

Figure 11 Dopamine release is reduced in aged VKI striata and is modestly altered with LRRK2 kinase inhibition 69

Figure S1 Vehicle treatment increases striatal glutamate release in both WT and VKI 3-month-old mice 129

Figure S2 Captisol® vehicle treatment selectively alters passive membrane properties of 6-month-old dorsolateral STR MSNs in VKI mice 131

Figure S3 sEPSCs in 6-month-old MSNs are differentially altered in the presence of Captisol® vehicle in WT and VKI mice 132

Figure S4 Captisol® vehicle treatment increases ChR2-evoked cortico-striatal glutamate release probability onto MSNs in both WT and VKI 6-month-old brain slices 134

Figure S5 Striatal glutamate release is reduced in aged female VKI vs WT brain slices 136

Figure S6 Striatal glutamate release is reduced in aged male VKI vs WT brain slices 138

Figure S7 Striatal dopamine release is reduced in aged female VKI vs WT brain slices 140

Figure S8 Striatal dopamine release is reduced in aged male VKI vs WT brain slices 141

List of abbreviations

AAV ..... adeno-associated virus

aCSF ..... artificial cerebrospinal fluid

AMPA ..... α-amino-3-hydroxy-5-methyl-4-isoxazolepropionic acid

AMPAR ..... AMPA receptor

ChR2 ..... channelrhodopsin-2

ChR2-PSC ..... channelrhodopsin-2-evoked postsynaptic current

CI-MPR ..... cation-independent mannose-6-phosphate receptor

CMA ..... chaperone-mediated autophagy

CME ..... clathrin-mediated endocytosis

CTX ..... cortex

co-IP ..... co-immunoprecipiate

D1R ..... D1-type dopamine receptor

D2R ..... D2-type dopamine receptor

D620N ..... aspartate to asparigine substitution at amino acid 620

DAT ..... dopamine transporter

FAM21 ..... family with sequence similarity 21

FRAP ..... fluorescence recovery after photobleaching

G2019S ..... glycine to serine substitution at amino acid 2019

GABA ..... γ-Aminobutyric acid

GBA ..... β-glucocerebrosidase

Gpe ..... globus pallidus external segment

GPi ..... globus pallidus internal segment

GWAS ..... genome-wide association studies

iGluSnFR ..... intensity-based glutamate-sensing fluorescent reporter

LAMP1 ..... lysosomal-associated membrane protein 1

LAMP2a ..... lysosomal-associated membrane protein 2a

L-DOPA l-3,4-dihydroxyphenylalanine

LED ..... light-emitting diode

LRRK2 ..... leucine-rich repeat kinase 2

LTP ..... long-term potentiation

MDV ..... mitochondria-derived vesicle

MLi-2 ..... cis-2,6-dimethyl-4-(6-(5-(1-methylcyclopropoxy)-1H-indazol-3-yl)pyrimidin-4-yl) morpholine

MSN or SPN ..... medium-sized spiny projection neurons

NMDA ..... N-methyl-D-aspartate

NMDAR ..... NMDA receptor

ns ..... not significant

P1, P2, etc. ..... stimulation pulse 1, pulse 2, etc.

PD ..... Parkinson's disease

PSC ..... postsynaptic current

Rab ..... Ras-associated binding

REM ..... rapid eye movement

sEPSC ..... spontaneous excitatory postsynaptic current

SNpc ..... substantia nigra pars compacta

SNpr ..... substantia nigra pars reticulata

STR ..... striatum

TH ..... tyrosine hydroxylase

VAMP2 ..... vesicle-associated membrane protein 2

veh ..... vehicle

VGlut1 ..... vesicular glutamate transporter 1

VKI ..... VPS35 D620N knock-in

VMAT ..... vesicular monoamine transporter

VPS35 ..... vacuolar protein sorting 35

WASH ..... Wiskott Aldrich Syndrome protein and scar homologue

WT ..... wild-type

β2AR ..... β2adrenergic receptor

ΔF/F ..... change fluorescence/baseline fluorescence

Chapter 1: Introduction

Parkinson's disease (PD) is often thought of as a movement disorder that results from the death of dopamine neurons in the substantia nigra pars compacta (SNpc). However, functional changes to neuronal activity precede cell death and PD cardinal motor symptom onset, including the loss of an enzyme required for dopamine synthesis, tyrosine hydroxylase (TH), at the cellular level[6]. At the clinical level, prodromal motor and non-motor changes include REM sleep behaviour disorder, loss of olfaction, and cognitive decline[7]. Initial dysfunction may therefore be the pathophysiological process which eventually leads to the death of nigral dopamine neurons[8].

The selective degeneration of SNpc dopamine neurons is believed to underlie the cardinal PD motor symptoms, as evidenced by alleviation with dopamine replacement therapy (often through administration of the TH substrate and dopamine precursor, L-DOPA). However, the excellent response of motor symptoms to L-DOPA is not matched in efficacy by treatments targeting other important aspects of the syndrome. Individuals with PD also suffer from a plethora of non-motor symptoms, including cognitive and psychiatric disturbances, which can precede motor symptom onset by several years[7,9,10]. These symptoms are very likely caused by alterations to other neurotransmitter systems, such as glutamate, as they are not responsive to L-DOPA. Moreover, other neuronal populations are also found to degenerate in PD, including cortical and thalamic nuclei[11,12]. We therefore need a better understanding of functional changes to dopaminergic transmission and glutamatergic transmission ahead of neurodegeneration in PD.

The onset of neurodegenerative disease is thought to be driven by a combination of genetic and environmental factors, and aging. To better understand how these factors converge to precipitate a Parkinsonian state, we can investigate neuronal dysfunction in models of monogenic

PD. Intriguingly, some mutations causal to PD have been shown to alter synaptic function, including mutations in LRRK2, VPS35, and α-synuclein[1,13,14].

The Milnerwood lab developed and characterises genetic mouse models with PD-linked mutations knocked-in to the endogenous mouse genome; including the substitution for aspartate with asparagine at amino acid 620 (D620N) in the protein vacuolar protein sorting 35 (VPS35)[1,4]. VPS35 was initially thought to only recycle manose-6-phosphate receptors from late endosomes to the trans-Golgi network for reuse[15]; however, recent advances from the Milnerwood lab and others demonstrate that VPS35 traffics many other cargoes, including neurotransmitter receptors, to plasma membranes in neuronal dendrites and axons[1,3,16,17]. In accordance with the findings that VPS35 cargoes include glutamate and dopamine receptors[1,3,17], our group has also reported increased cortical glutamate transmission *in vitro*[3] and increased dopamine release *ex vivo*[4] in young, VPS35 D620N knock-in mice. Such neuronal phenotypes are likely to change as animals age; augmented dopamine and glutamate release is similarly observed up to 6 months of age in knock-in mice harbouring the PD-linked G2019S mutation in the LRRK2 protein, but returns to wild-type levels by 12 months[18]. Glutamatergic and dopaminergic activity in the disease-relevant striatal brain region of VPS35 D620N knock-in mice may also be altered in an age-dependent manner. Therefore, striatal glutamatergic and dopaminergic transmission will be investigated in a VPS35 D620N knock-in mouse model using electrophysiological and optogenetic techniques.

Background

What is PD?

First described by James Parkinson in 1817, PD has been traditionally characterised as a neurodegenerative movement disorder, with clinical diagnosis requiring the presence of

bradykinesia and at least one of three other cardinal motor symptoms; resting tremor, rigidity, and postural instability[19]. Affected individuals often present with a host of additional non-motor symptoms which may precede motor symptom onset, including bladder and bowel dysfunction, anosmia, depression, changes in colour vision, cognitive impairments, sleep disturbances, and dementia[20,21]. The "gold standard" for treatment is dopamine replacement therapy, which can rescue the cardinal symptoms of PD and be effective for many years if well managed. Over time however, dopamine replacement loses efficacy for motor symptom treatment, and can lead to the development of a number of side-effects including dyskinesia, motor fluctuations, and addiction-like behaviours[22–24]. Moreover, dopamine replacement therapy does not prevent or slow the progression of PD, sadly making the case that current treatment options are not disease-modifying but serve only as symptom management.

Of all the neurological disorders included in the Global Burden of Disease 2015 study[25,26], Parkinson's disease was one of the fastest growing. Due to ageing populations, crude prevalence rates increased by ~74% from 1990 to 2016 and are expected to increase further[25]. The doubling of the number of individuals with PD between 1990 and 2016 is projected to occur again in the coming generation (*ibid*). It is therefore imperative that we develop a deeper understanding of disease etiology, which can more easily be done by studying isolated variables in cases where single gene mutations lead to the onset of PD.

Monogenic PD

While monogenetic mutations account for only 5-10% of all PD cases[27], studying the function of the proteins which are causal to PD could uncover a common etiology for multiple forms of PD.

Even if not, with 100,000 patients in Canada and as many as 10 million people affected world-wide, monogenetic PD affects >1 million people[28].

Genetic linkage has identified mutations in SNCA, LRRK2, VPS35, Parkin, PINK1, and DJ-1 genes, with additional variants greatly increasing the risk of developing PD such as GBA polymorphisms[29]. Autosomal dominant forms of familial PD, for example in cases caused by mutations in the LRRK2 or VPS35 genes, present as late-onset disease with symptoms that are indistinguishable from sporadic PD[30]. With the advancement of genetic tools like genome-wide association studies (GWAS), more information is being collected about the genetic variation and background associated with PD. By better understanding the genome and transcriptome of individuals with PD, we can prioritize studying the mechanism by which alterations to these PD-linked genes can lead to PD onset[31].

Striatal function and dysfunction in PD

The dorsal striatum (STR) is a central site of dysregulation in PD, characterized by a loss of nigral dopaminergic input[32]. As the largest structure and major integrative input nucleus of the basal ganglia, the STR is critical for associative learning, reward processing, and behavioural action selection[33]. It is believed to process ensembles of possible actions generated by the cortex, and select an action from among the possibilities[34–36]. While the ventral STR is involved in reward evaluation and incentive-based learning[37], the dorsal STR is involved in habit-based behaviour and action selection/initiation[38]. Impaired function of the dorsal STR leads to impaired locomotion, which is *the* major clinical manifestation of PD[39]. The dorsal STR, comprised of the caudate nucleus and putamen, receives glutamatergic input from the cortex and the thalamus[40], and is heavily modulated by dopaminergic input from the SNpc[41]. The dorsal STR can be further

delineated into dorsomedial and dorsolateral compartments, each with complementary functions. The dorsomedial STR is thought to process goal-oriented behaviour while dorsolateral STR function governs habit formation and maintenance[40,42,43]. As the dorsolateral STR is known to be dysregulated in PD[32,44], we chose to characterize neurotransmission in this brain region and investigate changes to neuronal function that might underpin the motor and non-motor changes related to PD.

Neuronal populations of the striatum

Medium-sized spiny projection neurons (MSNs a.k.a. SPNs), making up 90% of the striatal neuronal population, are GABAergic inhibitory neurons that can be generally divided into two classes based on expression of either D1- or D2-type dopamine receptors (D1R and D2R)[45]. D1R-expressing MSNs are "direct" pathway neurons which project to the substantia nigra pars reticula (SNpr) and globus pallidus internal segment (GPi), to ultimately disinhibit output thalamic nuclei involved in motor commands. Functionally, direct pathway neurons oppose D2R-expressing, "indirect" pathway neurons which project to the globus pallidus external segment (GPe)[33,46,47].

Interestingly, MSNs respond to dopamine differentially based on receptor expression; dopamine excites D1R-expressing MSNs and inhibits D2R-expressing MSNs through activation or suppression, respectively, of the second messenger adenylyl cyclase[48]. Dopamine also modulates glutamatergic input onto MSNs differentially based on receptor expression, amplifying N-methyl-D-aspartate receptor (NMDAR)-mediated currents in D1R-MSNs[49] and reducing α-amino-3-hydroxy-5-methyl-4-isoxazolepropionic acid receptor (AMPAR)-mediated currents in D2R-MSNs[50]. The general classification of MSNs into direct and indirect pathways is likely oversimplified. Subpopulations of striatal MSNs express both D1- and D2-receptors[51,52], and

moreover, there is evidence to suggest that the two pathways can work in cooperation rather than in opposition with one another[53,54].

Striatal MSNs are additionally subdivided into striosomes or "patches," or into "matrix" compartments. These visually distinct populations are differentially innervated, and differ in their expression of opioid receptors and neurochemicals including acetylcholinesterase[55–58]. Regardless of their classification, MSNs are perfectly positioned to integrate both dopaminergic and glutamatergic input to initiate motor output sequences. The high density of dopamine terminals in the STR (~2.9 billion in rats arising from only ~16,000 SNpc neurons[59]) and the high density of glutamate and dopamine receptors[60–63] in the dorsal STR is of particular interest in PD, not only for its function in motor control but because of the potential impact of even small changes to dopaminergic or glutamatergic transmission here.

Glutamatergic and dopaminergic inputs onto MSNs can also be locally modulated through a number of GABAergic or cholinergic interneuron populations, both directly and indirectly[58,64–66]. The levels of complexity briefly discussed here afford the striatum the ability to support learning, initiating, and maintaining complex behaviours. This also means that the delicate balance required to maintain healthy striatal function is particularly vulnerable to age-related changes, as well as the genetic and environmental changes that contribute to PD onset.

What is VPS35 and why is it linked to PD?

VPS35 is a core subunit of the retromer complex that canonically functions to traffic cargo from recycling endosomes to the trans-Golgi network or out to the plasma membrane[15]. Since its discovery in Swiss and Austrian families in 2011, mutations in VPS35 have been linked to over 15,000 cases of PD[67–69]. The frequency of carriers of the D620N is low, accounting for up to 1%

of all PD cases. At present, the brain pathology remains unknown, as only one partial autopsy has been conducted[69,70]. Patients with this form of PD have clinically typical motor and non-motor symptoms[67], suggesting dysregulation of dopamine neurotransmission and beyond.

In mammals, VPS35 mRNA and protein is ubiquitously expressed through the body and the brain (Human Protein Atlas, proteinatlas.org)[71]. More specifically, RNA-seq data from mouse brains show *VPS35* expression is found in neuronal, neuronal precursor, vascular, and glial cells[72]. It should be noted that VPS35 D620N mutations may affect non-neuronal cell populations of the brain which could contribute to PD pathology and/or changes to neurotransmission. For instance VPS35 D620N knock-in mice show increased SNpc reactive astrogliosis at an advanced age[73]. It may be that phagocytic clearance, a process that implicates VPS35[74], may be directly affected by the D620N mutation. While a reduction of phagocytic clearance could contribute PD etiology[75], little else is known about non-neuronal effects of VPS35 D620N in PD. We will, however, discuss the neuronal roles of VPS35 before exploring the potential implications of the D620N mutation in VPS35 neuronal function.

VPS35 regulates neuronal and embryonic viability

VPS35 is ubiquitously expressed in the brain, including in neurons of the cerebral cortex, hippocampus, brainstem, and substantia nigra[76], suggesting VPS35 could play a role in regulating the development and maintenance of neurons. We know that VPS35 is required for proper embryonic development as its complete knockout is embryonic lethal[77,78]. Multiple reports suggest that a reduction in embryonic VPS35 levels disrupts neurite outgrowth and morphology[77,79–82]. Furthermore, VPS35 may regulate the communication between vasculature and developing neurons as knock-out of VPS35 in embryonic neurons reduces the number and branching of brain vasculature[83]. Coupled with an impairment in terminal neuronal differentiation, embryonic

knockout of VPS35 increases cortical atrophy and reactive gliosis, both features of Alzheimer's disease-like neurodegeneration in young adult mice[77,83,84]. Selective knockout of VPS35 in dopaminergic neurons show PD-like neurodegeneration and loss of motor coordination[85]. The induction of neurodegenerative processes may begin with changes to neurodevelopment, and both could converge on VPS35 modulation of Wnt/β-catenin signaling[86–90]. In fact, Wnt signaling in *C.elegans* guides neuronal polarity in a VPS35-dependent manner[91]. Together, VPS35 function may be required for the development, maturation, and maintenance of neurons.

VPS35 synaptic function

The Milnerwood lab, and others, have demonstrated that VPS35 is localized to axons and dendrites of many neurons, including cortical neurons[1,16,81,92,93]. This implicates VPS35 in synaptic transmission through activity in both pre- and post-synaptic neuronal compartments. Presynaptic function of VPS35 is somewhat contentious. In a report by Vazquez-Sanchez et al., knock-down of VPS35 in mouse hippocampal neurons does not seem to alter synaptic vesicle size or number docked at active zones, but does decrease the number of VAMP2-positive synapses. However knockout of VPS35 in drosophila does show a reduction the number and size of most synaptic vesicles, while a small number of vesicles are significant enlarged[81]. The discrepancy between these findings may be a result of incomplete knock-down in the former report, or a species-dependent role for VPS35 at synaptic boutons. In addition to VAMP2 localization, VPS35 and the PD-linked D620N mutation has been shown to influence the localization and expression of other presynaptic proteins specific to dopaminergic and glutamatergic neurons, including DAT, VMAT2, and VGLUT1[3,4,94,95]. Finally, VPS35 may also regulate the release of extracellular vesicles from presynaptic compartments, and could transmit potentially pathogenic proteins associated with neurodegeneration from one neuron to another[13,96,97].

VPS35 may further function at the postsynapse to regulate neurotransmission through its binding to neurotransmitter receptors including D1- and D2- type dopamine receptors[3,17], GluN1 NMDARs and GluA1 AMPAR subunits[1,3], and β2-adregenergic receptors[16]. Knock-down of VPS35 reduces endosome to surface delivery of β2-adregenergic receptors (*ibid*); conversely, overexpression of VPS35 increases D1 receptor trafficking from endosomes to cell membranes[16]. Acute VPS35 knock-down also decreases excitatory post-synaptic currents and blocks long term potentiation (LTP) in hippocampal slices through an impairment in AMPA receptor surface delivery[2,16]. Interestingly, overexpression of wild-type (WT) VPS35 in cultured hippocampal neurons (after acute knock down of VPS35) rescues LTP deficits, whereas overexpression of VPS35 containing the PD-linked D620N mutation does not[2]. The Milnerwood lab has also shown that AMPAR delivery is modified by VPS35 expression and mutation[1,3]. Altogether, these data directly implicate VPS35 in the regulation of pre- and post-synaptic activity in a number of neuronal populations, likely through its canonical role in endosomal sorting.

VPS35 influences mitochondrial function

VPS35 mutations can dysregulate mitochondrial homeostasis, a key player in PD pathogenesis[98]. Mitochondrial fragmentation can be mediated through recruitment of the protein DLP1 which is thought to inhibit mitochondrial fission perhaps through occupation of fission sites on the outer membrane[99]. Interaction of DLP1 with proteins such as VPS35 can disinhibit DLP1-mediated fission sites and increase trafficking of mitochondrial-derived vesicles (MDVs) to lysosomes, promoting mitochondrial fission[100]. Indeed, VPS35 interacts with DLP1 through binding to the FLV motif[101], and the D620N mutation increases this interaction, promoting mitochondrial turnover[100].

Mitophagy can also be mediated by Rab7, a retromer effector that is found on many subcellular membranes including late endosomes, lysosomes, and mitochondrial membranes[102]. Rab7 localization and activity can be maintained by VPS35's retromer complex, and overactivation of Rab7 results in the reduction of the ability of autophagic protein ATG9a (another VPS35-interactor) to form autophagosomes around damaged mitochondria (*ibid*). VPS35 mutations may therefore impact cellular homeostasis through dysregulated trafficking of cellular components, ultimately resulting in the death of neurons underlying motor and non-motor clinical manifestations of PD.

VPS35 influences lysosomal function

Neuronal function is dependent on lysosomal regulation of cellular health, a process that is altered in cases of both sporadic and genetic PD[103,104]. VPS35 function is critical for lysosomal degradation of autophagic cargo, and this seems to be evolutionarily conserved[53,105–107]. One such cargo is the synaptic protein α-synuclein, whose dysregulation and subsequent aggregation is a hallmark of PD pathology[108]. α-synuclein is degraded through two lysosome-dependent autophagic processes: chaperone-mediated autophagy, and macroautophagy[109], which both require VPS35 function[110]. In fact, VPS35 knockdown alters levels and trafficking of lysosomal proteins, including LAMP1, LAMP2a, ATG9, and cathepsin D[107,110–113]. This suggests mutations in VPS35 associated with PD may perturb cellular pathways required to repair or degrade proteins that maintain neurons in a healthy state. Furthermore, lysosomes may be involved in intracellular signaling, as they can fuse with cell membranes to release contents[114], contributing another potential mechanism to the spread of PD pathology.

VPS35 interacts with LRRK2

VPS35 has also been implicated in the function of other proteins that 1) contribute to lysosomal and synaptic function and 2) are mutated in familial PD[30]. The most frequent familial mutations alter leucine-rich repeat kinase 2 (LRRK2) proteins. Of these mutations, G2019S, and other pathogenic LRRK2 mutations have all been shown to increase LRRK2 kinase activity[115]. Mir et al. (2018) found the VPS35 D620N mutation also increases LRRK2-mediated phosphorylation of its target substrates, Rab GTPases, including Rab 8A, Rab10, and Rab12. As elevated phosphorylation of Rab10 in VPS35-mutant cells was rescued with the application of a LRRK2 kinase inhibitor[3,5], VPS35 mutation effects are potentially upstream of LRRK2 dysfunction in a common pathway to PD.

LRRK2 G2019S mutations also affect lysosomal function in a similar manner to VPS35 suppression, leading to lysosomal swelling and mis-localized endosomal cargo[104]. In addition to a potential convergence with LRRK2 in lysosomal function, LRRK2 and VPS35 may functionally converge to regulate presynaptic release of synaptic vesicles and neurite outgrowth[81]. Similar to the increase observed in cortical cultures from VPS35 D620N knock-in mice[3], data from the Milnerwood lab suggests that LRRK2 G2019S mutations increases both glutamate and dopamine transmission in the mouse striatum, and that this occurs in an age-dependent manner[18]. In summary, VPS35 function may implicate other proteins that are found to be mutated in PD, including, but not limited to LRRK2.

VPS35 interacts with GBA

One of the first-described cargos of the VPS35 retromer complex is the cation-independent mannose-6-phosphate receptor (CI-MPR), which traffics lysosomal enzymes, including PD-linked β-glucocerebrosidase (GBA)[30], although there is evidence that GBA can also be trafficked

in a CI-MPR-independent manner[116]. Regardless, a reduction in both VPS35 and GBA protein levels is observed in post-mortem brain tissue from patients harbouring LRRK2-mutations, linking the function of VPS35 to multiple proteins previously mentioned in the development of PD[117]. Mutations in VPS35, LRRK2, GBA, and α-Syn can all inhibit cellular functions such as chaperone mediated autophagy[30,118], again suggesting a degree of convergence in the etiology of genetic and sporadic PD. It is therefore vital that we develop an improved understanding of VPS35 function and the impact of D620N mutations in specific brain regions and cell types affected in PD; critically, the STR and striatal MSNs.

D620N mutation in VPS35

The PD-linked D620N mutation in VPS35 causes a c-terminal substitution, aspartate to asparagine at amino acid 620, that is proposed to disrupt molecular electrostatic interactions[68]. Since the c-terminus of VPS35 participates in binding to VPS29 and homodimerization with VPS35 of other retromer complexes, it is hypothesized that D620N mutations could alter retromer core complex assembly[119–121]. However, the D620N mutation does not significantly alter binding capacity to other core complex components, including with VPS26a and VPS29[1,3,15], but does seem to increase perinuclear localization of retromer and reduces the strength of interaction with WASH complex components[3,113,122–124]. The WASH, or Wiskott Aldrich Syndrome protein and scar homologue, complex includes proteins such as WASH1 and FAM21, and functions to regulate actin polymerization on endosomes through the activation of Arp1/2 protein[125,126]. As WASH complex is recruited to VPS35-positive endosomes to facilitate endosomal tubulation and movement of cargoes, it may be that the D620N mutation leads to tubulation defects and reduction of cargo recycling/budding off from endosomal membranes[113,127,128]. The nature of the cargo may then determine the functional implications of VPS35 D620N mutations. The consequences of VPS35

D620N on neurons are next discussed in the context of either knock-in animal models or patient-derived studies, so as to avoid the potential confound of altering levels of VPS35 itself.

Effects of VPS35 D620N in human neurons

Asides one report suggesting VPS35 D620N increases LRRK2-mediated phosphorylation of Rab proteins in human neutrophils and monocytes[5], very little is known about VPS35 D620N function in humans and human neurons. A previous study in patient-derived induced pluripotent stem cell neurons suggests that the presence of the D620N mutation increases neuron surface expression of GluA1 AMPA receptor subunits in dopaminergic-like neurons[1]. Patient-derived neurons of various subtypes show impairments in mitochondrial respiration and a sustained increase in mitophagy following CCCP exposure[129]. These neurons also show a reduction in lysosomal size, lysosomal protein expression, and an accumulation in total α-synuclein levels (*ibid*). VPS35 D620N-expressing human fibroblasts have increased fragmentation of the mitochondrial network, which is reversed when inhibiting mitochondrial fission[101]. Whether the observed impairments in lysosomal and mitochondrial dynamics in VPS35 D620N human neurons are implicated in PD pathogenesis remains to be seen. However, data from knock-in animal models of PD suggest VPS35 D620N mutations can alter lysosomal, mitochondrial, and synaptic function.

Effects of VPS35 D620N in knock-in mouse models of PD

To date, several different knock-in mouse models VPS35 D620N have been generated with similar, but slightly different phenotypes (possibly due to methodological or housing differences). Central and peripheral nervous system-specific knock-in of the D620N mutation leads to impairment of neurogenesis in the hippocampal dentate gyrus by 3 months as well as reduced neurite outgrowth and dendritic brancing[80]. These mice also show increased phosphorylation of AD-associated amyloid precursor protein, which may be evidence of early dysregulation of neuronal protein

homeostasis. Multiple assessments of VPS35 D620N effects on striatal neurotransmission show altered dopamine levels in animals, however some reports show elevated levels of basal and evoked striatal dopamine release[4,130], while another suggests decreased evoked dopamine release[78]. The differences in striatal dopamine measures may result from differences in age, peripheral expression of wild-type VPS35, the method of assessment (whether *in* or *ex vivo*, whether microdialysis or voltammetry, whether electrical or KCl stimulation, etc), or even that basal and evoked dopamine release are altered by VPS35 D620N in opposing ways. Mice could also be exposed to different immune, environmental, and psychological factors arising from differences in housing conditions and background strains. Regardless of the knock-in model, D620N mutations in VPS35 seem to alter striatal dopamine release in both young and aged mice.

Aged VPS35 D620N mice show a reduction in TH+ neuron number in most knock-in models[73,78,122], but this is not observed in 22 month-old mice harbouring mutations only in the central and peripheral nervous system[130]. Aged VPS35 D620N knock-in mice do not show differences in levels of dopamine transporter (DAT) or D2 dopamine receptor, nor in dopamine metabolism[78,130]. However, this contrasts an early reduction in DAT function and expression, as well as increase in dopamine metabolism and vesicular monoamine transporter (VMAT) levels in the striatum of young knock-in mice[4]. Taken together, these studies present functional, biochemical, and anatomical evidence of age-related changes to striatal dopaminergic neurotransmission with VPS35 D620N mutation.

Moreover, aged mutant mice show neurodegenerative changes including widespread axonal damage, increased levels of α-synuclein, aberrant tau phosphorylation and conformation, and reactive gliosis[73,122]. VPS35 D620N may also induce changes to midbrain retromer-dependent lysosomal and mitochondrial function[73] in aged animals, but this is not observed in every knock-

in model[78,130]. Intriguingly, aged mutant mice show altered VPS35 levels[122,130] and reduced WASH1 levels[122], suggesting VPS35 D620N mutation may alter the expression of VPS35 interactors with age, and that this could contribute to the enhanced degeneration of SNpc dopaminergic neurons in PD. Despite multiple reports of neurodegenerative changes in aged VPS35 D620N knock-in mice, changes to locomotion and gait are modest at best[73,78,122,130], suggesting the changes induced by the mutation in mice can be accommodated for in terms of behaviour.

Considering markers of neurodegeneration are found throughout the brain[73,122], VPS35 D620N may affect other cell types and neurotransmitter systems. Our data from primary mouse cortical neurons cultured from heterozygous and homozygous knock-in mice show glutamatergic transmission is increased in both pre- and post-synaptic measures[3]. As with findings in patient-derived human neurons, GluA1 surface expression in mouse primary cortical neurons is increased *in vitro*[1]. An increase in phosphorylated Rab10 is also observed in these neurons, which can be rescued with acute LRRK2 kinase inhibition, and is in line with reports from mouse embryonic fibroblasts[5]. However, acute LRRK2 kinase inhibition does not alter glutamatergic phenotypes observed in knock-in neurons[3].

A thorough investigation of the subtle phenotypic differences between experimental models of VPS35 PD may reveal the specific changes required to contribute to a Parkinsonian state. Still, a growing body of literature demonstrates early dysregulation to both glutamatergic and dopaminergic transmission, and separately, eventual neurodegeneration. Early dysfunction seems to be characterized by an elevation in neurotransmission, and later neurodegeneration would theoretically reduce neurotransmission; however, the potential transition from dysfunction to degeneration has not been characterized in the same model of VPS35 D620N-linked PD.

Rationale for this study

Currently, individuals carrying PD-linked mutations have no disease modifying therapeutic options which serve to stop or halt disease progression. We need to better understand early cellular events that lead to the progression of motor and non-motor symptoms of the disease. Since PD caused by VPS35 D620N mutations presents similarly to idiopathic PD symptoms[30], this model serves can serve as a powerful tool to better understand not only VPS35-linked PD, but idiopathic cases as well. Moreover, the effects of VPS35 D620N on both dopaminergic and glutamatergic neurons are variable and may depend on the level of protein expression, cell-type specificity of the mutation, age of the animal, and method of assessment[2–4,73,78,85,106,122,130]. It is imperative, therefore, to assess longitudinal changes to dopaminergic and glutamatergic neurotransmission in the striatum in the same model using standardized techniques to better characterize the progression of changes throughout adulthood.

As VPS35 D620N heterozygous knock-in mice can be used to model autosomal dominant carriers of the mutation, they are compared to wild-type mice throughout adulthood. Alterations to neurotransmission are assessed in the dorsal striatum, a region which is canonically affected in PD and receives both glutamatergic and dopaminergic input. We also assess potential convergence of VPS35 D620N with LRRK2 kinase activity by repeating measures in the presence of LRRK2 kinase inhibition.

In better understanding how dopaminergic and glutamatergic inputs change across age, and the potential mechanistic involvement of LRRK2 kinase in synaptic phenotypes, we will further the understanding of the progression of striatal pathology in the VPS35 D620N model of PD. We

hope that our findings eventually lead to the development of drugs and/or therapeutic windows which confer neuroprotection against VPS35-linked PD, and potentially beyond.

Hypothesis

We hypothesize that **1)** VPS35 D620N heterozygous mutations increase striatal glutamate and dopamine transmission in young adult mice, which **2)** drives the eventual loss of striatal neurotransmission in aged mice. **3)** Changes to striatal neurotransmission are mediated by increased activation of LRRK2 kinase.

Specific objectives

1) Compare *ex vivo* striatal glutamate transmission between young adult mice (1- to 6-month-old) and aged (22- to 27-month-old) mice that are either wild-type (WT) or VPS35 D620N heterozygous knock-in (herein VKI).
2) Assess *ex vivo* striatal dopamine release in young adult and aged WT and VKI mice.
3) Investigate the sensitivity of striatal neurotransmission in young and aged WT and VKI mice to acute LRRK2 kinase inhibition.

Materials and Methods

Animals

VPS35 D620N knock-in (VKI) generated as previously described[4] were maintained on a C57Bl6/J wild-type background, and housed and bred in accordance with the Canadian Council on Animal Care regulations (Animal Use Protocol 2017-7888B). All procedures were approved by and governed in accordance with the Neuro Centre of Neurological Disease Models (Animal Use Protocol 2017-7888B) and with Memorial University Animal Care Committee (Animal Use Protocol 18-01-MP). Heterozygous, and wild-type littermates were used throughout. 1- to 6-month-old male mice were used for all experiments characterizing "young adult" mice, and 23- to 27-month-old male and female mice used for the "aged" mice cohort.

Genotyping

All animals were genotyped from ear samples taken at time of weaning and confirmed after collection of post-mortem tissue. Samples collected from tail tips or ears were digested in 100µL 10% Chelex (Bio-Rad 142–1253) for 20 minutes at 95°C, vortexing twice during the process. Digested samples were centrifuged for 2 minutes at 12,000 RPM. 2µL of the DNA-containing supernatant was added to 18µL of polymerase chain reaction (PCR) master mix (Qiagen 201203). Master mix was made using the Qiagen kit instructions and contained: taq polymerase, DNAse and RNAse-free water, 10X buffer, 10mM dNTPs, and custom DNA oligo primers (ThermoFisher: Forward-TGGTAGTCACATTGCCTCTG, Reverse-ATGAACCAACCATCAATAGGAACAC). Sample mixes were amplified using a PCR machine (program cycle available upon request) and combined with fluorescent DNA dye (ZmTech LB-001G). 10µL of the mix was then run through 4% agarose gel and visualized with a BioRad ultraviolet gel imaging machine.

Surgery

Experiments using channelrhodopsin-2 (ChR2), intensity-based glutamate-sensing fluorescent reporter (iGluSnFR), or modified dopamine D1 receptor fluorescent reporter (dLight1.3b), required stereotaxic injection of AAV constructs. Mice were injected subcutaneously with carprofen (2-4 mg/mL, 20mg/kg) and 0.9% NaCl and allowed to rest for >15 minutes. Mice were then anaesthetized with isoflurane (5% for induction, 1-2% for maintenance) and secured in a stereotaxic head frame (Kopf Instruments). Marcaine was injected subcutaneously below the site of incision and the scalp hair was removed either using chemical (Nair) or mechanical (Wahl clippers) means. A small incision was made in the scalp and the skull leveled using Bregma and Lambda sutures as points of reference. A micro-burr dentistry drill was used to perform a 0.5mm craniotomy over the site of injection. A 10µL syringe (Nanofil), attached to a microinjector (Harvard Apparatus Pump11 Elite) and lowered into the injection site. The z-coordinates were zeroed to the brain surface, and x, y coordinates to Bregma as origin. Injections for iGluSnFR and dLight were occasionally performed bilaterally; two craniotomies were therefore required to create openings, one in each hemisphere.

Injections were performed one hemisphere at a time with a 5-minute settling period post-injection. After injection the needle was removed, and the scalp rehydrated using additional Marcaine. The scalp was sutured closed with 4-0 silk sutures (Ethicon 683G) and sealed with Vetbond tissue adhesive (3M 1469SB) and the animals were given subcutaneous 0.9% NaCl to replace fluids lost during surgery (0.2-0.5mL/10mg). Mice were monitored for pain and discomfort after they regained consciousness and returned to their home cage within 1 hour. Post-operative monitoring was done for 3 days following surgery, during which mice were administered

Carprofen daily. Over the three-year period during which these experiments were performed, mortality from surgery or arising complications was less than 2%.

Construct specific injection details

For ChR2 experiments, AAV9-CAG-ChR2-mCherry (Neurophotonics Centre, U de Laval, lot #834 = $4x10^{12}$ GC/mL) was injected 4-6 weeks in advance of slice experiments. 650nL was delivered at 1nL/sec into the primary motor cortex (M1): 1.5 mm anterior, 1.0 mm lateral, 0.8 mm ventral to Bregma. For iGluSnFR or dLight experiments in 3- to 6-month-olds, mice were injected 3-6 weeks ahead of slice recording experiments. For glutamate release experiments, 1uL of AAV1.hSyn.iGluSnFr.WPRE.SV40 (Addgene 98929-AAV1, $2.8x10^{13}$ GC/mL) was injected into the dorsolateral striatum (STR) at 2nL/sec. For dopamine release experiments, 300nL of AAV5-CAG-dLight1.3b (Addgene 125560-AAV5, $1.5x10^{13}$ GC/mL) was injected into the dorsolateral STR at 1nL/sec. Dorsolateral STR coordinates: 2.0 mm anterior, 1.0 lateral, 3.2 ventral to Bregma.

Surgeries on 23-27-month-old animals were modified to maximize recording potential from each animal. As such, mice were injected bilaterally with iGluSnFR in one hemisphere and dLight in the other (separate needles were used for each virus). Needles were swapped between bilateral injections and reset to position Bregma at the origin before proceeding to the second hemisphere. Additional considerations were made to account for the advanced age of the animals: a prophylactic dose of carprofen was administered the day before surgery. Animals were also inspected to ensure they were healthy enough to tolerate surgery and DietGels were placed in cages during post-operative care to increase fluid intake. Surgeries were performed 2-4 weeks ahead of slice experiments.

Preparation of acute brain slices

For all recordings of neurotransmission, 300µm acute coronal brain slices were prepared from unanaesthetised mice. Mice were restrained, swiftly decapitated, and brains rapidly collected and placed in ice-cold recovery solution for 1 minute to firm the brain for subsequent slicing. Recovery solution contained in mM: 93 NMDG, 93 HCl, 2.5 KCl, 1.2 NaH_2PO_4, 30 $NaHCO_3$, 20 HEPES, 25 glucose, 5 sodium ascorbate, 3 sodium pyruvate, 10 $MgSO_4 \cdot 7H_2O$, 0.5 $CaCl_2 \cdot 2H_2O$ (pH 7.3-7.4, 290-310 mOsm). Following removal of extra-striatal rostral and caudal brain regions, the remaining brain was mounted on a vibrating-blade microtome platform using sodium acrylate and hemisected when required (as in the case of ~25-month-old animals injected with dLight and iGluSnFR in opposite hemispheres). The mounted brain was submerged in ice-cold recovery solution and sectioned coronally with the vibrating-blade microtome (Leica Microsystems VT 1200S). Slices were then transferred to 35°C recovery solution for 15 minutes before final transfer into holding chambers containing room-temperature (22-25°C) carbogen-infused artificial cerebrospinal fluid (aCSF) for at least 45 minutes prior to experiments. aCSF contained in mM: 125 NaCl, 2.5 KCl, 25 $NaHCO_3$, 1.25 NaH_2PO_4, 2 $MgCl_2$, 2 aCl_2, 10 glucose (pH 7.2-7.4, 300-310 mOsm).

Whole-cell patch-clamp electrophysiology

Whole-cell patch-clamp electrophysiology was used to obtain recordings of spontaneous and ChR2-evoked glutamatergic transmission events in MSNs of the dorsolateral caudate-putamen / corpus striatum[18]. Brain slices were transferred into a recording chamber perfused with room-temperature aCSF containing 100µM picrotoxin (Tocris 1128) at a rate of ~1.5mL/min. Slices were visualized on an Olympus BX51 microscope (40x magnification, 2x digital zoom) using IR-DIC

and recording using a Q-Imaging Electro camera. MSNs were identified visually within the dorsolateral STR based on somatic size (8-20μM) and distinct morphology, 50-150μM below the surface of the slice. Borosilicate glass capillary tubes (Harvard Apparatus 640805) were pulled using a Sutter P-1000 micropipette puller to form pipettes with a resistance of 4-8 MOhms when filled. Pipettes were filled with cesium-based internal solution containing in mM: 130 Cs methanesulfonate, 5 CsCl, 4 NaCl, 1 $MgCl_2$, 5 EGTA, 10 HEPES, 5 QX-314, 0.5 GTP, 10 Na_2 phosphocreatine, 5 MgATP, and 0.1 spermine (pH 7.2, 290mOsm). Filled pipettes were loaded onto an AgCl wire-containing motorized micromanipulator (Sutter Instrument MP-285) and lowered to patch onto identified MSNs. Recordings were obtained using a MultiClamp 700B amplifier in voltage-clamp configuration and filtered at 2kHz and digitized at 10kHz (Molecular Devices Axon Digidata 1440A). Membrane properties were initially determined using the membrane-test function while holding the cell at -70mV. Synaptic recordings following a 2-minute settling period. For all recordings, tolerance for access resistance was maximum 27 MOhms and recordings were discarded if this changed >10%.

Spontaneous excitatory post-synaptic currents (sEPSCs) were recorded over a minimum 2-minute period at -70mV with primary output gain 20, and analyzed using Clampfit 10 software (Molecular Devices) to detect glutamatergic sEPSCs. A 5pA peak event threshold tool was used to isolate EPSC events, with each checked by eye; non-unitary events were retained for inter-event interval analysis, but only unitary events were used for analysis of EPSC amplitude and decay constants. Cumulative distributions were used to evaluate amplitude and inter-event intervals of sEPSCs for each recorded MSN. Unitary sEPSCs within each recording were averaged and decay tau was measured using a 1-term exponential fitting function.

Following sEPSC recordings, patched MSNs maintained for subsequent ChR2-evoked post-synaptic current (ChR2-PSC) recordings. ChR2 was stimulated using wide-field illumination with blue light (473nm, XCite Series 120Q) transmitted through 40x immersion objective generating 2.7 mW. 5ms pulses were controlled by a Lambda SC Smart Shutter Controller (Sutter Instruments). Pulses were administered in trains of 4 pulses at 100ms inter-pulse intervals. Trains were repeated every 30 seconds, 5-10 times. Recordings at 70mV holding potential and Gain 2 were used to determine ChR2-PSC amplitudes, which were averaged across repetitions for each of the 4 pulses in the train.

Synaptic currents mediated by α-amino-3-hydroxy-5-methyl-4-isoxazolepropionic acid receptors (AMPARs) and N-methyl-D-aspartate receptors (NMDARs) were recorded. Single 5ms pulse stimulations repeated 5x every 30 seconds, were applied during recordings of ChR2-PSCs at -70mV holding potential to determine AMPAR-mediated currents. Recordings with single pulse stimulations were repeated at +40mV holding potential to assess AMPAR+NMDAR-mediated currents. Peaks of NMDAR-mediated currents were estimated at 40ms post AMPA peak. AMPAR-mediated currents then were isolated in experiments repeated at +40mV in bath-applied 10μM D-APV (NMDAR blocker, Tocris 0106). AMPA rectification indices were calculated by dividing isolated AMPAR ChR2-PSC at +40mV by ChR2-PSC at +70mV.

iGluSnFR and dLight imaging

Imaging of iGluSnFR and dLight to assay striatal glutamate and dopamine release, respectively, was performed on hemisected acute brain slices. Live recordings were obtained using the 2X objective focused on the dorsolateral STR. Slices were wide-field illuminated with green light (473nm, CoolLED pE-340fura), with a shutter controlled by Clampex software and Digidata

1550B hardware. Clampex and digitizer outputs were also used to trigger recordings with the EM-CCD camera (Andor iXon Ultra 897) and stimulus isolator (WPI A365). The stimulus isolator was connected to a monopolar tungsten stimulating electrode (A-M Systems 574000) which was lowered into the dorsolateral striatum 50-100µM beneath the surface of the tissue. Recordings were captured using Andor Solis software, using 4x4 binning and 205 frames/second (Hz) acquisition rate. N.B. The higher temporal resolution afforded by this acquisition rate allowed for more accurate analysis of event decays and expand the capability of this technique to capture and analyze spontaneous activity for future experiments. For these experiments, spontaneous activity was excluded from analysis of both iGluSnFR and dLight responses to electrical stimulation.

For iGluSnFR recordings, the stimulation was given at 150uA in a train of 10 x 0.2ms pulses with 100ms inter-pulse intervals. No-stimulation and stimulation trials were alternated at 1-minute intervals such that the stimulation was repeated every 2 minutes, until 4 stimulation and 5 no-stimulation trials were recorded. An 11^{th} pulse was delivered with each repetition of the stimulation trial, with inter-pulse intervals alternating between 500ms, 1000ms, 2500ms and 5000ms. The same protocol was used to obtained dLight 10-pulse recordings, which proceeded 2-pulse experiments. To obtain 2-pulse dLight input-output curves, 2 pulses of electrical stimulation with 4s inter-pulse interval, was delivered at 50uA, 100uA, 200uA, 300uA, 400uA, 500uA, (and in some cases, 600uA) with 2 minutes between each change in stimulus intensity. Responses were concatenated in FIJI software to determine the stimulus intensity corresponding to 50-60% maximum response, which was used for the subsequent 10-pulse dLight experiment. For recordings from old mice, only 2-pulse dLight data were obtained. For analysis of both iGluSnFR and dLight recordings, videos were converted into plots of fluorescent intensity over time using FIJI software and peaks and decays were analyzed within Clampfit (with decays measured by

fitting 1-term exponential function onto each trace). 10-pulse responses were averaged across all 4 stimulation trials.

Acute LRRK2 kinase inhibition

LRRK2 kinase was inhibited acutely in 3- and 6-month-old brain slice experiments using bath-applied MLi-2 (500 nM, Tocris 5756) dissolved in 45% captisol in PBS. Vehicle-control experiments were conducted with bath-applied 45% captisol in PBS (377.6µL/L aCSF). Slices were incubated for >1.5hours and remained perfused with either MLi-2 or captisol vehicle throughout recordings. Acute LRRK2 kinase inhibition was also delivered *in vivo* in aged animals by intraperitoneal injection of MLi-2 or 45% captisol in PBS at a dose of 5mg/kg for >1.5hours in advance of slice preparation. Slices were then incubated with MLi-2 or captisol as previously described, for > 45 minutes.

Statistical analysis

All statistical analysis was performed on GraphPad 10. Data were assessed for parametric or non-parametric distributions using D'Agostino and Pearson normality tests. This determined whether to follow with unpaired t-test/1-way ANOVA if normally distributed or Mann-Whitney U-test/Kruskal-Wallis test if one or more groups were not normally distributed. *Post-hoc* analysis was performed for analysis where significance was reached ($p < 0.05$) using the Holm-Šídák multiple comparisons test. Specific statistical analysis for each experiment is described in figure legends. Asterisks on figures represent $p < 0.05$ and a trend towards statistical significance ($0.10 > p > 0.05$) is represented as a numerical p value on figures. Comparisons yielding significance of $p>0.10$ were not plotted on graphs. Data are presented as n=cells from (n) animals (ie. WT = 6(3) describes that the wild-type dataset includes 6 cells from 3 animals).

Chapter 2: Investigating striatal glutamate transmission in VKI mice

Effects of VPS35 D620N mutation on striatal glutamate transmission in young adult mice

2.1 Membrane properties of dorsolateral striatal medium spiny neurons are transiently altered in VKI mice

Acute coronal brain slices were taken from WT and heterozygous VKI mice (Figure 1 A i). Whole-cell patch-clamp electrophysiological recordings were obtained from MSNs of the dorsolateral STR (Figure 1 A ii). WT and VKI neurons have similar membrane capacitance and resistance in 1-month-old animals, but VKI MSNs show a small but significant reduction in membrane tau (Figure 1 B i-iii). By 3 months, membrane tau measurements are similar to WT MSNs, as are membrane resistance measurements (Figure 1 C ii & iii). VKI MSNs show a trend towards increased membrane capacitance at this age (Figure 1 C i). This trend is also observed in 6-month-old VKI MSNs (Figure 1 D i). Membrane resistance at 6 months is significantly lower in VKI versus WT MSNs (Figure 1 D ii). Membrane tau measurements at 6 months are similar across genotypes (Figure 1 D iii). Altogether, changes in membrane properties are observed in dorsolateral VKI MSNs. These changes are age-dependent and may correspond to changes in membrane excitability of MSNs, which was measured next.

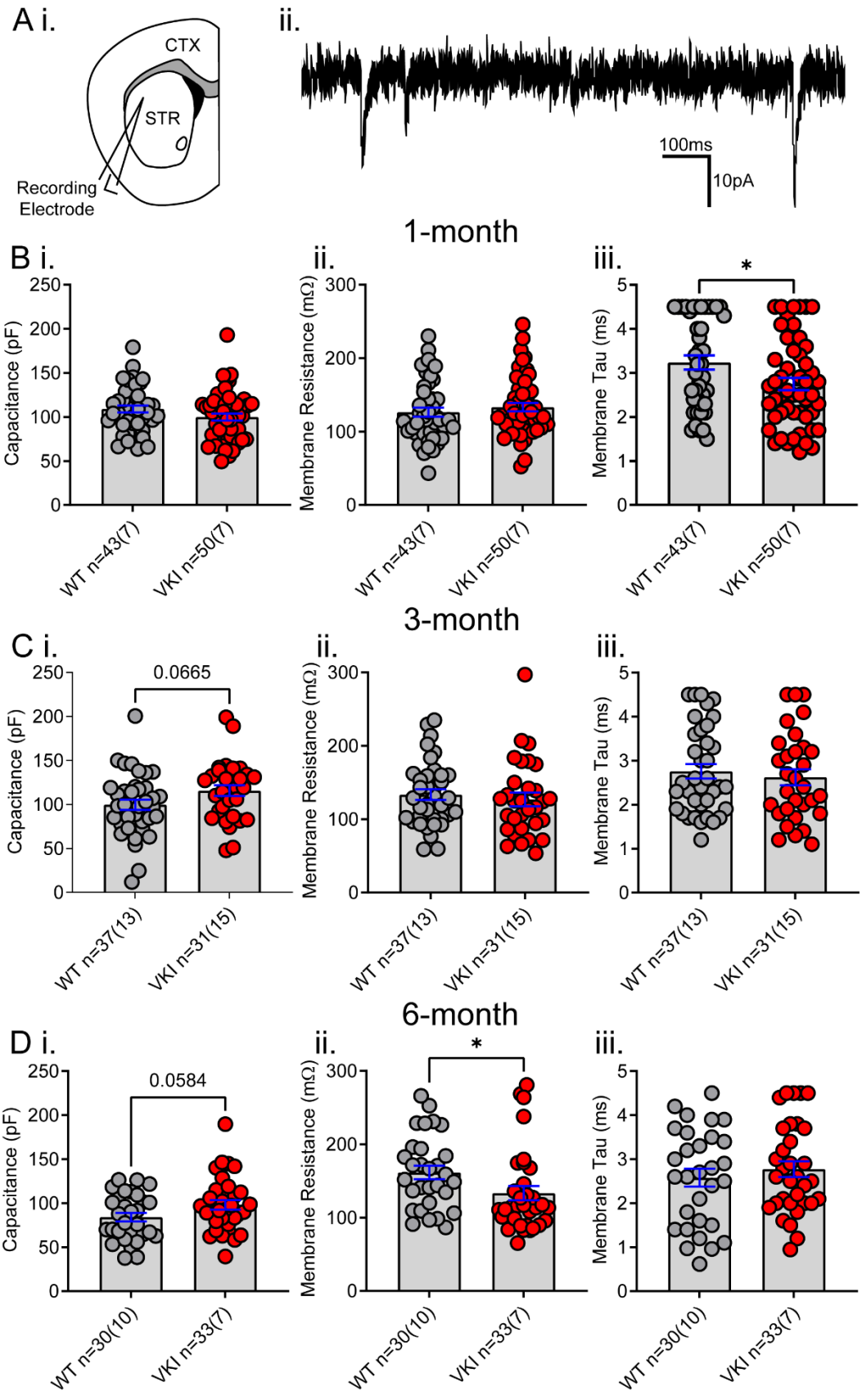
A i.
CTX
STR
Recording Electrode
ii.
100ms
10pA
1-month
B i.
ii.
iii.
Capacitance (pF)
Membrane Resistance (mΩ)
Membrane Tau (ms)
*
WT n=43(7)
VKI n=50(7)
3-month
C i.
ii.
iii.
0.0665
WT n=37(13)
VKI n=31(15)
6-month
D i.
ii.
iii.
0.0584
*
WT n=30(10)
VKI n=33(7)

(Previous Page) **Figure 1. Membrane properties of dorsolateral striatum medium spiny neurons are modestly altered in VKI vs WT mice in an age-dependent manner.**

A i) Schematic depicting whole-cell patch-clamp recording of medium spiny neurons in the dorsolateral striatum (STR) of acute coronal brain sections also containing cortex (CTX). **ii)** Representative trace of voltage-clamp recording of spontaneous excitatory post-synaptic currents (sEPSCs) from dorsolateral STR MSNs during which, passive membrane properties were recorded. **B** At 1 month, **i)** membrane capacitance of recorded MSNs is not different between WT and VKI mice (Mann-Whitney U-test p=0.13). **ii)** Membrane resistance of neurons is not different between WT and VKI mice (Unpaired t-test p=0.42). **iii)** Membrane tau is slower in WT neurons vs VKI neurons (Mann-Whitney U-test p=0.03). **C** At 3 months, **i)** VKI neurons trend towards significantly higher membrane capacitance measures vs WT neurons (Unpaired t-test p=0.07). **ii)** Membrane resistance of neurons is not different between genotypes (Mann-Whitney U-test p=0.39). **iii)** Membrane tau is not significantly different between genotypes (Mann-Whitney U-test p=0.61). **C** At 6 months, **i)** VKI neurons trend towards significantly higher membrane capacitance measures (Unpaired t-test p=0.06). **ii)** Membrane resistance is significantly lower in VKI vs WT neurons (Mann-Whitney U-test p=0.01). **iii)** Membrane tau of neurons is not significantly different between genotypes (Unpaired t-test p=0.47). Experimental n = x(y), where x = # of recordings and y = # of mice.

2.2 Spontaneous glutamate transmission in the dorsolateral STR is increased in VKI MSNs by 6 months

Spontaneous excitatory post-synaptic currents (sEPSCs) were obtained in voltage-clamp configuration to assess spontaneous glutamate transmission in WT and VKI dorsolateral STR MSNs (Figure 2). At 1 month, WT and VKI MSNs are similar in sEPSC amplitude, inter-event interval, and decay tau, suggesting that spontaneous glutamatergic activity is similar in MSNs across both genotypes at this age (Figure 2 A i-iii). At 3 months, VKI MSNs show increased sEPSCs amplitudes compared to WT neurons, as revealed by the cumulative probability plot, with no change in the inter-event interval of spontaneous glutamatergic events (Figure 2 B i & ii). At this age, decay tau of sEPSCs is reduced in VKIs (Figure 2 B iii). Intriguingly at 6 months, no change in decay tau is observed in VKI versus WT MSNs (Figure 2 C iii). However, the increase in probability of higher-amplitude events in VKIs is more robust than at 3 months and is now accompanied by an increased probability of a smaller inter-event intervals (Figure 2 C i & ii). These data suggest that changes to spontaneous glutamatergic transmission in VKI MSNs emerge at 3 months and become more robust by 6 months.

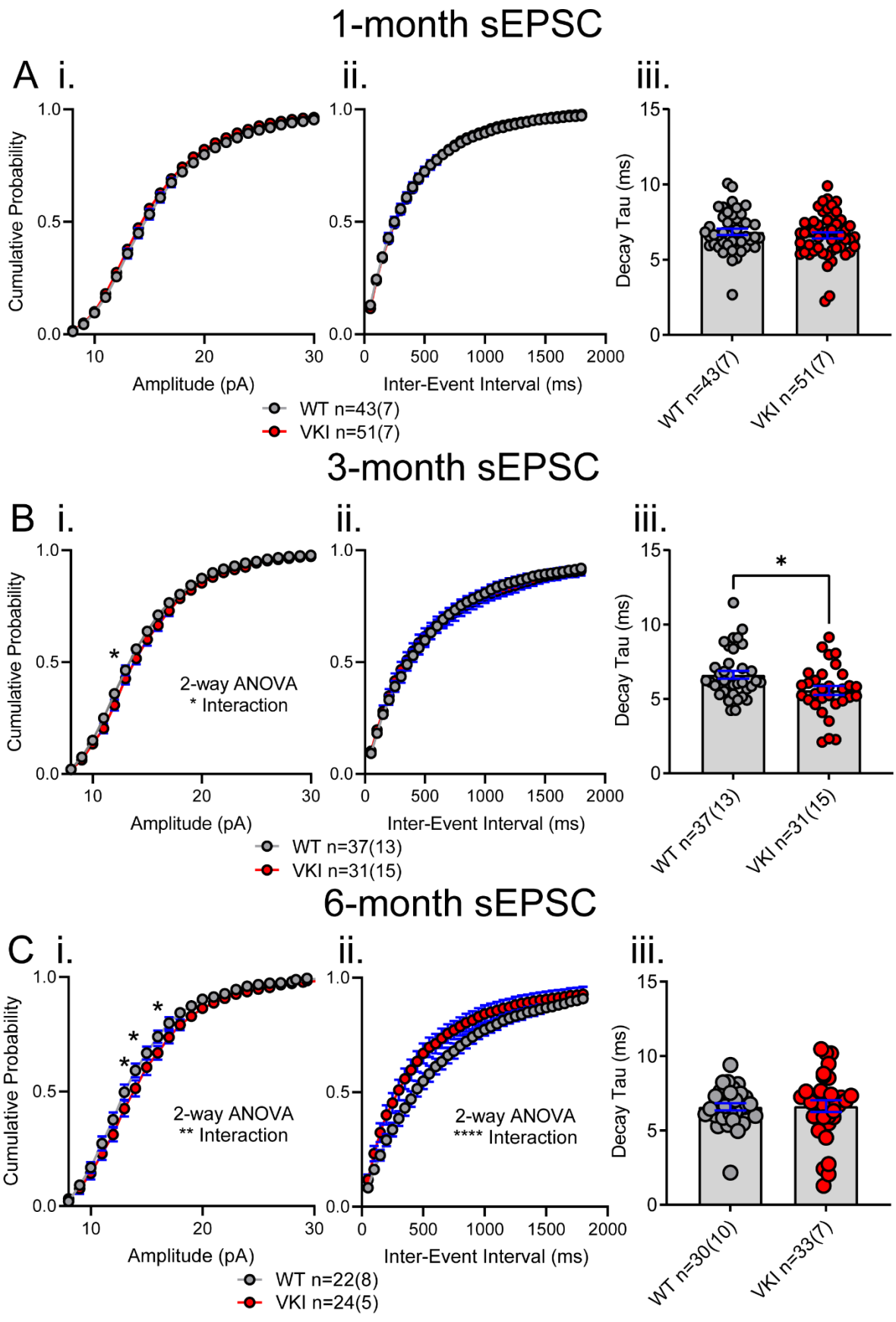
1-month sEPSC
A i.
ii.
iii.
Cumulative Probability
Amplitude (pA)
Inter-Event Interval (ms)
Decay Tau (ms)
WT n=43(7)
VKI n=51(7)
3-month sEPSC
B i.
ii.
iii.
2-way ANOVA
* Interaction
WT n=37(13)
VKI n=31(15)
6-month sEPSC
C i.
ii.
iii.
2-way ANOVA
** Interaction
2-way ANOVA
**** Interaction
WT n=22(8)
VKI n=24(5)
WT n=30(10)
VKI n=33(7)

(Previous Page) **Figure 2. Spontaneous glutamate transmission is increased in VKI MSNs by 6 months.**

A At 1 month, **i)** Cumulative distribution of sEPSC event amplitude show no significant difference between WT vs VKI recordings (2-way ANOVA interaction p>0.99, genotype p=0.21) **ii)** Cumulative distribution of sEPSC inter-event interval is not significantly different between genotypes (2-way ANOVA interaction p>0.99, genotype p=0.93). **iii)** Average sEPSC decay taus are not significantly different between WT vs VKI recordings (unpaired t-test p=0.43). **B** At 3 months **i)** Cumulative distributions show VKI sEPSC amplitudes are significantly more likely to be larger vs WT amplitudes (2-way ANOVA interaction p=0.02, genotype p=0.21, Holm-Šídák's multiple comparisons test WT vs VKI @ 12pA p=0.04) **ii.** Cumulative distributions of sEPSC inter-event intervals are not significantly different between genotypes (2-way ANOVA interaction p=0.34, genotype p=0.95). **iii.** Average sEPSC decay tau is significantly faster in VKI vs WT neurons (Mann-Whitney U-test p=0.01). **C** At 6 months **i)** cumulative distributions show a significantly higher number of larger-amplitude sEPSCs in VKI neurons (2-way ANOVA interaction p=0.005, genotype p=0.24, Holm-Šídák's multiple comparisons test WT vs VKI @ 14pA p=0.03 and @ 16pA p=0.04) **ii.** Cumulative distributions of sEPSC inter-event intervals indicate VKI neurons are significantly more likely to have sEPSCs with smaller inter-event intervals vs WT neurons (2-way ANOVA interaction p<0.0001, genotype p=0.04). **iii.** Average sEPSC decay taus are not significantly different in VKI vs WT neurons (Mann-Whitney U-test p=0.54).

2.3 Evoked corticostriatal glutamate transmission is increased in VKIs by 6 months

To assess evoked glutamate transmission changes in dorsolateral STR MSNs, channelrhodopsin-2 (ChR2)-expressing virus was injected into the primary and supplementary motor cortices, 4-6 weeks ahead of acute slice experiments. Due to the requirement of ~5-weeks post-surgery for viral expression of ChR2, experiments were conducted in 3- and 6-month-old cohorts only. Presynaptic cortical afferents were stimulated using wide-field illumination while MSNs of the dorsolateral STR were recorded (Figure 3 A i). 4 pulses of light were given at 100ms inter-pulse intervals and corresponding postsynaptic currents (PSCs) were assessed for amplitude and paired-pulse ratios (Figure 3 A ii). At 3 months, VKI MSNs show a trend towards higher amplitude PSCs for each of the 4 stimulation pulses compared to WT MSNs (Figure 3 B i). There was no difference in paired-pulse ratios, indicating no change in probability of glutamate release at cortico-striatal synapses (Figure 3 B ii). By 6 months, compared to WT MSNs, VKI MSNs show significantly different PSC amplitude and a trend towards reduced paired pulse ratios (Figure 3 C i & ii). Therefore, there is a modest increase in cortico-striatal glutamate transmission onto VKI MSNs by 3 months and remains elevated at 6 months.

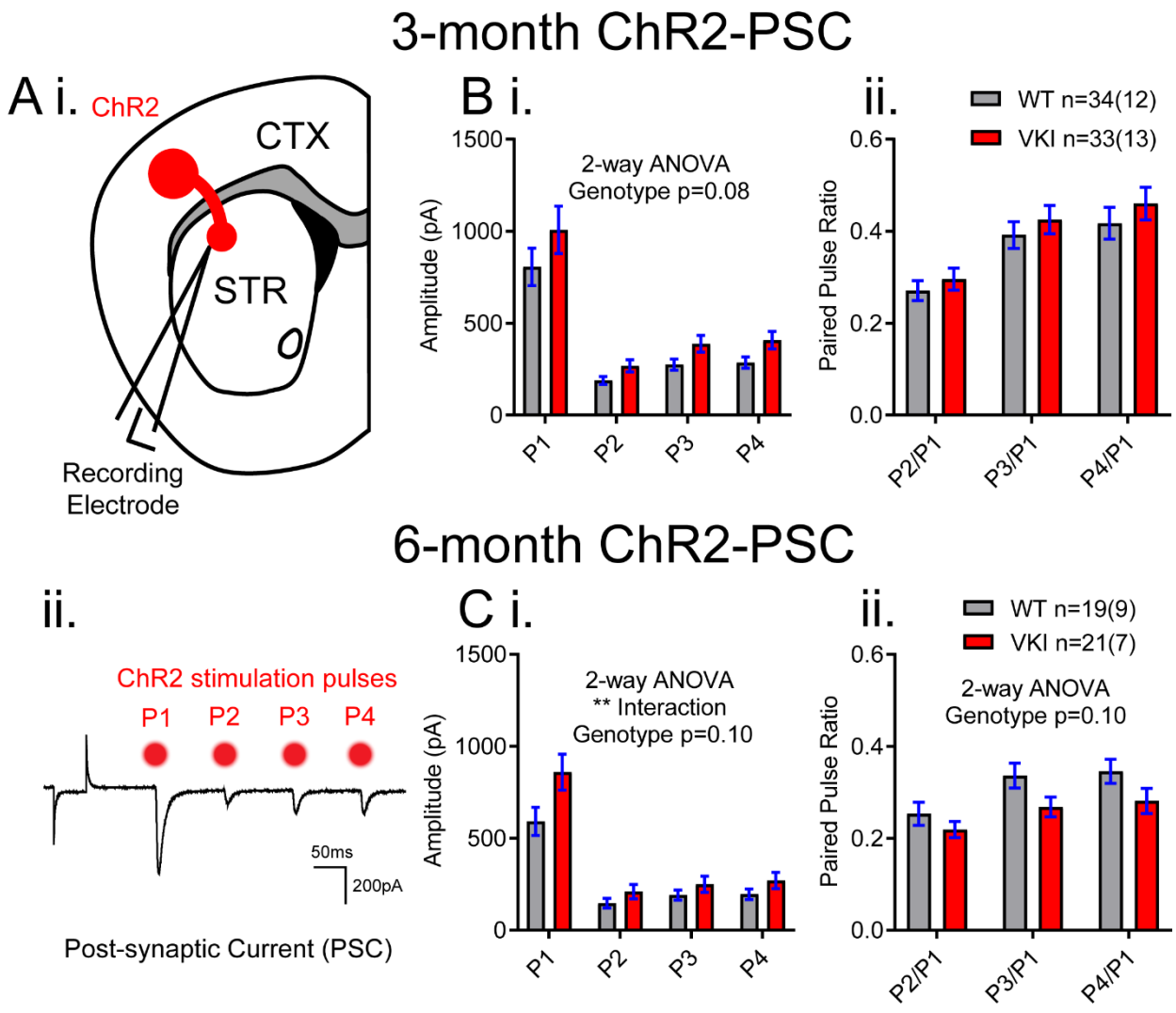

Figure 3. Corticostriatal glutamate transmission is increased in VKI MSNs by 6 months.

A i) Schematic representing channelrhodopsin-2 (ChR2) expression at injection site (primary + supplementary motor CTX), projecting to dorsolateral STR where MSNs were recorded. **ii)** Representative ChR2-mediated postsynaptic current (PSC) trace showing evoked currents corresponding to 4 pulses of light stimulation (P1-P4). **B** At 3 months, **i)** ChR2-PSCs show a trend towards significantly higher amplitudes in VKI vs WT MSNs (2-way ANOVA interaction p=0.64, genotype p=0.08) and **ii)** are not different in paired pulse ratios (2-way ANOVA interaction p=0.70, genotype p=0.41). **C** At 6 months, **i)** ChR2-evoked PSC amplitudes in VKI MSNs are significantly different from WT MSNs (2-way ANOVA interaction p=0.001, genotype p=0.10) **ii.** Paired pulse ratios of ChR2-PSCs trend towards significantly smaller values in VKI vs WT MSNs (2-way ANOVA interaction p=0.13, genotype p=0.10).

2.4 Corticostriatal glutamate transmission through AMPA and NMDA receptors are significantly increased in VKIs by 6 months

Using pharmacological and electrical manipulation, ChR2-evoked glutamatergic currents in dorsolateral STR MSNs were separated AMPAR- and NMDAR- mediated current (Figure 4 A i & ii). At 3 months, there is no significant difference between WT and VKI PSCs from AMPARs, NMDARs, or the ratio of the two currents (Figure 4 B i-iii). There is also no change in AMPA rectification index (Figure 4 B iv). At 6 months, VKIs show increased AMPAR current and NMDAR current, without a change in the ratio of AMPA: NMDA mediated currents (Figure 4 C i-iii). Like at 3 months, VKI MSNs did not differ from WT MSNs in AMPA rectification index measures at 6 months (Figure 4 C iv). Altogether, glutamate transmission through AMPARs and NMDARs are increased at 6, but not 3 months. This increase affects both receptors to the same extent, which may be the result of upstream increases in glutamate release.

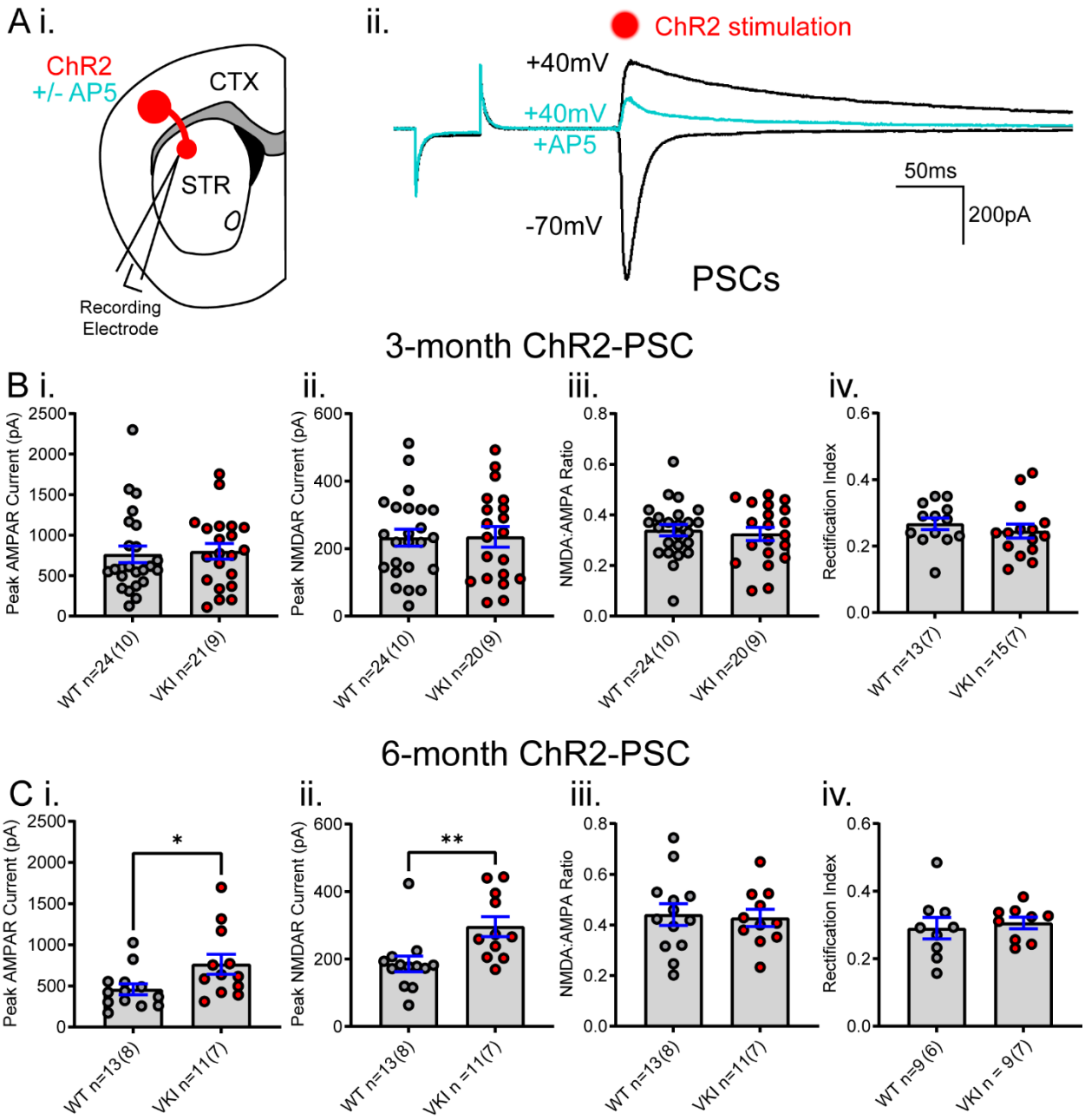

Figure 4. AMPAR and NMDAR-mediated ChR2-PSCs are significantly higher in VKI MSNs by 6 months.

A i) Schematic depicting ChR2-evoked corticostriatal glutamate release onto dorsolateral medium spiny neurons, which were recorded +/- NMDAR inhibitor, AP5. **ii)** Representative ChR2-PSC traces in response to single pulses of light. MSNs that were held at membrane potentials of -70mV or +40mV (in black), and +40mV in the presence of AP5 (in cyan) **B** At 3 months, **i)** the peak amplitude of AMPAR-mediated currents at -70mV are not significantly different between WT and VKI MSNs (Mann-Whitney U-test p=0.63). **ii)** Amplitude of NMDAR-mediated currents are not significantly different between genotypes at +40mV (Unpaired t-test p=0.95). **iii)** Ratios of +40mV NMDAR current to -70mV AMPAR current are not significantly different between WT and VKI MSNs (Unpaired t-test p=0.68). **iv)** Rectification Index of AMPA current is not significantly different between WT and VKI MSNs (Unpaired t-test p=0.45). **C** At 6 months, **i)** VKI MSNs show larger PSCs than WT MSNs, in peak amplitude of both AMPAR-mediated

(Figure 4 cont'd) current (Mann-Whitney U-test p=0.02) and **ii)** NMDAR-mediated current (Mann-Whitney U-test p=0.003). **iii)** Ratio of NMDA:AMPA currents are not significantly different between genotypes (Unpaired t-test p=0.81). **iv)** AMPA Rectification Index is not significantly different between WT and VKI MSNs (Unpaired t-test p=0.67).

2.5 Electrically-evoked glutamate release onto dorsolateral STR MSNs is altered in VKI mice by 6 months

To directly measure glutamate release, mice were injected in the STR with virus encoding intensity-based glutamate-sensing fluorescent reporter (iGluSnFR), 4-6 weeks prior to acute slice experiments. Changes in fluorescence corresponding to local electrical stimulation were normalized to baseline fluorescence (Figure 5 A i). A high frequency stimulation protocol of 10 pulses at 10Hz was applied, with a subsequent 11th pulse delivered at varying intervals to assess the capacity of the STR to recover glutamate after release (Figure 5 A ii). At 3 months, VKI iGluSNFR responses are lower in amplitude than WT responses when normalized to baseline fluorescence (Figure 5 B i). Relative to the 1st response in the 10-pulse train, VKIs show a faster initial depletion of glutamate which normalize to wild-type levels by the end of the pulse train (Figure 5 B ii). Following the pulse train, VKIs show reduced capacity to recover from glutamate depletion compared to WT mice (Figure 5 B iii). Decay taus of the 10th (and last) pulse in the train are significantly faster in VKIs than WTs (Figure 5 B iv). At 6 months, 10th pulse decay tau are no different from WT mice (Figure 5 C iv). At this age, VKIs show a trend towards altered iGluSnFR response amplitude relative to baseline (Figure 5 C i). VKIs are also significantly more likely to release glutamate during the 10-pulse train stimulation than WT mice (Figure 6 C ii). Finally, VKIs trend towards a significantly faster recovery from 10-pulse train stimulation (Figure 6 iii). Therefore, VKIs show increased probability of striatal glutamate release as early as 3 months, and are more capable of recovering from that increased release by 6 months.

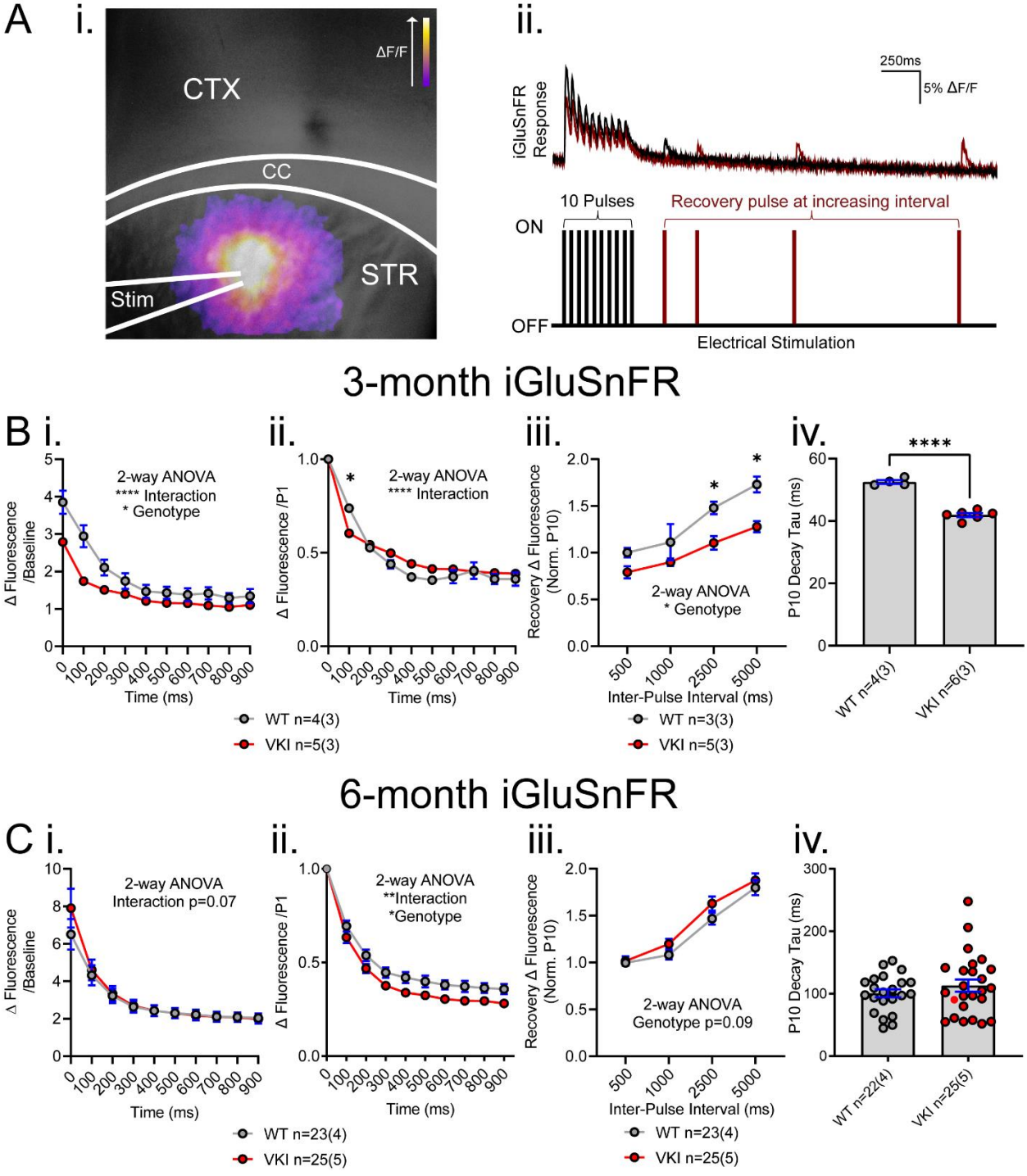

Figure 5. Glutamate release in the dorsolateral STR is increased in VKI mice by 6 months.

A i) Visualization of intensity-based glutamate-sensing fluorescent reporter (iGluSnFR) change in fluorescence from baseline (ΔF/F) in dorsolateral STR in response to local electrical stimulation (low to high ΔF/F represented as a gradient from purple to yellow, respectively). Boundaries of the corpus callosum (CC) separate CTX and STR in a coronal brain slice. **ii)** Representative iGluSnFR response in dorsolateral STR corresponding to train of 10x10Hz pulses of electrical stimulation followed by 11th pulse at increasing interval with each repetition of the protocol. Black trace represents 1st of 4 stimulations with subsequent stimulations overlayed in brown. **B** At 3 months, **i)** VKI vs WT

(Figure 5 cont'd) iGluSnFR Δ fluorescence/baseline is significantly smaller in VKI brain slices (2-way ANOVA interaction $p<0.0001$, genotype $p=0.03$). **ii)** When normalized to 1st pulse (P1), VKI iGluSnFR responses are significantly smaller relative to P1 (2-way ANOVA interaction $p<0.0001$, genotype $p=0.40$, Holm-Šídák's multiple comparisons test WT vs VKI @ 100ms $p=0.02$). **iii)** VKI responses show significantly smaller responses after 10x10Hz stimulation when normalized to 10th pulse (P10) when compared to WT responses (2-way ANOVA interaction $p=0.17$, genotype $p=0.01$, Holm-Šídák's multiple comparisons test WT vs VKI @ 2500ms inter-pulse interval (IPI) $p=0.04$, and @ 5000ms IPI $p=0.05$) **iv)** P10 decay of iGluSnFR Δ fluorescence is significantly faster in VKIs vs WT (Unpaired t-test $p<0.0001$). **C** At 6 months, **i)** VKI iGluSnFR Δ fluorescence/baseline trends towards significantly different response vs WT (2-way ANOVA interaction $p=0.07$, genotype p=0.74). **ii)** VKI responses are significantly smaller when normalized to P1 when compared to WT responses (2-way ANOVA interaction $p=0.004$, genotype $p=0.03$). **iii)** VKI responses after 10x10Hz stimulation trends towards significantly higher values when normalized to P10 than WT responses (2-way ANOVA interaction $p=0.63$, genotype $p=0.09$). **iv)** P10 decay of iGluSnFR Δ fluorescence is not significantly different between WTs and VKIs at 6 months (Unpaired t-test $p=0.31$).

Effects of acute LRRK2 kinase inhibition on striatal glutamate transmission in young adult mice

2.6 Acute inhibition of LRRK2 kinase activity does not alter STR glutamatergic transmission in 6-month-old mice

As LRRK2 kinase activity is increased in PD patients with VPS35 D620N mutation and may function downstream of VPS35 in endo-lysosomal pathways[5], it may be that LRRK2 kinase inhibition can reduce glutamate transmission in VKI mice. sEPSCs and ChR2-PSCs were recorded from dorsolateral STR MSNs which were bath-perfused for >1.5 hours with LRRK2-kinase inhibitor, MLi-2 or its vehicle, Captisol® (Figure 6). sEPSC recordings from 6-month-old animals show no difference in average amplitude, frequency, or decay tau of spontaneous glutamatergic events when comparing WT to VKI MSNs in both vehicle- and MLi-2 treated conditions (Figure 6 A i-iii). Strikingly, with MLi-2 treatment, WT MSNs show reduced amplitude of ChR2-evoked PSCs without change in paired-pulse ratios (Figure 6 B i & ii). There is no difference with MLi-2 treatment in VKI MSNs in either ChR2-evoked PSC amplitude or paired-pulse ratio (Figure 6 C i & ii). This suggests that acute treatment with LRRK2 kinase inhibitor MLi-2 does not alter glutamatergic transmission in the dorsolateral STR of VKI mice but may reduce corticostriatal glutamate transmission in WT mice.

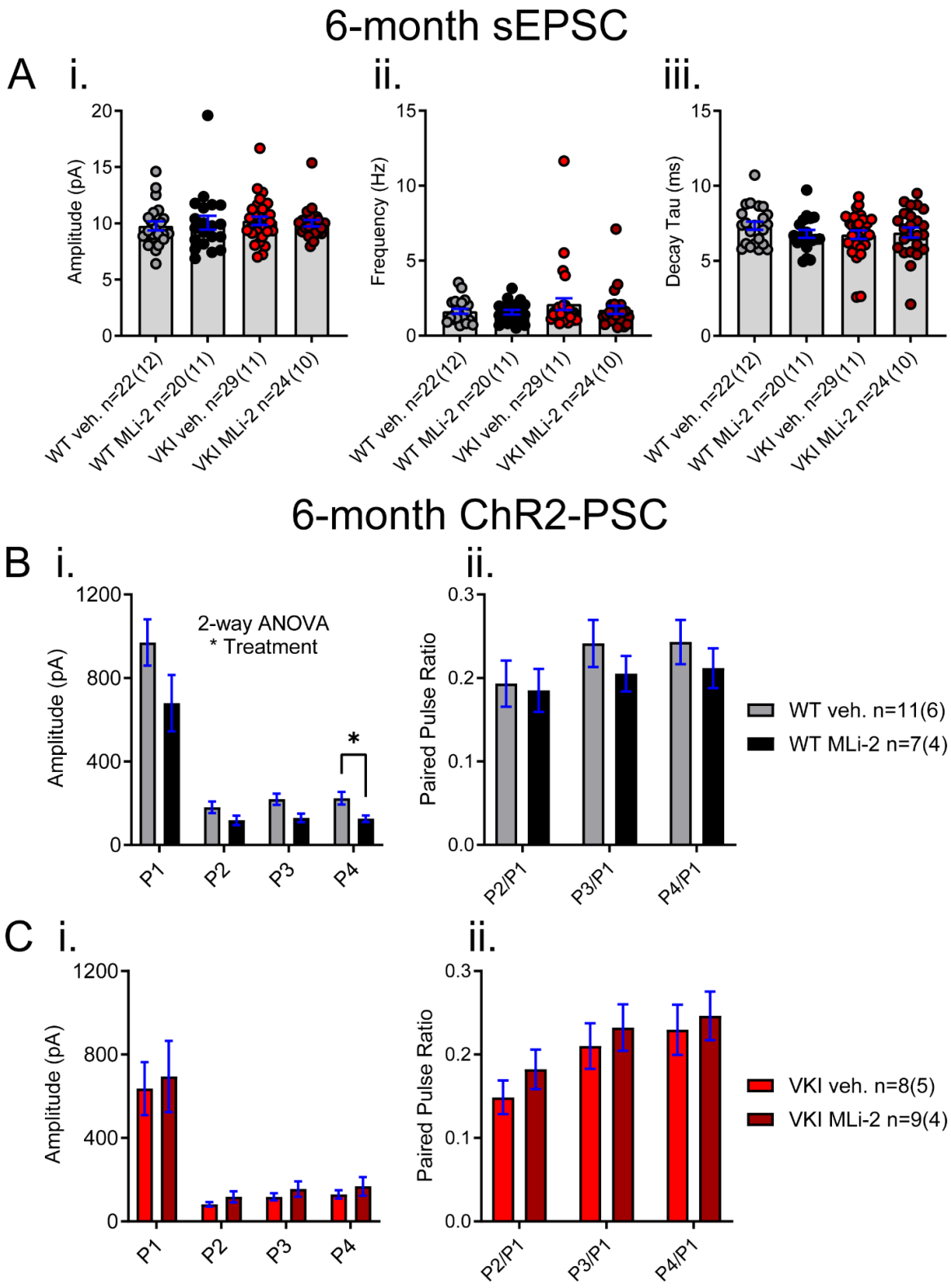

Figure 6. At 6 months, striatal glutamate transmission in WT but not VKI mice is sensitive to acute LRRK2 kinase inhibition with MLi-2.

(Figure 6 cont'd) A At 6 months, **i)** average sEPSC amplitude is not significantly different between WT and VKI neurons when comparing MLi-2 treatment vs vehicle (Kruskal-Wallis test p=0.61). **ii)** Average sEPSC frequency is not significantly different with MLi-2 treatment in WT and VKI neurons (Kruskal-Wallis test p=0.90). **iii)** Average sEPSC decay tau is not significantly different with MLi-2 treatment in WT and VKI neurons (Kruskal-Wallis test p=0.90). **B** At 6 months, **i)** MLi-2 treatment reduces WT ChR2-PSCs (2-way ANOVA interaction p=0.17, treatment p=0.05, Holm-Šídák's multiple comparisons test WT veh. vs WT MLi-2 @ P4 p=0.04). **ii)** MLi-2 treatment does not alter WT neuron ChR2-evoked PSC paired-pulse ratio (2-way ANOVA interaction p=0.56, treatment p=0.50). **C** At 6 months, **i)** MLi-2 treatment does not affect the amplitude of ChR2-PSCs in VKI neurons (2-way ANOVA interaction p>0.99, treatment p=0.61). **ii)** MLi-2 treatment does not affect paired-pulse ratio of ChR2-PSCs in VKI neurons (2-way ANOVA interaction p=0.57, treatment p=0.52).

2.7 Captisol® vehicle treatment differentially alters striatal glutamate transmission and membrane properties in VKI and WT MSNs

Spontaneous glutamate transmission is elevated in 6-month-old untreated WT vs VKI striata (Figure 2C), but not in vehicle-treated WT vs VKI striata of the same age (Figure 6A). Therefore, we next investigated whether vehicle treatment alone was sufficient to alter striatal glutamate transmission. To address this, MLi-2 and vehicle-treated slices were compared to untreated WT and VKI slices in 3 experimental paradigms.

First, iGluSnFR recordings of responses to 10 x 10Hz pulse train electrical stimulation revealed that vehicle treatment increased glutamate release in both WT and VKI striata relative to perfusion with artificial cerebrospinal fluid (aCSF) alone (Figure S1 A i & B i, Appendix). MLi-2 treatment does not significantly alter the size of iGluSnFR responses when compared with vehicle treatment, but both MLi-2 and vehicle treatment significantly increase the iGluSnFR response size when compared to aCSF conditions.

iGluSnFR responses, when normalized to 1st pulse peak, show greater facilitation or less extensive glutamate release in both WT and VKI aCSF perfused slices when compared with vehicle or MLi-2 treatment (Figure S1 A ii & B ii). Finally, decay tau of the response to the 10th/last pulse is significantly faster in aCSF-perfused WT and VKI brain slices when compared with vehicle or MLi-2 treatment (Figure S1 A iii & B iii). There is no significant difference between

Captisol® and MLi-2 treated iGluSnFR response decay. These findings indicate that Captisol® may be sufficient to increase striatal glutamate release to a similar extent as MLi-2 in 3-month-old animals, regardless of genotype.

Further, whole-cell patch-clamp experiments in 6-month-old MSNs revealed a significant difference in passive membrane properties with Captisol® vehicle treatment in VKI, but not WT mice (Figure S2, Appendix). Vehicle treatment in VKI brain slices decreases MSN membrane capacitance and membrane tau while increasing membrane resistance (Figure S2 A - C). There is no effect on these membrane properties in VKI MSNs with MLi-2 when compared to aCSF or vehicle conditions. WT MSN membrane properties are not affected by either vehicle or MLi-2 treatment. Therefore, there seems to be a selective alteration of membrane properties in VKIs by Captisol®.

MSNs were also recorded to compare spontaneous glutamatergic transmission across different treatment conditions (Figure S3, Appendix). Cumulative distribution of WT sEPSC amplitude, but not inter-event interval, is significantly altered with Captisol® vehicle and MLi-2 treatment when compared to aCSF alone (Figure S3 A i & ii). Cumulative distribution of VKI sEPSC amplitude and inter-event interval is significantly altered when comparing across treatment conditions (Figure S3 B i & ii). In both genotypes sEPSC amplitude, but not inter-event distribution is affected significantly by vehicle and MLi-2 treatment in when compared to recordings in aCSF, reflected by more numerous lower-amplitude events with either treatment. Neither sEPSC amplitude nor inter-event interval distribution in either genotype is affected by MLi-2 treatment when compared to vehicle alone. Average sEPSC decay taus are not different across treatment conditions or genotypes (Figure S3 C). Altogether, using Captisol® may differentially alter membrane properties of VKIs, and increases the proportion of lower amplitude,

spontaneous glutamate transmission events in MSNs in both WT and VKI mice. MLi-2 treatment does not seem to alter membrane properties or sEPSC characteristics in either genotype beyond what is observed with vehicle treatment alone.

Finally, ChR2- PSCs in 6-month-old mice were compared across treatment conditions to determine the influence of Captisol® vehicle treatment on corticostriatal glutamate release (Figure S4, Appendix). In WT MSNs, Captisol® vehicle treatment increases the initial ChR2-PSC while reducing paired-pulse ratios by the end of the 4-pulse train (Figure S4 A i & ii). MLi-2 effects were not significantly different from vehicle treatment alone. In VKI MSNs, vehicle treatment does not affect the initial amplitude, but reduces P2-P4 amplitudes (Figure S4 B i). A significant difference in paired-pulse ratio is only observed with vehicle treatment when comparing P2:P1 (Figure S4 B ii). No further differences in absolute or relative ChR2 responses are observed in VKIs treated with MLi-2 when compared to vehicle or aCSF control experiments. In summary, Captisol® alone may be sufficient to increase corticostriatal glutamate transmission onto WT MSNs and seems to increase the probability of glutamate release in both genotypes.

Effects of VPS35 D620N mutation +/- acute LRRK2 kinase inhibition on striatal glutamate release in aged mice

2.8 STR glutamate release is reduced in 25-month-old VKI mice and does not respond to acute LRRK2 kinase inhibition

iGluSnFR recordings (10-pulse, 10Hz electrical stimulation with subsequent recovery stimulation at variable intervals) were repeated in male and female mice aged 22-27 months and pooled (Figure 7 A). Mice were injected intraperitoneally with MLi-2 or vehicle 1.5 hours in advance of slicing. Pooled data show VKI responses to electrical stimulation trend towards smaller changes in

fluorescence than in WT, under vehicle-treated conditions (Figure 7 C i). There is no change in iGluSnFR response size with acute treatment with MLi-2 in either genotype (Figure 7 C ii & iii). When normalized to the size of the 1st pulse response, vehicle-treated VKI slices show significantly larger subsequent responses (Figure 7 D i). 1st pulse-normalized responses are not responsive to MLi-2 in either genotype (Figure 7 D ii & iii). Recovery following 10-pulse train was slower in vehicle-treated VKI versus WT slices (Figure 7 E i), but not sensitive to MLi-2 treatment in either genotype (Figure 7 E ii & iii). Decay tau of the 10th pulse was not different across genotype or treatment condition (Figure 7 B). While experimental numbers are underpowered to appreciate possible sex differences in observed phenotypes, preliminary data suggests that male and female VKI mice respond differentially to high frequency stimulation, and that there may be a sex-dependent effect of MLi-2 in WT mice (Figures S5 & S6). To summarize, iGluSnFR recordings from ~25-month-old mice suggest that glutamate release is reduced in the dorsolateral STR of VKI mice.

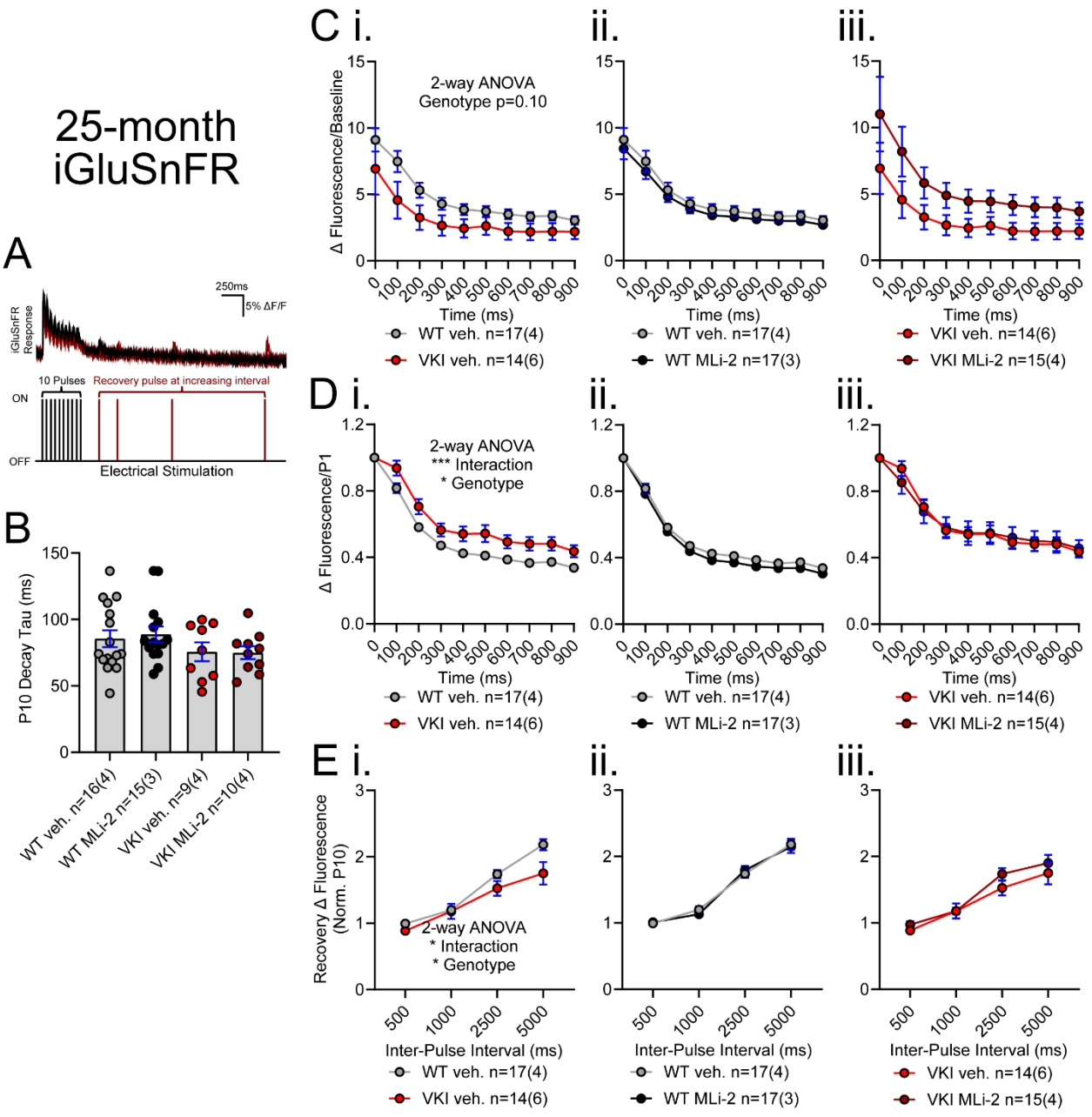

Figure 7. Evoked glutamate release in aged mice is reduced in VKI striata when compared to WT responses and is not altered with acute MLi-2 treatment.

A) Representative iGluSnFR response (in black) in dorsolateral STR corresponding to train of 10x10Hz pulses of electrical stimulation followed by 11th pulse at increasing interval with each repetition of the protocol (repetitions in brown). **B)** P10 decay tau of iGluSnFR responses are not significantly different in either genotype, with MLi-2 treatment (1-way ANOVA p=0.32). **C** At ~25 months, **i)** vehicle-treated WT responses trend towards significantly higher peak Δfluorescence/baseline measures when compared to VKIs (2-way ANOVA interaction p=0.19, genotype p=0.10). **ii)** WT iGluSnFR responses are not significantly altered with MLi-2 treatment (2-way ANOVA interaction p=0.99, treatment p=0.45). **iii)** VKI iGluSnFR responses are not significantly altered with MLi-2 treatment (2-way ANOVA interaction p=0.49, treatment p=0.11). **D** At ~25 months, **i)** iGluSnFR responses normalized to P1 peak

(Figure 7 cont'd) Δ fluorescence/baseline are significantly lower in vehicle-treated VKI vs WT brain slices (2-way ANOVA interaction p=0.0001, genotype p=0.01). **ii)** WT responses normalized to P1 peak are not significantly altered with MLi-2 treatment (2-way ANOVA interaction p=0.44, treatment p=0.14). **iii)** VKI responses normalized to P1 peak are not significantly altered with MLi-2 treatment (2-way ANOVA interaction p=0.29, treatment p>0.99). **E** At ~25 months, **i)** iGluSnFR response following 10x10Hz pulse stimulation, when normalized to P10 peak, is significantly lower in vehicle-treated VKI vs WT striata (2-way ANOVA interaction p=0.02, genotype p=0.04). **ii)** P10-normalized iGluSnFR responses following pulse train stimulation are not significantly different in WT brain slices treated with MLi-2 vs vehicle (2-way ANOVA interaction p=0.44, treatment p=0.90). **iii)** P10-normalized iGluSnFR responses following pulse train stimulation are not significantly different in VKI brain slices treated with MLi-2 vs vehicle (2-way ANOVA interaction p=0.67, treatment p=0.24).

Chapter 3: Investigating striatal dopamine release in VKI mice

Effects of VPS35 D620N mutation on striatal dopamine release in young adult mice

3.1 STR dopamine release is not significantly different between WT and VKI mice at 3 months

VKI mice have previously been shown to have increased dopamine transmission at 3 months by fast-scan cyclic voltammetry[4]. Here, STR dopamine release was instead measured with the fluorescent dopamine sensor, dLight, which was expressed using a viral vector injected into the STR, 3-4 weeks prior to slice experiments. Acute coronal slices were incubated in Captisol® vehicle >1.5hours prior to recording. STR change in fluorescence, normalized to baseline fluorescence, in response to 2 pulses of electrical stimulation with 4s inter-pulse interval were compared between vehicle-treated WT and VKI brain slices (Figure 8 A). No difference is observed between WT and VKI dLight response to increasing stimulus intensity (Figure 8 B i).

Neither the ratio of the 2nd pulse response size to the 1st, nor the decay tau of the 1st pulse is different between genotypes at this age (Figure 8 B ii & iii). Vehicle-treated WT and VKI brain slices were further evaluated for responses to high frequency 10-pulse, 10Hz stimulation with an 11th pulse given at an increasing interval (Figure 8 C). 3-month vehicle-treated WT and VKI responses were similar in size of peak fluorescence change (Figure 8 D i). WT and VKI responses

were also similar in size of the 10th pulse in the pulse train relative to the 1st and were similar in decay tau of the 10th pulse (Figure 8 D ii & iii). Finally, recovery from the 10-pulse train was similar between vehicle-treated WT and VKI brain slices. Contrary to previously published findings[4], no difference is observed in vehicle-treated WT vs VKI dopamine release at 3 months when assessed using dLight.

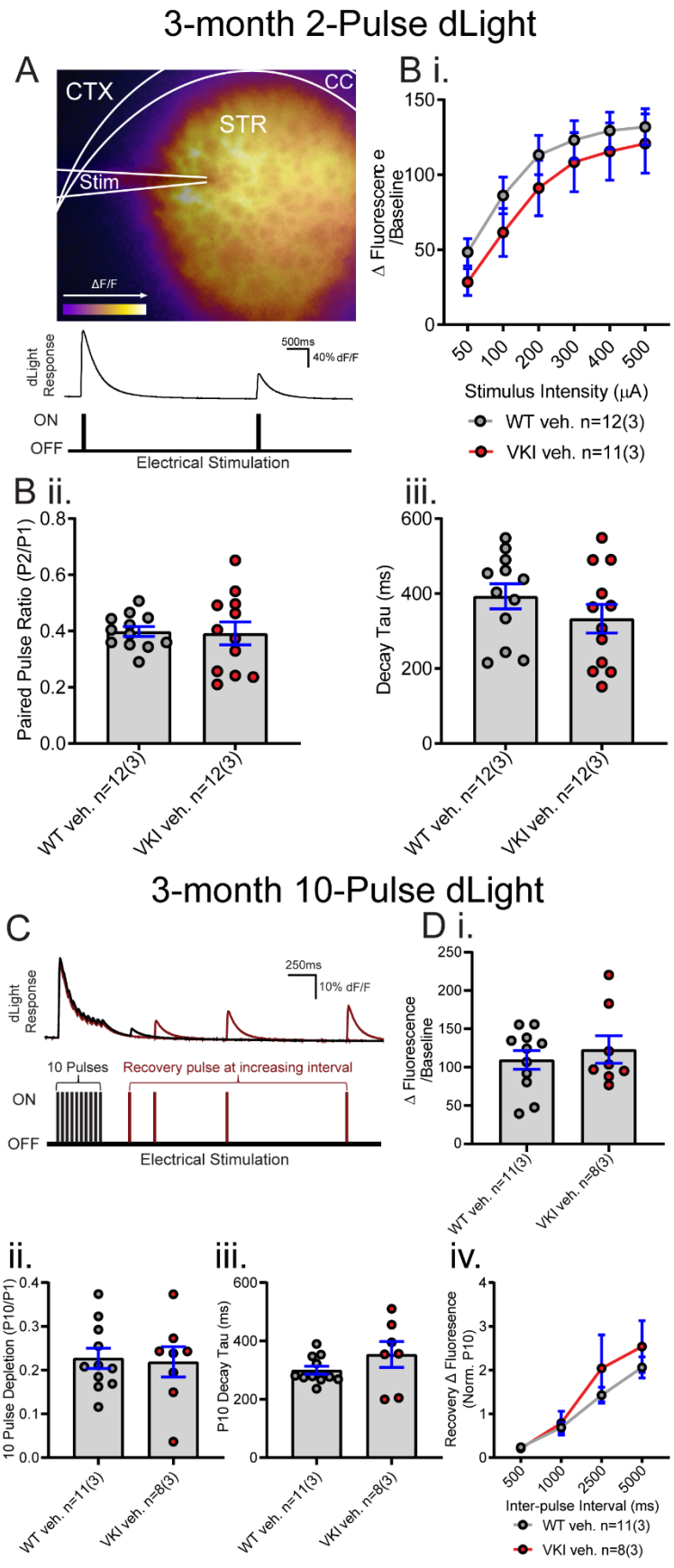

Figure 8. Electrically-evoked striatal dopamine release is not significantly different between WT and VKI mice at 3 months.

A) Upper: Visualization of change in dLight fluorescence over baseline in the dorsolateral striatum (ΔF/F) with local electrical stimulation (low to high ΔF/F represented as a gradient from purple to yellow, respectively). Boundaries of the corpus callosum (CC) separate CTX and STR in a coronal brain slice. Stimulating electrode (Stim) was placed in dorsolateral STR. Lower: Representative dLight ΔF/F trace plotted over time, in response to 2 pulses of electrical stimulation with 4s inter-pulse interval. **B** At 3 months, **i)** dLight response to increasing stimulation intensity is not significantly different in WT vs VKI striata (2-way ANOVA interaction p=0.77, genotype p=0.38). **ii.** Average paired-pulse ratio (P2:P1) is not significantly different between WT and VKI striata (Unpaired t-test p=0.87). **iii.** Average P1 decay tau of dLight responses is not significantly different between WT and VKI brain slices (Unpaired t-test p=0.25). **C** Representative trace showing dLight ΔF/F plotted over time (in black) in response to 10x10Hz pulses of electrical stimulation followed by 11th pulse at increasing intervals with each repetition of the protocol (in brown). **D** At 3 months, **i)** dorsolateral STR dLight responses to 10x10Hz pulse stimulation are not significantly different between WT and VKI mice in peak response size (Unpaired t-test p=0.53). **ii.** Ratio of P10:P1 is not significantly different between WT and VKI striatal responses (Unpaired t-test p=0.84). **iii.** P10 decay tau of dLight response is not significantly different between WT and VKI slices (Unpaired t-test p=0.19). **iv.** WT vs VKI responses following 10x10Hz pulse stimulations show no significant difference in response size following pulse train (2-way ANOVA interaction p=0.45, genotype p=0.45).

3.2 STR dopamine release evoked with paired electrical stimulation is significantly higher in 6-month VKI mice

Slice recordings of dLight in 6-month-old mice were combined with electrical stimulation, again using a pair of pulses with 4s inter-pulse interval. dLight responses were compared in slices treated with vehicle or MLi-2 for >1.5hours. At 6 months, vehicle-treated VKI slices show an increased change in fluorescence relative to baseline at lower stimulation intensities when compared to WT slices (Figure 9 A i). WT slices treated with MLi-2, compared to vehicle-treated slices, trend towards a reduction in dLight response size with increasing stimulus intensity (Figure 9 A ii). VKI dLight responses are not changed with acute MLi-2 treatment (Figure 9 A iii). At this age, there is no change to paired-pulse ratio when comparing across genotype or treatment conditions (Figure 9 B i). However, vehicle- and MLi-2-treated VKI slices show significantly higher decay taus of the 1st pulse response than in WT slices (Figure 9 B iii). Taken together, the data suggest an emergent increase in STR dopamine release as well as slower decay kinetics occurs in VKI mice at 6 months, which is not responsive to MLi-2 treatment. WT striatal dopamine release is, however, modestly reduced with MLi-2 treatment.

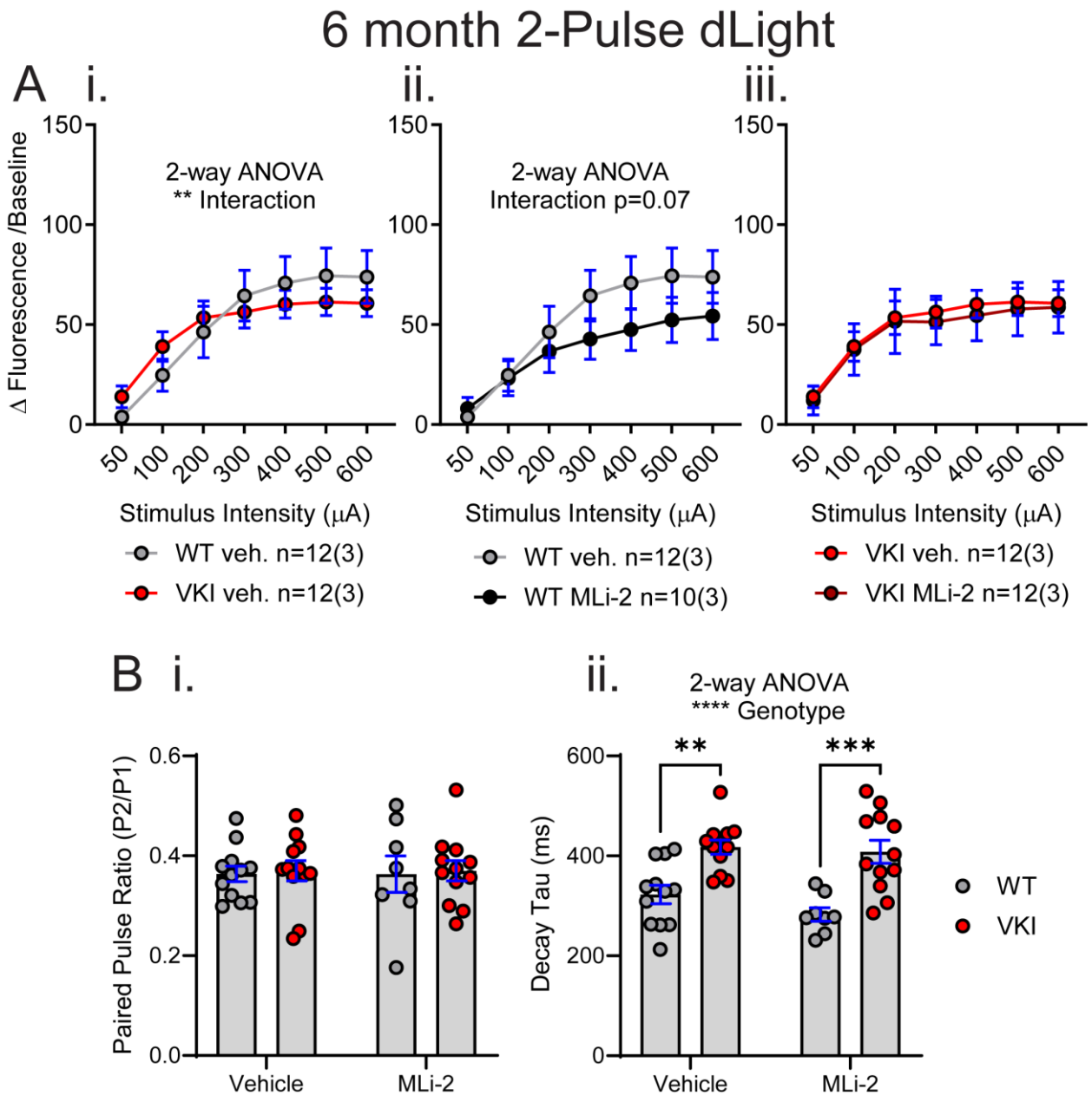

Figure 9. Dorsolateral STR dopamine release at 6 months is altered in VKI brain slices and is not responsive to acute MLi-2 treatment.

A At 6 months **i)** P1 dLight responses to increasing stimulation intensity is significantly different in WT vs VKI Δ fluorescence/baseline (2-way ANOVA interaction p=0.004, genotype p=0.88). **ii)** WT MLi-2- vs vehicle-treated brain slices trend towards significantly different P1 responses with increasing stimulation intensity (2-way ANOVA interaction p=0.07, treatment p=0.35). **iii)** VKI MLi-2 vs vehicle-treated brain slices do not show significantly different response peaks with increasing stimulation intensity (2-way ANOVA interaction p=0.98, treatment p=0.83). **B** At 6 months **i)** Ratio of P2:P1 dLight responses are not significantly different across genotype or treatment condition (2-way ANOVA interaction p>0.99, genotype p=0.78, treatment p=0.99) **ii)** P1 decay tau of dLight response are significantly increased in VKIs vs WT mice in both treatment conditions and are not responsive to MLi-2 treatment in either genotype (2-way ANOVA interaction p=0.42, genotype p<0.0001, treatment p=0.20, Holm-Šídák's multiple

(Fig 9 cont'd) comparisons test WT veh. vs WT MLi-2 p=0.65, WT veh vs. VKI veh p=0.0033, WT MLi-2 vs VKI MLi-2 p=0.0004, VKI veh. vs VKI MLi-2 p>0.99).

3.3 STR dopamine release from high frequency electrical stimulation is significantly increased in 6-month-old VKI mice and is not responsive to MLi-2 treatment

As before, a 10-pulse, 10Hz train of electrical stimulation, followed by an 11th pulse with variable inter-pulse interval was delivered to striatal brain slices expressing dLight (Figure 10). At 6 months, no difference in dLight fluorescence change, relative to baseline, is observed when comparing vehicle- and MLi-2 treated WT and VKI slices (Figure 10 A i). The 10th pulse response size relative to the initial response is significantly lower in VKI versus WT slices, indicating a greater depletion of dopamine in VKI mice (Figure 10 A ii). MLi-2 does not alter the relative size of 10th pulse responses in either genotype. There is no change in 10th pulse decay tau across genotype or treatment condition (Figure 10 A iii). Recovery from the 10-pulse stimulation is significantly faster in vehicle-treated VKI slices than WT (Figure 10 B i). No difference in recovery after 10-pulse stimulation is observed with acute treatment MLi-2 versus vehicle alone in either WT or VKI slices (Figure 10 B ii & iii). Taken together, VKI mice seem more likely to release dopamine with repeated high frequency stimulation by 6 months and demonstrate a greater capacity to recover from the more extensive release. Furthermore, striatal dopamine release is unaltered with acute MLi-2 treatment in either genotype at this age.

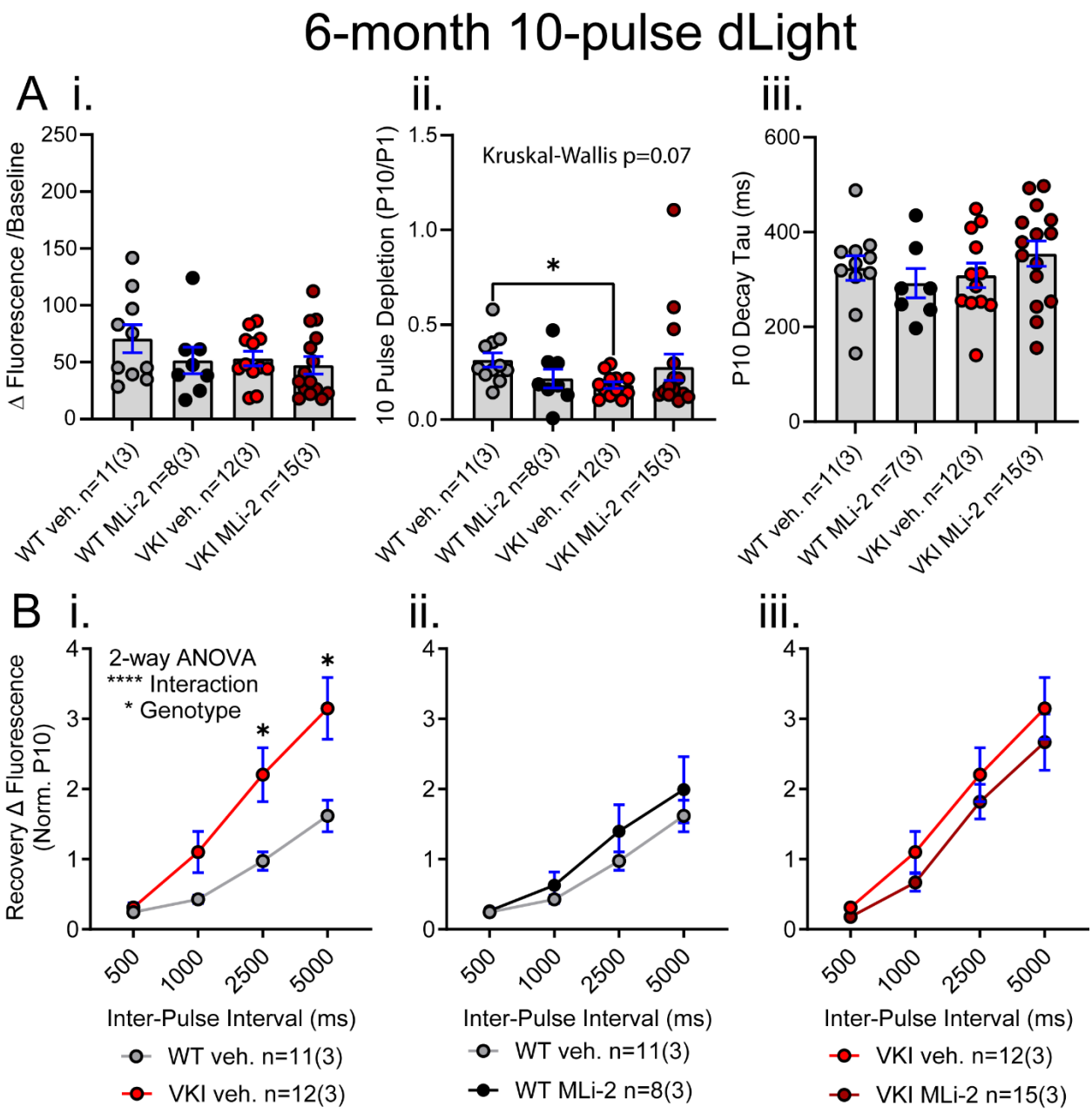

Figure 10. Striatal dopamine release is more exhaustive in VKI vs WT dorsolateral STR at 6 months and is not sensitive to acute LRRK2 kinase inhibition.

A At 6 months, **i)** dLight responses to 10x10Hz pulse stimulation are not significantly different across genotype or treatment condition in Δfluorescence/baseline measures (Kruskal-Wallis test p=0.35). **ii)** Ratio of P10:P1 is significantly lower in vehicle-treated VKI vs WT slices and are not responsive to MLi-2 treatment with either genotype (Dunn's multiple comparisons test WT veh. vs VKI veh. p=0.04, WT veh. vs WT MLi-2 p=0.40, VKI veh. vs VKI MLi-2 p>0.99). **iii)** P10 decay tau of dLight responses are not significantly different across genotype or treatment condition (1-way ANOVA p=0.92). **B** At 6 months, **i)** dLight response following 10x10Hz pulse stimulation is significantly higher in vehicle-treated VKI vs WT brain slices (2-way ANOVA interaction p<0.0001, genotype p=0.01, Holm-Šídák's multiple comparisons test WT vs VKI @ 2500ms IPI p=0.005, and @ 5000ms IPI p=0.0003). **ii)** WT responses following 10x10Hz pulse stimulation are not significantly altered by MLi-2 treatment (2-way ANOVA, interaction p=0.47, treatment p=0.30) **iii)** VKI responses following 10x10Hz pulse stimulation are not significantly different with MLi-2 treatment (2-way ANOVA, interaction p=0.80, treatment p=0.28).

Effects of VPS35 D620N mutation +/- acute LRRK2 kinase inhibition on striatal dopamine release in aged mice

3.4 STR dopamine release is reduced in aged VKI mice and is partially responsive to LRRK2 kinase inhibition

dLight recordings of responses to 2-pulse, 4s inter-pulse interval electrical stimulation was pooled from 22-27-month-old male and female mice (labeled ~25-month-old mice; Figure 11 A). Increasing stimulus intensity elicits consistently and significantly smaller dLight responses from vehicle treated VKI mice compared to WT (Figure 11 B i). While WT responses are unchanged with acute MLi-2 treatment, VKI responses show significant interaction between treatment condition and response to increasing stimulus intensities (Figure 11 B ii & iii). Furthermore, the ratio of 2^{nd} to 1^{st} pulse is not different by genotype or treatment condition (Figure 11 C). 1^{st} pulse decay tau is also not different between genotype or treatment condition (Figure 11 D). As with iGluSnFR data, male and female VKI dLight responses may differentially respond to both electrical stimulation and MLi-2 treatment but require further experimentation (Figures S7 & S8). In conclusion, dorsolateral STR dopamine release in aged VKI mice is lower than in WT mice and may be partially responsive to acute treatment with LRRK2 kinase inhibitor, MLi-2.

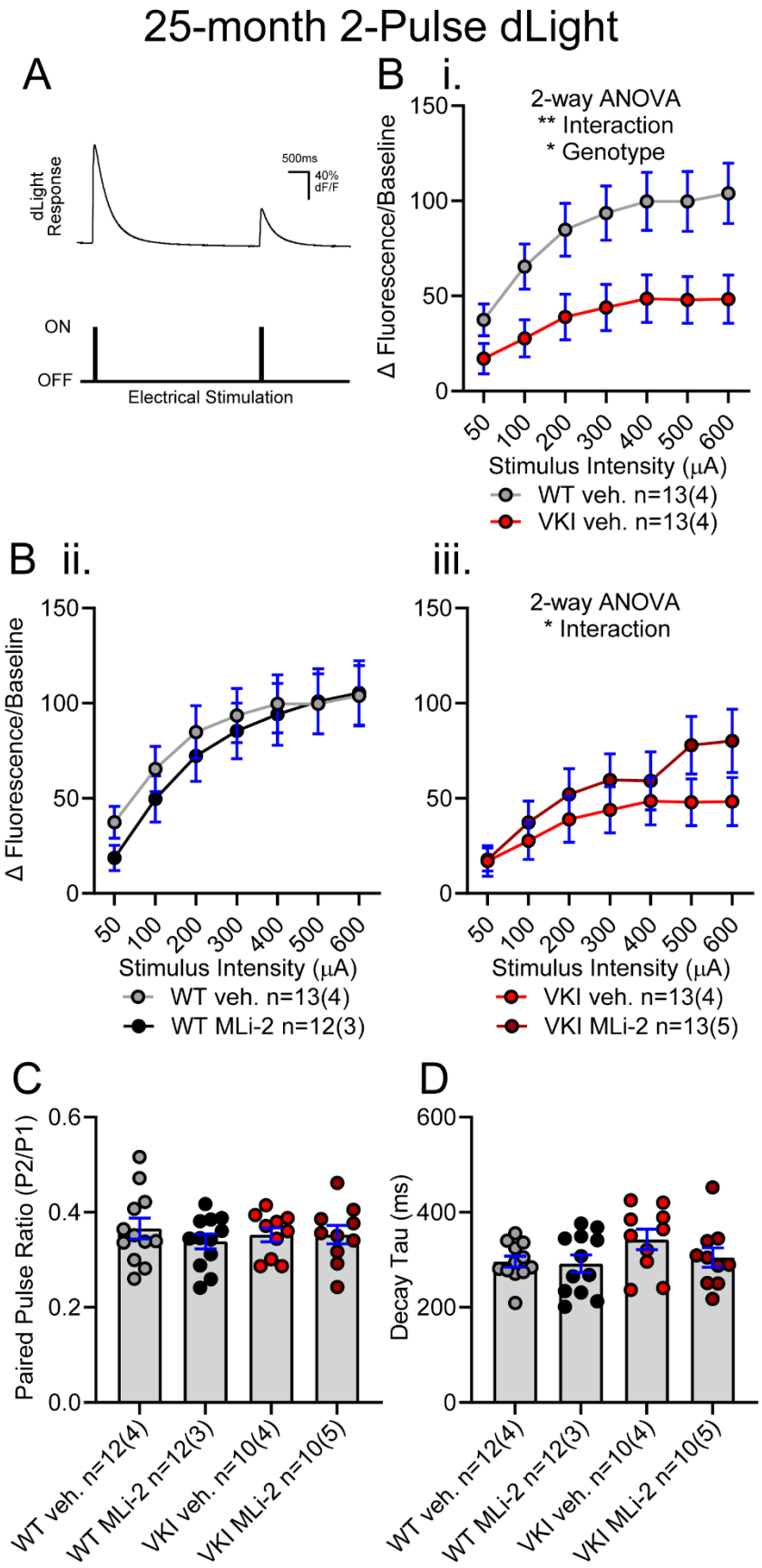

Figure 11. Dopamine release is reduced in aged VKI striata and is modestly altered with LRRK2 kinase inhibition.

A) Representative dLight trace showing Δfluorescence/baseline plotted over time, in response to 2x0.2ms pulses with 4s inter-pulse interval. **B** At ~25 months, **i)** P1 peak with increasing stimulation intensity is significantly lower in vehicle-treated VKI brain slices vs WT (2-way ANOVA interaction p=0.0014, genotype p=0.015). **ii)** WT P1 peak with increasing stimulation intensity is not significantly altered with MLi-2 treatment (2-way ANOVA interaction p=0.27, treatment p=0.67). **iii)** VKI P1 peak with increasing stimulation intensity is significantly altered with MLi-2 treatment (2-way ANOVA interaction p=0.04, treatment p=0.34). **C)** Ratio of P2:P1 peaks are not significantly different across genotype or treatment condition (1-way ANOVA p=0.76). **D)** P1 decay tau is not significantly different across genotype or treatment condition (1-way ANOVA p=0.20)

Chapter 4: Discussion

In 2011, two reports of heterozygous carriers of VPS35 D620N first linked the mutation to PD[68,69]. Since then, progress has been made in better understanding effects of the D620N on VPS35 function. However, how this mutation leads to PD-like changes to neurotransmission has not been well characterized. Thus, dopamine and glutamate neurotransmission was assessed in the disease-relevant dorsolateral striatal brain region of VKI mice throughout their lifetime.

Glutamate transmission is altered in the dorsolateral STR of VKI mice

Previously, the Milnerwood lab showed that glutamate transmission is increased in primary cortical cultures from VKI mice[3]. The lab also reported that in a similar model of genetic PD caused by the G2019S mutation in LRRK2, elevations to striatal neurotransmission are age-dependent[18]. To address whether A) glutamate transmission is altered in the striatum of VKI mice and B) whether any alterations observed are age-dependent; spontaneous and evoked glutamatergic transmission was measured in *ex vivo* brain slice preparations from WT and VKI mice. Relative to WT mice, multiple measures of striatal glutamate transmission are indeed increased in young adult VKI mice, and this precedes the eventual loss of glutamate transmission in old age.

Spontaneous striatal glutamatergic transmission is increased in young adult VKI mice

Whole-cell patch-clamp electrophysiology was employed to first assess changes to spontaneous glutamatergic transmission onto MSNs in the dorsolateral STR. Although sEPSCs are not different between 1-month-old WT and VKI neurons, an increase in the number of higher amplitude sEPSCs in VKIs emerges at 3 months and is sustained at 6 months. An increase in sEPSC inter-event

interval also emerges in VKIs, but not until 6 months. Inter-event interval is inversely proportional to the frequency of spontaneous transmission events. Changes to spontaneous event frequency can be interpreted as alterations to the probability of presynaptic glutamate release at a similar number of synapses[131,132], or as a similar probability of release at altered number of synapses[133,134]. Similarly, altered amplitude is canonically interpreted as changes to postsynaptic receptor availability according to quantal theory for glutamate transmission[135]. An increase in sEPSC amplitude could also reflect more glutamate being packaged into a single vesicle and released[136], or more vesicles containing glutamate being released in one event (multi-vesicular release)[137,138].

As VPS35 is involved in the regulation of both presynaptic synaptic vesicle cycling[81] and postsynaptic receptor membrane trafficking[2,3,16], it is possible pre- and post-synaptic compartments are affected by the D620N mutation in the striatum of young adult mice. In a previous study of glutamatergic transmission in VKI primary cortical neurons, we found increased glutamatergic activity independent of changes to synapse density[3]. PSD95 and synapsin-1 co-localization, which was used to measure the number of active synapses, is similar in VKI dorsolateral STR at 3 months[4]. Thus, we conclude that changes to sEPSC inter-event interval/frequency in VKI MSNs are likely due to the increased probability of presynaptic release and not synapse number.

Although there is less evidence to suggest VPS35 D620N can modulate packaging of vesicular glutamate, it cannot be ruled out that VGLUT1 and 2 (which are expressed in cortical and thalamic afferents to the STR, respectively) could be recycled in a retromer-mediated fashion. For instance, in *C. elegans*, endosomal recycling of the nematode ortholog V-GLU2 implicates another retromer subunit SNX-1[139]. VGLUT1 cluster intensity is significantly reduced in homozygous, but not heterozygous primary cortical neurons from VKI mice[3]. An absence of

VGLUT1 effects in heterozygous neurons may be a result of the physiological age of the cortical neurons. To better correlate with time points at which we observe increased glutamate release, assessment of VGLUT1 and VGLUT2 levels in VKI striata from 6-month-old mice would prove useful.

In postsynaptic compartments, VPS35 D620N may affect neurotransmitter receptor expression and localization. AMPAR subunit GluA1 shows increased surface expression in VKI primary cortical neuron cultures[3]. Furthermore, VPS35 co-IPs with GluA1, NMDAR subunit GluN1, and dopamine receptor D2R (*ibid*). VPS35 is also required for the delivery of β2-adrenergic receptors (β2ARs) to dendritic shafts from recycling endosomes[16]. Fluorescence recovery after photobleaching (FRAP) experiments in primary cortical neurons show a reduction in fluorescent recovery with overexpression of WT VPS35, which is not observed when overexpressing VPS35 D620N[1]. This could mean that VPS35 stabilizes AMPARs at postsynaptic membranes or reduces the rate of AMPAR delivery to the dendritic surface. It may also mean that AMPARs are trafficked to dendrites similar to β2ARs; ie. retromer mediates the delivery of AMPARs to the dendritic shaft or spine but other mechanisms govern the diffusion of AMPARs to postsynaptic densities. While VPS35 D620N overexpression does not alter the recovery after photobleaching[1], endogenous levels of VPS35 D620N expression could increase in the plasma membrane delivery of AMPAR by mutant VPS35 and may underlie the increased surface expression in VKI primary cortical neurons[3]. Further assessment of MSN GluA1 surface expression, presynaptic VGlut-1 and -2 expression, and characterization of presynaptic vesicle morphology, number, and density would directly address pre- and post-synaptic changes underlying sEPSC differences in VKI MSNs. Regardless, our sEPSC recordings suggest

spontaneous glutamate activity in the dorsolateral striata of VKI mice begins to diverge from WT measures at 3 months of age and is clearly increased by 6 months.

Corticostriatal glutamatergic transmission is increased in young adult VKI mice

Since we had previously observed that cortical glutamatergic transmission in altered *in vitro* in VKIs[3], we next investigated glutamatergic transmission onto MSNs from cortical afferents. ChR2 expression in M1/S1 afferents was used to evoke corticostriatal glutamate transmission onto dorsolateral STR MSNs. VKI MSNs show a trend towards higher amplitude ChR2-PSCs at 3 months which become significant by 6 months. Modest changes to the paired-pulse ratio, indicating altered probability of corticostriatal glutamate release also appear by 6 months in VKIs.

Similarly, by 6 months, we find significant increases in AMPAR- and NMDAR- mediated currents in VKI MSNs, but not in the ratio of AMPA:NMDA. This suggests that both AMPAR- and NMDAR-mediated transmission is increased to the same extent. This could be explained by increased postsynaptic surface expression of both AMPAR and NMDAR as we have shown that that cultured VKI neurons exhibit increased GluA1 surface expression, and that VPS35 D620N also binds GluN1 subunits of NMDARs[3]. However, the more parsimonious (and generally accepted) interpretation is that more glutamate is released upstream from presynaptic terminals, leading to a global increase in the activation of all postsynaptic glutamate receptors.

Combined with our observations of sEPSC changes in VKIs, we see evidence of presynaptic glutamate release increase in both spontaneous and evoked measures of MSN glutamate transmission by 6 months. As the mechanisms governing evoked synaptic transmission may differ from spontaneous glutamate transmission in terms of synaptic machinery and vesicle

dynamics[140–142], more work is required to understand the specific role of VPS35 in both forms of glutamatergic neurotransmission.

Striatal glutamate release is increased in young adult VKI mice

With multiple lines of evidence suggesting that presynaptic glutamate release is altered by 6 months in VKI mice, we next directly assessed presynaptic release using intensity-based glutamate-sensing fluorescent reporter, iGluSnFR. This reporter was directly expressed in the striatum of WT and VKI mice and fluorescent changes in response to local electrical stimulation were compared.

As early as 3 months, iGluSnFR recordings reveal alterations to glutamate release in VKIs. Initial release probability may be lower in VKIs, as we see smaller-amplitude iGluSnFR fluorescence changes than in WT mice. Interpretation of amplitude changes as being directly related to the amount of glutamate released is confounded by viral expression levels of iGluSnFR, LED intensity, and electrical stimulation intensity. However, amplitude changes in 3-month-old VKIs are also observed in spontaneous and ChR2-evoked patch-clamp recordings, which suggests that initial release capacity may be higher in iGluSnFR experiments as well. To overcome the limitations of absolute amplitude analysis, we also quantified the likelihood of glutamate release and capacity for re-release using trains of stimulation by normalizing iGluSnFR responses to the first response.

At 3 months, glutamate release is increased in VKIs early in the stimulation train and normalizes to WT levels upon subsequent stimulation. By 6 months, VKIs consistently show a greater capacity to release glutamate throughout the pulse train. Reflecting our observations of

ChR2-evoked responses, iGluSnFR data suggest striatal glutamate release remains elevated at 6 months in VKIs in contrast to WT release, which seems to reduce between 3 and 6 months.

We also measured iGluSnFR responsiveness following pulse train stimulation to assess the capacity to recovery following extensive glutamate release. At 3 months, VKI responses are smaller following pulse train stimulation, indicating a reduction in the rate and extent of recovery after pulse train stimulation. This contrasts a faster rate of recovery observed in 6-month-old VKI mice relative to WT. Recovery rate could reflect the capacity to replenish vesicular stores of readily releasable glutamate, perhaps through glutamate repackaging into recycled vesicles, generation of new glutamate-containing vesicles, or mobilization of existing vesicles to the readily-releasable pool[143–146]. Therefore, a reduced recovery rate in 3-month-old VKIs may reflect impaired vesicular recycling or mobilization of glutamate-containing vesicles to the readily-releasable pool and may reflect compensation against the observed increased release probability with repeated stimulation. A failure of compensatory action may be reflected in the increased rate of recovery in 6-month-old VKIs, and lead to the observed increase in glutamate release in mutants. Altogether, striatal glutamate release in VKIs diverges from WT levels by 6 months.

Clearance of glutamate is transiently altered in young adult VKI mice

Since the rate of clearance of glutamate mitigates against glutamate-mediated excitotoxicity[147], we next investigated whether glutamate clearance is altered in VKI mice. In iGluSnFR experiments, the rate of clearance was measured by the speed of the decay of the last pulse of the 10-pulse train stimulation. We found that the rate of decay of the iGluSnFR response is significantly faster in 3-month-old VKIs but normalizes to WT levels beyond 6 months. This transient increase in the speed of glutamatergic transmission decay is also observed in the decay kinetics of sEPSCs in VKI

MSNs. Taken together, these observations reflect an increase in the rate of glutamate clearance from VKI striatal synapses at 3 months, which normalizes to wild-type levels with age. This may reflect initial compensatory changes against elevated glutamate release in VKI striata but is reduced or lost with age. Further study into mechanisms of glutamate clearance, such as astrocytic clearance through excitatory amino acid transporters (EAATs)[148], would shed light on the capacity of the striatal network to navigate the potentially excitotoxic changes to glutamate transmission in VKI brains.

Subunit composition of AMPA receptors is not altered in young adult VKIs

Apart from glutamate clearance, changes to sEPSC decay kinetics may also reflect an alteration to the subunit composition of postsynaptic AMPAR receptors[149]. Thus, AMPA rectification, which can be used to infer subunit composition, was compared between WT and VKI MSNs[150,151]. In recordings of corticostriatal glutamatergic transmission, we see no change to the rectification index of VKI neurons at 3 or 6 months, indicating a similar subunit composition of AMPARs to WT neurons, at least in young adulthood. Therefore, we see no evidence of a change in AMPAR subunit composition in the striatum, despite previous observations of an increase in GluA1 expression in primary cortical neuron from VKI mice[3]. It may be that VKI striata contain more AMPARs that are positive for GluA1 without an alteration to the composition of individual AMPARs themselves. Another explanation is that the distribution of GluA1-containing AMPARs is altered, which would explain changes to VKI sEPSC decay at 3 months, independent of changes to subunit composition[152]. Further characterization of the expression and distribution of GluA1 in VKI striata from 3- to 6-month-old mice would clarify the degree of post-synaptic alterations to AMPAR composition and localization (if any).

Passive membrane properties are transiently altered in young adult VKI mice

Since passive membrane properties govern the ability of neuronal membranes to integrate synaptic inputs both temporally and spatially[153,154], we characterized membrane capacitance, membrane resistance, and membrane tau in 1- to 6-month-old MSNs. VKI MSNs show small, transient differences in passive membrane properties from 1-6 months. MSN membrane tau is smaller in 1-month-old VKIs but normalizes to WT levels by 3 months old. Since membrane tau is a product of membrane resistance and conductance, it is a measure of how quickly synaptic inputs can integrate signals[155]. A smaller value indicates faster decay of membrane charge, so VKI MSNs at 1 month may be less likely to fire in response to asynchronous input. The difference, though significant, is small. Perhaps other cell types which are intrinsically more likely to fire could be affected more significantly (ie. cortical cells). By 3 months, VKI MSNs show modestly, but not significantly increased membrane capacitance. This trend towards a significant increase is maintained in 6-month-old VKI MSNs, suggesting that the MSNs of VKI mice have a slightly higher capacity to hold change in their membranes. Membrane resistance is also significantly reduced by 6 months in VKIs and may result from a larger soma, larger-diameter processes, or a greater density of open channels[153,154].

The transient and subtle nature of passive membrane property changes could reflect slight differences in the development or maintenance of neuronal membranes at soma and/or neurites in VKI striata. While dendritic arborization of primary cortical neurons are not different in VKI cultures at DIV 21[3], by 13 months, VKI mice show markers of axonal damage in multiple brain regions[122]. Therefore, the slight changes to passive membrane properties of striatal MSNs we observe in 1- to 6-month-old VKIs could reflect an intermediate stage that precedes neurodegeneration. Characterization of membrane lipid profile and morphology of VKI MSNs

during this stage would provide further insight into cellular changes underlying neurodegeneration. More work also is required to parse out somatic, dendritic, and axonal membrane properties to elucidate the network consequences of potential changes to VKI MSNs, as membrane properties intrinsically differ between these neuronal compartments[153].

Altogether, VKI MSNs show small changes in passive membrane properties by 6 months of age, which potentially compensate for the reduced membrane tau of 1-month-old VKI MSNs. Given that VKI MSNs show reduced membrane tau at 1 month, but not at 3 or 6 months, it may be that VKI MSNs initially show a reduced capacity to integrate synaptic inputs, which is compensated for by 3-6 months through changes to membrane area and/or composition.

Striatal glutamate release is reduced in aged VKI mice

The progressive emergence of increased glutamate release in the striatum of young adult VKI mice prompted further investigation into striatal glutamate release in aged mice. We recorded iGluSnFR responses in ~25-old-month as it is generally accepted as "old age" and likely corresponds to 60-70 years in humans[156]. Since mean age of PD onset is 52 for VPS35 D620N-linked cases[68,69], it would also correspond to a pseudo-Parkinsonian state in VKI mice. N.B. Unpublished rotarod experiments by the Milnerwood lab show no change in motor performance in 3- or 18 month-old VKI mice but behavioural characterization has not been performed beyond this age.

By 25 months, iGluSnFR responses in VKI striata are reduced in average amplitude and show significantly greater facilitation than responses in WT striata. The rate of recovery following the train of stimulation is also reduced, with no change to the decay of the iGluSnFR pulse train response. Taken together, glutamate release in aged mice is impaired in VKI striata, as is the capacity to recover from extensive release.

Whether functional loss of glutamatergic neurotransmission is related to glutamatergic neurodegeneration remains to be seen, but widespread neurite damage and increased levels of markers of neurodegeneration are both observed in VKI mice as early as 13 months[122]. Therefore, loss of striatal glutamate transmission in aged VKIs may result from a number of mechanisms: loss of glutamatergic innervation, a reduction in the excitatory neuromodulation by glutamatergic axons in the striatum[50,157–160], a reduction in the stores of glutamate at presynaptic terminals, and/or changes to the synaptic machinery at terminals.

Other caveats and limitations

Spontaneous EPSCs represent miniature EPSCs in MSNs

sEPSCs reflect both spontaneous, action potential-independent and -dependent release of glutamate. As MSNs have a very low probability of firing in brain slice recordings[161,162], and as we recorded with cesium-based internal solution to prevent postsynaptic action potential generation, we expect that sEPSCs are not contaminated by postsynaptic action potentials. The Milnerwood lab previously demonstrated that MSN sEPSC frequency and amplitude are not altered by tetrodotoxin application (voltage-gated sodium channel blocker) which blocks presynaptic action potentials[163]. Therefore, we conclude that sEPSC recordings in MSNs are equivalent to action potential-independent miniature EPSCs (mEPSCs) that occur as a result of quantal release of glutamate onto recorded MSN synapses.

ChR2 stimulation is supra-physiological

One limitation of our ChR2 experiments is that the evoked release is likely supra-physiological. The low paired-pulse ratio of 0.2-0.3 observed in both WT and VKI MSNs indicates a very high level of initial release, and subsequently low release on the second pulse; this ratio is much lower

than that typical of striatal MSN facilitation produced by local electrical stimulation (where paired-pulse ratios range from 0.9-1.5)[164–166]. Lower paired-pulse ratios have been previously reported for ChR2-induced glutamate release onto MSNs[167], and is likely due to depolarisation of a large number of corticostriatal terminals by ChR2. In addition, the influx of Ca^{2+} through the cation non-selective ChR2 channel could maximize the release probability at each terminal. The efficiency of ChR2-activated glutamate release depends on several factors including: the site and intensity of light stimulation, AAV serotype and titre[168], efficiency and volume of injection[169], cortical region of injection, mouse strain[170], etc. Nonetheless, stimulation with ChR2 reveals a progressive increase in glutamatergic transmission in young adult VKIs, and this pattern of emergence is also found in several other measures of glutamatergic transmission.

Electrical, but not ChR2, stimulation reveals significant changes to presynaptic release in 3-month-old VKIs

At 3 months, iGluSnFR responses show evidence of alterations to glutamate release in VKI striata, while ChR2-evoked postsynaptic current amplitude only modestly increases in VKI MSNs. It may be that the subtlety of the phenotype is masked by the intense activation of corticostriatal glutamate release with ChR2. It could also be that initial increase in release probability manifests as changes to the amplitude of ChR2-PSCs. Another possibility is that the local electrical stimulation used for iGluSnFR recordings activates a number of presynaptic inputs within the striatum that contribute to glutamate release differentially to monosynaptic glutamate release from cortical afferents[64].

An increase in corticostriatal glutamate transmission may only represent a portion of the changes to glutamate transmission observed with iGluSnFR assessment. Other sources of glutamate include thalamic input into the striatum[165,167,171,172] and potential co-release from dopamine terminals, however the latter contribution is likely small in the dorsolateral

striatum[173,174]. Thus, the more pronounced phenotype observed using electrical stimulation versus ChR2 in 3-month-old VKIs may be attributed to an increase in glutamatergic striatal transmission beyond what we observe when activating corticostriatal circuits in isolation.

Electrical stimulation induces local polysynaptic activation in the STR

The STR comprises a complex network of input neurons and inhibitory interneurons that have capacity to locally regulate glutamate (and dopamine release)[64]. Therefore, electrical stimulation of the dorsolateral STR could activate a polysynaptic network that contributes to glutamate release increases in VKI striata *ex vivo* but may not necessarily reflect physiological glutamate release probability changes. Moreover, a number of these neuromodulators can alter glutamate release including acetylcholine, adenosine, dynorphin, dopamine, serotonin, and endocannabinoids[157–160]. Repeated electrical stimulation may recruit activity-dependent enhancement of glutamate release in young adult VKIs, and the loss of this neuromodulation could underpin the reduction in glutamate transmission in aged VKIs.

Changes to glutamatergic transmission onto MSNs may be cell-type specific

MSNs can be divided into dopamine receptor D1- and D2-expressing subpopulations. Here, we did not differentiate between the two subpopulations, thus we cannot elucidate cell-type specific differences in passive membrane properties of VKI MSNs, nor differences in spontaneous or evoked glutamatergic transmission onto MSNs. Further study of D1- and D2- subtypes in VKI animals (throughout adulthood) would allow for a greater understanding of the functional consequences of our observed changes. As D1- and D2-subpopulations play opposing, but complementary roles in regulating basal ganglia output, dysregulation of these populations could to contribute to the development of PD symptoms[175–179].

Changes to MSN neurotransmission may be sex-dependent

Reviews of clinical research suggest the onset of Parkinson's disease is earlier and greater in men versus women[180,181]. It also seems that women progress more rapidly once diagnosed than men (*ibid*). We pooled both male and female mice for the characterization of striatal glutamate release 25-month-old animals and differentiating the data by sex may show more pronounced reductions in glutamate release in female versus male VKIs. However, our animal numbers are quite limited, and we lack statistical power, especially in males, to analyze sex-based differences. Several complications arise from working with mice older than 18 months, including comorbidities compromising the health of the mice and age-related, limited animal availability. As such, more experiments assaying glutamate release in 22- to 27-month-old mice will be required to determine whether changes to glutamate release in aged VKIs is dependent on sex. Moreover, data from young mice are limited to observations in male mice, and these experiments will also need to be repeated in female mice as several recent reports indicate striatal function, mRNA transcription, and addictive behaviour differs between male and female rodents[182–185].

iGluSnFR recordings in aged mice were obtained in the presence of Captisol®

Glutamate release in aged mice were compared between vehicle-treated WT and VKI brain slices. These slices, treated with the vehicle, Captisol®, served as a control for LRRK2 kinase inhibition experiments (discussed later). As such the presence of Captisol® is unique to the ~25-month-old data set and may skew measures of glutamate release. To characterize the effects of Captisol® iGluSnFR responses were compared in 3-month-old WT and VKI striata treated with vehicle or artificial cerebrospinal fluid (aCSF) alone.

Absolute iGluSnFR fluorescence changes in response to electrical stimulation are significantly higher in both genotypes when treated with vehicle instead of aCSF alone. iGluSnFR

responses relative to the initial peak also shows glutamate release probability is lower in aCSF recordings than in the presence of Captisol®. Decay tau of the iGluSnFR response train is dramatically increased with vehicle treatment versus aCSF alone. Altogether, the presence of Captisol® may augment the release of glutamate and increase the time it takes to clear released glutamate. These differences allude to an effect of the vehicle, Captisol®, on glutamate transmission. It would be prudent to repeat these experiments within, instead of across, animals to account for variables including differences in viral expression of iGluSnFR, breeding and housing conditions between litters, and slice preparation differences across experimental days. If in 25-month-old mice, vehicle treatment increases glutamate release as well, it would imply that the reduction in glutamate release observed in VKIs may be even more robust in aCSF alone. Since Captisol® effects on iGluSnFR responses do not seem to be different between genotypes, the reduction in VKI glutamate release compared to WT release at 25 months likely would be present in the absence of vehicle.

Conclusion

We repeatedly observe that striatal glutamate transmission is elevated in young adult VKI mice and is largely driven by increased presynaptic glutamate release. While robustly elevated at 6 months, striatal glutamate release in VKIs is paradoxically reduced below WT levels by ~25 months. Multiple lines of evidence point to compensatory changes that could function to reduce glutamate transmission in VKI striata at 3 months old, including changes to MSN passive membrane properties, faster decay of glutamate transients, and a reduction in the recovery of releasable glutamate following extensive stimulation. However, these potentially compensatory changes to decay and recovery seem to be lost by 6 months. In fact, recovery following extensive

glutamate release in VKI striata from 6-month-old mice show an increased rate of recovery, which could positively feed back to increase striatal glutamate release further.

The mechanisms by which VPS35 D620N mutations may contribute to loss of synaptic integrity are discussed in detail at the end of this chapter. But to summarize, subtle changes in glutamatergic transmission observed between 1-6 months could indicate a progressive loss of compensatory mechanisms which reduce glutamatergic input into MSNs, leaving neurons vulnerable to damage incurred from the increased synaptic burden. This may also lead to increased glutamate-mediated excitotoxicity, degrading the integrity of striatal synapses further, and contribute to the eventually loss of striatal glutamate transmission observed in 25-month-old VKIs. In short, early elevations to striatal glutamate transmission in VKI mice may contribute to the eventual loss of striatal glutamate release in old age.

Dopamine transmission is altered in the dorsolateral STR of VKI mice

Striatal dopamine release is increased in young adult VKI mice

Elevated striatal neurotransmission in 3-month-old VKIs is not limited to the glutamatergic system. Previously, fast-scan cyclic voltammetry (FSCV) experiments in 3-month-old VKI and WT mice revealed that dopamine release in the dorsolateral STR is increased in heterozygous and homozygous mice alongside a reduction in DAT expression in striatal tissue[4]. As FSCV offers low temporal (10Hz data sampling) and spatial resolution (limited by the size of the carbon fiber electrode surface area), we opted to use the fluorescent reporter, dLight1.3b to assess dopamine release across the entire dorsolateral STR at 20X the temporal resolution.

First, 2 pulses of electrical stimulation with 4s inter-pulse interval were delivered every 2 minutes with increasing stimulus intensity over each round of stimulation. This protocol replicates previous inter-pulse and inter-stimulus intervals used for FSCV[4,18]. dLight responses at 3 months are not different between vehicle-treated WT and VKI mice in amplitude nor the capacity for secondary release. N.B. Our PPR of ~0.4 is similar to PPRs derived from voltametric recordings, which also show high variability and no difference between VKI and WT release at 3 months[4].

We also applied a more exhaustive 10-pulse train stimulation (as was used in iGluSnFR experiments) to assess initial response size, the extent of dopamine depletion over the stimulation train, and the rate of recovery following the train. Here too, there is no difference between vehicle-treated WT and VKI dLight responses at 3 months in any measure of dopamine release. Altogether, VKI mice do not differ from WT mice at 3 months when comparing dopamine release in the dorsolateral STR by dLight.

In contrast, at 6 months, we see a significant increase in STR dopamine release in VKI compared to WT vehicle-treated striatal brain slices. 2-pulse stimulation experiments show dopamine release in VKIs is increased at low stimulation intensities compared to WT mice without an alteration to the capacity for secondary release. Again, we tested release capacity using the 10-pulse stimulation protocol in VKI and WT mice aged 6 months. Although the size of the initial stimulus is not different, by the end of the pulse train, VKI mice show far greater depletion of dopamine stores than WT mice. Recovery from the pulse train, assessed using additional stimuli following the train, is significantly faster in VKI mice.

This suggests that the capacity for both release and recovery of released dopamine at striatal synapses is increased by 6 months in VKI mice. For one, young adult VKI mice may have

increased vesicular dopamine packaging by VMATs. In fact, levels of VMAT2 are increased in the STR of young VKI mice[4]. Young VKI mice also show increased responsiveness to D2R agonism (*ibid*). This, combined with the fact that VPS35 has been shown to co-IP with D2R[3], suggests that VPS35 directly modulates presynaptic activity in dopaminergic terminals. Other changes could explain increased release at glutamatergic and dopaminergic terminals, including alterations synaptic vesicle cycle and/or machinery (as discussed earlier). Altogether, VKI mice show increased dopamine release and replenishment of dopamine stores by 6 months old, likely through changes at presynaptic terminals.

Striatal dopamine release is reduced in aged VKI mice

As PD is characterized by a reduction in striatal dopamine release, we were especially curious about striatal dopamine in release in aged VKI mice. We repeated 2-pulse stimulation experiments and compared resulting dLight response to increasing stimulus intensity, and measured capacity for secondary release. In aged mice, we observe a drastic reduction in the dLight response size to 2-pulse stimulation with increasing stimulus intensity in vehicle-treated VKI versus WT mice. It seems that by ~25 months, VKI striata are consistently less capable of releasing dopamine, regardless of the intensity of the stimulation. There was no change to the capacity for secondary release as measured by the ratio of the second to first response amplitude, suggesting mechanisms governing release at 4 second inter-pulse intervals are not different in VKI mice. Since these data pool measurements from male and female mice, it may also be that there are sex-specific changes to dopamine release in old animals with and without VPS35 D620N mutations. As previously discussed in the context of glutamate release assays, a larger sample number is required to address potential sex differences in dLight recordings of dopamine release. Together, striatal dopamine

release is consistently reduced in aged VKI mice and this contrasts earlier elevations in dopamine release in young adult VKI mice.

Clearance of striatal dopamine is slowed in young adult VKI mice

The decay of the dLight response, which would be dependent on DAT-mediated clearance of extracellular dopamine, is similar between vehicle-treated WT and VKI brain slices at 3 months, regardless of whether the stimulation was delivered in pairs or in a train. By 6 months, the decay of the initial response during 2-pulse stimulation is significantly slower in VKI mice, suggesting an impairment in the clearance of individual dopamine release events. During 10-pulse stimulation protocols, the decay of the final dLight response of the train is not significantly different between VKI and WT mice, which may be due to a saturation of DAT-mediated clearance in both genotypes. Moreover, decay of dLight responses at 25 months is not significantly different in VKI and WT striata. It may be that the reduction in dopamine release in aged mice also reduces the clearance load on DAT.

It was previously been shown that 3-month-old VKI mice have reduced STR expression of DAT and slower decay of FSCV transients[4]. VPS35 D620N transgenic C.*elegans* worms show reduced recycling of DAT from endosomes to the plasma membrane, reducing DAT surface expression levels[186]. To determine whether DAT function is itself altered, dLight responses from brain slices could be recorded in the presence of the selective DAT inhibitor, GBR-12909, and its effects in VKIs relative to that in WT mice would shed light on the contribution of acute DAT activity to extracellular dopamine clearance. In summary, clearance of dopamine, likely through DAT, is robustly reduced in 6-month-old VKI striata, but this impairment may be relieved in old age as dopamine release itself is reduced in VKIs.

Other caveats and limitations

FSCV, but not dLight, recordings show increased dopamine release in 3-month-old VKIs

While we do not observe differences in striatal dopamine release at 3 months between VKI and WT dLight responses, FSCV recordings of VKIs at the same age do show a nearly two-fold increase in dopamine release compared to WT mice[4]. The differences in observations may be dependent on technical differences between fast-scan cyclic voltammetry and dLight recordings, which have their unique limitations.

For instance, because dopamine release is measured via dopamine oxidation on the carbon fiber electrodes, both spatial and temporal resolution are limited to the physical properties of the electrode's detection area. A triangular waveform is applied to the electrode which causes a redox reaction with nearby dopamine and induces a shift in the current measured from the electrode across the waveform[187]. Although this waveform is only 10ms long, repeating it beyond 10Hz result in adsorption of dopamine onto the carbon fiber and a reduction in the detected current over time[188]. Moreover, fast-scan cyclic voltammetry can only detect extracellular dopamine released directly onto the electrode, which limits the spatial resolution of this technique. A larger peak in FSCV may actually equate to a larger area of extracellular dopamine being released, which would increase the size of the pool of dopamine available to be detected by the electrode[189]. In other words, peaks in FSCV detect how much dopamine is in contact with electrode. It would not be able to distinguish between a low concentration of dopamine released over a larger area from a high concentration localized to a smaller area, if the same number of dopamine molecules were ultimately contacting the electrode.

With dLight imaging, we can achieve a 20-fold increase in the temporal resolution and sample areas an order of magnitude larger, as the expression of dlight depends on the area and efficiency of the viral injection. dLight imaging, however, is limited in its current form when compared to FSCV, as only relative, but not initial, dopamine release can be quantified using this technique. This could be overcome by normalizing responses to known concentrations of dopamine applied to the dLight expression area using a microinjection system, akin to what is done to determine the concentration of released dopamine in FSCV. Still, multiple stimulations can allow us to quantify responses relative to the initial response and allow us to quantify the dynamics of dopamine release with repeated stimulation.

Given these technical differences, it may be that at 3 months, the spread of dopamine release in VKIs is what is altered. Dopamine may either more rapidly released, or diffuse across a larger area of the STR in VKIs, and this is supported by the observation of reduced DAT-mediated clearance[4]. Diffusion of dopamine may contribute to the increased dopamine release and slowing of decay kinetics (*ibid*) when measured using the smaller carbon fiber electrode recording area in FSCV experiments, but would not affect peaks of dLight recordings. Further analysis of the spread of the change in dLight fluorescence over time would address whether diffusion is itself altered in VKIs.

It could also be that dLight responses are saturated at 3 months, given that the change in fluorescence is anywhere from 30-150% increase from baseline (compared to <10% with iGluSnFR). This may obscure changes between genotypes, which could become obvious with less intense stimulation. Repeating the 2-pulse stimulation protocol with stimulation intensities lower than 50μA, may reveal differences in VKIs at 3 months old. Finally, there may also be physiological differences in mice used for these versus previous FSCV experiments, including

mouse colony handling, food, water, and microbiome differences. Further investigation of the differences between simultaneous FSCV and dLight recordings could impart a greater mechanistic understanding of dopamine release changes in VKIs. However, the similarities in VKI phenotypes across the two techniques suggest that striatal dopamine release is indeed altered in young adult VKI mice.

Recordings were obtained in the presence of Captisol®

Another important variable of our dLight recordings is that these experiments were performed in the presence of Captisol®, which acutely seems to increase glutamate release in both VKI and WT striata. It could be that Captisol® directly increases dopamine release through similar effects on nigral cell synaptic membranes, obscuring differences at between genotypes at 3 months. Further assessment of dLight responses in the striata of 3-month-old mice aCSF alone to vehicle treatment is necessary to rule out secondary effects of Captisol® on dopamine release.

Captisol® may even have an indirect effect through elevated glutamate release, as glutamate can influence the activity of striatal cholinergic interneurons[165,190,191], which can in turn modulate dopamine release through nicotinic acetylcholine receptors[192]. In fact, acetylcholine release onto distal dopaminergic axons in the striatum is sufficient to initiate action potentials, release dopamine, and alter movement dynamics in freely-moving mice[193]. Therefore, it may be that the increase in glutamate release observed in Captisol® conditions, could indirectly drive dopamine release through cholinergic interneuron activity. Further assessment cholinergic contributions to dopamine release using pharmacological blockade of nicotinic acetylcholine receptor with mecamylamine would address if cholinergic interneurons contribute to dopamine release differentially in VKI mice.

Furthermore, Captisol®, the brand name for sulfobutylether-β-cyclodextrin, is capable of forming ring-like pores in lipid membranes and binding drugs in its cavity[194,195], which makes it suitable for solubilizing and delivering compounds like MLi-2 to brain tissue. However, this very action positions Captisol® to damage lipid membrane integrity and modulate cholesterol levels, both of which can affect neurotransmission in a non-cell type-specific manner at pre-and post-synapses[196,197]. In fact, there have been reports of other cyclodextrins altering glutamatergic, GABAergic, and cholinergic transmission attributed to disrupted lipid homeostasis at synaptic membranes[198–200]. With all of these neurotransmitters present in the STR[64], Captisol® could possibly increase dopamine release in the striatum of both WT and VKI through network activation. However, as we see a clear reduction in dopamine release in aged VKIs even with vehicle treatment, we assume that this reduction would only be made *more* apparent in aCSF alone.

Conclusion

As with glutamate release, we see robust increases in dopamine release in young adult VKI mice, implicating VPS35 at presynaptic dopamine terminals. As touched on earlier, VPS35 D620N may modulate dopamine release through interactions with vesicular transporter proteins. VPS35 in COS7 cells is shown to localize with the monoamine transporter VMAT2 in perinuclear structures[201]. Knocking down VPS35 levels reduces the half-life of VMAT2, impairs perinuclear trans-golgi network localization, and increases co-localization of VMAT2 with lysosomal structures[201]. Therefore, VPS35 seems to be required for retrograde trafficking of VMAT2 from synaptic vesicles to the trans-golgi network, where they can get sorted into new synaptic vesicles instead of being degraded. This retrograde trafficking may be affected by the D620N mutation in our mice, resulting in early accumulation of VMAT2 in synaptic vesicles followed eventual loss as it gets mis-localized to lysosomes instead of being recycled to synaptic vesicles. As total

VMAT2 protein expression is increased in young VKIs[4], increased packaging of dopamine into synaptic vesicles may explain the increase in extracellular dopamine release by 6 months. However, VMAT2 staining in 3-month-old VKIs show no differences in VMAT2 puncta density or area[4], suggesting that its cellular distribution in the STR is mostly conserved at this age. Characterization of VMAT2 staining in 6- to 25-month-old animals may show a difference in distribution or activity contributing to the progression of the dopamine release phenotype in VKI mice.

As previously discussed, DAT dysfunction or reduced expression could also be implicated in the increased dopamine release in young adult VKI mice. As less dopamine is recovered following release, there may be an increased demand on *de novo* monoamine synthesis, which increases oxidative stress in dopamine neurons and may contribute to selective neurodegeneration of dopaminergic neurons[202]. The inability to replenish stores of dopamine coupled with an accumulation of oxidative stress, could lead to a PD-like reduction in dorsolateral STR dopamine release, as is observed in our aged VKI mice. In summary, striatal brain slice experiments reveal elevated dopamine release by 6 months in VKIs, which may drive later loss of striatal dopamine release at ~25 months old.

Acute LRRK2 kinase inhibition does not alter glutamatergic or dopaminergic striatal neurotransmission.

Once basal neurotransmission changes were characterized in VKI mice, we then assessed potential involvement of LRRK2 kinase activity in the VKI phenotype. Mechanistically, VPS35 D620N function has been suggested to lie upstream of LRRK2 kinase activity. Firstly, autosomal dominant mutations in both LRRK2 and VPS35 are linked to clinically typical, late-onset PD. LRRK2

mutations increase LRRK2's kinase activity, its autophosphorylation, and the phosphorylation of its target RabGTPases[203]. Furthermore, VPS35 D620N mutations also result in increased LRRK2 kinase activity, autophosphorylation, and Rab10 phosphorylation in patient cell lines and knock-in mice; this was reduced with LRRK2 kinase inhibition[5]. These markers of LRRK2 kinase overactivity have been reported in one study of post-mortem brain tissue from a donor with idiopathic PD[204]. As kinase inhibitors targeting LRRK2 are now in phase II clinical trials[205], we investigated the potential of the selective LRRK2 kinase inhibitor, MLi-2[206], to reverse the changes to glutamatergic striatal neurotransmission in VKI mice.

Acute LRRK2 kinase inhibition does not alter striatal glutamatergic transmission

We previously showed that 1.5-hour treatment with MLi-2, either administered intraperitoneally in mice, or in the case of primary cortical neuron cultures, with bath-incubation, was sufficient to reduce hyperphosphorylation of the LRRK2 effector, Rab10[3]. Therefore, experiments measuring striatal glutamate transmission in mice were repeated with >1.5-hour bath incubation of brain slices in MLi-2 or it's vehicle, Captisol®.

iGluSnFR recordings in 3-month-old striatal brain slices reveal that in both WT and VKI brain slices, acute MLi-2 treatment significantly increases iGluSnFR response amplitude and probability of release when compared aCSF alone, but does not when compared to vehicle treatment. Decay tau of the iGluSnFR response train is also increased in both genotypes with MLi-2 treatment when compared to aCSF alone, but is not significantly different from vehicle controls. At 6 months, when glutamatergic neurotransmission is robustly increased in the dorsolateral STR of VKIs, we see no effect on either genotype with MLi-2 treatment versus vehicle control on spontaneous glutamatergic neurotransmission onto MSNs. There is also no effect of MLi-2 on

MSN membrane properties when compared to aCSF or vehicle treatment conditions in either genotype. Furthermore, no effect of acute MLi-2 treatment was observed on most measures of ChR2-evoked corticostriatal glutamatergic transmission when compared to vehicle treatment, and this was true of both WT and VKI responses.

At 6 months, the only significant effect of MLi-2 versus vehicle alone is a reduction in the ChR2-PSC amplitude in WT MSNs. This could indicate a decreased amount of glutamate released with repeated stimulation, and/or a higher probability of initial glutamate release leading to suppression of subsequent glutamate release. Moreover, MLi-2 inhibition in primary cortical neuron cultures increases mEPSC frequency in WT neurons, which indicates increased presynaptic spontaneous glutamate release[3]. *In vivo,* acute LRRK2 kinase inhibition selectively increases glutamate content in synaptosomal fractions from striatal but not cortical brain regions of 3-month-old WT mice[207]. Therefore, acute LRRK2 kinase activity may negatively regulate striatal glutamate release in WT mice. Since LRRK2 kinase inhibition does not acutely alter glutamate release in VKI striata, it may be that the regulation of glutamate release is not as discretely modulated by LRRK2 kinase activity when it is constitutively increased. This is further substantiated by a lack of LRRK2 kinase inhibition effects on striatal glutamate release in another model of LRRK2 kinase hyperactivation, LRRK2 G2019S knock-in young adult mice[207].

We repeated glutamate release assays on old animals, this time opting to deliver either MLi-2 or vehicle alone using *in vivo* intra-peritoneal injections and bath-incubation with the corresponding treatment throughout perfusion of brain slices. iGluSnFR responses were compared between vehicle-treated and MLi-2-treated animals only, as we were limited by the smaller number of viable aged animals. In ~25-month-old VKIs, acute MLi-2 treatment did not affect glutamate release in either genotype when compared to vehicle controls. There may be sex-specific MLi-2

effects on WT striatal glutamate release, which could be masked by pooling both male and female sexes within the dataset. As it stands, acute MLi-2 treatment does not reverse the reduction in striatal glutamate release observed in vehicle-treated VKI 25-month-old mice, but more work is required to investigate whether MLi-2 treatment could have sex-specific effects in aged animals of either genotype.

Taken together, acute treatment of MLi-2 does not modulate striatal glutamate transmission in VKI mice, nor does it alter membrane properties when compared to vehicle controls. This may be a result of acute kinase inhibition altering mechanisms not immediately involved in glutamate release, especially if LRRK2 kinase hyperactivity is a compensatory action rather a direct downstream effect of VPS35 D620N mutation. In contrast, acute LRRK2 kinase inhibition with MLi-2 may selectively increase the probability of glutamate release onto striatal MSNs under wild-type conditions through mechanisms that have yet to be characterized.

Acute LRRK2 kinase inhibition does not alter striatal dopamine release

We next investigated the effects of acute LRRK2 kinase inhibition on dopamine release at 6 months, at which point we observe robust increases in striatal dopamine release in VKIs. In 2-pulse stimulation experiments, WT brain slices show a trend towards reduced responses at higher intensity stimulation in the presence of MLi-2. WT responses, however, are not sensitive to acute MLi-2 treatment with regards to the capacity for repeated dopamine release, decay kinetics, nor responses to pulse train stimulation. Previously, it has been reported that WT synaptosomal dopamine content after KCl treatment is reduced with acute treatment with LRRK2 kinase inhibitor, GSK2578215A, at certain concentrations[207]. Therefore, it may be that dopamine release

is reduced in the WT striatum LRRK2 kinase inhibition, but that this particular to stimulation with higher intensity.

In contrast to WT responses, VKI dLight responses at 6 months are not altered by acute MLi-2 treatment in any of the measure we compared. Intriguingly, a pre-print report does show reduced dopamine release with *chronic* MLi-2 treatment in 3-5-month-old VKI mice[208]. One explanation for this difference is that acute LRRK2 kinase activity is not mechanistically involved in dopamine release regulation in VKI animals. Another pre-print report suggest that VPS35 D620N increases LRRK2 kinase-mediated phosphorylation and recruitment of RILPL1 complexes to the lysosome[209], which can disrupt Sonic-hedgehog mediated neuroprotective mechanisms as well as ciliogenesis in striatal cholinergic neurons[210,211]. Therefore, it may be that elevated striatal neurotransmission, or even compensatory action towards it, increases cellular stress which leads to an accumulation of lysosomal damage. This may then recruit LRRK2 to the lysosomes and increase kinase activity to act as a break to prevent further damage. Since chronic MLi-2 treatment is able to reduce lysosomal recruitment of RILPL1[209] in VKI mouse tissue, and reduce elevated dopamine release in VKI striata[208], this may be sufficient time to remove the "breaks" from the endolysosomal system. In turn, other cargo that may not have been sufficiently recycled, including DAT, may be allowed to reintegrate into the cell membrane to reduce the levels of extracellular dopamine release over time.

Another potential mechanism to explain dopamine release alterations with chronic, but not acute, LRRK2 kinase inhibition, is that LRRK2 kinase inhibition influences dopamine release through extra-striatal action. As we bath-apply MLi-2 onto acute striatal brain slices, there is the potential that MLi-2 acts on nigral cell bodies which are absent in our acute slice preparations.

However, this would be accounted for in experiments in our aged mice, where either MLi-2 or vehicle alone was delivered intraperitoneally prior to acute slice preparation.

In vivo LRRK2 kinase inhibition in ~25-month-old mice does not alter dopamine release in WT striata compared to vehicle alone, but it seems to alter dopamine release in VKIs in 2-pulse experiments as stimulus intensity is increased. This suggests that there is the potential for acute MLi-2 treatment to increase dopamine release in aged animals but that it may require supra-physiological stimulation to see significant effects. It would therefore be interesting to repeat dLight experiments in 25-month-old mice with 10-pulse train stimulation, as it may reveal further differences in the capacity of WT and VKI brain slices to regulate dopamine release and recycle dopamine with higher frequency stimulation. This could conversely reveal that MLi-2 is not beneficial for reversing the reduction in VKI striatal dopamine release during lower frequency, *in vivo* activity. As with other data from 25-month-old animals, both sexes were pooled for analysis of MLi-2 effects on striatal dopamine release, and more experiments are necessary to characterize the effects of MLi-2 (and vehicle) by sex.

In summary, acute LRRK2 kinase inhibition with MLi-2 does not seem to profoundly alter striatal dopamine release in VKI mice in 6-month-old animals but could augment release in 25-month-old VKIs when stimulating with higher intensity. In 6-month-old WT mice, striatal dopamine release may be reduced with MLi-2 treatment but requires higher intensity stimulation (which is perhaps supra-physiological). As WT mice age to 25 months, no difference in striatal dopamine release with acute MLi-2 treatment is observed.

Other caveats and limitations

Captisol® selectively alters membrane properties of VKI MSNs

Since Captisol® alone increases striatal glutamate release in 3-month-old mice, we also investigated the effects of Captisol® and MLi-2 treatment on 6-month-old MSN membrane properties in both genotypes. Membrane properties were not altered with MLi-2 treatment in either genotype, when compared to vehicle or aCSF alone. Compared to aCSF, Captisol® vehicle treatment alters membrane properties selectively in VKI, but not WT, MSNs. In 6-month-old VKI MSNs, membrane capacitance is lowered with vehicle treatment, as is membrane tau. Membrane resistance is increased with vehicle treatment in VKIs. Further, the changes to membrane properties in Captisol®-treated VKI MSNs oppose the observed increase in membrane capacitance and reduction in membrane resistance at 6 months. This may indicate that VKI membranes have a larger membrane surface area to be targeted to a greater extent by lypophilic compounds like Captisol®. Since age-related processes can compromise membrane integrity[212,213], it may be that similar mechanisms in VKI MSNs render their membranes more frail and easier to manipulate. Together, 1) VKI MSN membrane properties are selective altered by vehicle treatment. 2) vehicle treatment seems to oppose the VKI phenotype in aCSF conditions, and 3) acute treatment with MLi-2 does not seem to alter membrane properties further.

Captisol® effects may confound MLi-2 effects on striatal glutamate and dopamine release

While vehicle treatment selectively alters passive membrane properties in VKI MSNs, Captisol® increases the proportion of lower-amplitude spontaneous glutamatergic transmission events in both genotypes. Inter-event interval distribution is only affected by vehicle condition in VKI MSNs and not WT MSNs. It may be that amplitude (canonically postsynaptic), but not inter-event interval (canonically presynaptic) is dependent on the membrane properties that are affected by Captisol®

treatment in VKIs. Furthermore, no change in sEPSC decay tau is observed between genotypes or treatment conditions. Overall, spontaneous glutamate transmission onto VKI MSNs seems to be altered in both pre- and post-synaptic measures in the presence of Captisol®. In addition, vehicle treatment may also alter postsynaptic sEPSC amplitudes in WT MSNs.

Recordings of ChR2-evoked cortico-striatal glutamate transmission at 6 months further reveals that both WT and VKI MSNs respond to vehicle treatment alone. In WT neurons, vehicle treatment increases the amplitude of the first response in a train of 4 pulses, when compared to aCSF alone. Subsequent release towards the end of the pulse train was significantly reduced relative to initial pulse response. This suggests that in WT neurons, the probability of glutamate release is increased with vehicle treatment. Captisol® does not seem to alter initial glutamate release in VKI MSNs but does decrease the size of subsequent responses, reducing the paired-pulse ratio. Taken together, Captisol® seems to increase the probability of repeated glutamate release in both genotypes and may also increase the capacity for initial release in WT MSNs.

As previously discussed, Captisol® may also alter dopamine release, either directly or through effects on the striatal network. As we've already demonstrated that Captisol® augments glutamate release in both genotypes in young adult mice, it may have profound effects on striatal dopamine release in 25-month-old mice as well. Again, as Captisol® appears to increase neurotransmission, sham-injected control experiments may reveal that the reduction in dopamine release in VKI mice at this age is even more profound in the absence of Captisol®. Altogether, we cannot rule out that acute LRRK2 kinase inhibition could influence glutamate and dopamine transmission in young and aged animals but may be masked by off-target Captisol® vehicle effects. Further assessment of glutamate and dopamine release comparing sham-injected to vehicle-injected aged mice would clarify whether the changes to striatal neurotransmission in VKI

mice are altered in the presence of Captisol®. Alternating the delivery method of MLi-2 or using a more soluble LRRK2 kinase inhibitor may reveal that a reduction in acute LRRK2 kinase alters glutamate or dopamine transmission in the absence of cyclodextrins such as Captisol®.

Conclusion

Acute LRRK2 kinase does not seem to reverse or alter changes to striatal glutamatergic or dopaminergic neurotransmission in VKIs in a physiologically relevant manner. However, this does not rule out the efficacy of LRRK2 kinase inhibitors in treating changes to neurotransmission when administered chronically. It may be that LRRK2 kinase hyperactivity, observed in VPS35 D620N-PD or idiopathic PD[5,204], is a compensatory change to mitigate VPS35 dysfunction, and that acutely reducing LRRK2 kinase activity is not enough to relieve the dysfunction contributing to altered neurotransmission.

Since lysosomal stress can directly trigger an increase in LRRK2 kinase activity and localization to lysosomal membrances[214], LRRK2 kinase activity could be increased in response to the stress. For instance, Rab29 which can be phosphorylated by LRRK2 kinase[115] is mobilized onto lysosomal membranes following lysosomal stress, and this can also occur independent of LRRK2 kinase activity[215]. Therefore, chronic LRRK2 kinase inhibition may shift the phosphorylation of select Rab effectors away from LRRK2 kinase-dependent pathways, and promote clearance of lysosomal proteins that through LRRK-kinase independent mechanisms. If this interpretation holds true, longer-term chronic MLi-2 treatment may have adverse effects as it may eventually redirect the cellular dysregulation rather restoring balance. I.e., a system without breaks is just as dysregulated (or maybe even more dysregulated) as a system with constitutively active breaks. The lack of clear effects of MLi-2 treatment on striatal glutamatergic and

dopaminergic transmission in VKIs, and the presence of MLi-2 effects on distinct properties of striatal glutamate and dopamine release in young adult WT mice, necessitates further investigation into the interaction of LRRK2 and VPS35 at the presynapse, especially given that LRRK2 kinase inhibitors are being developed as treatments for genetic and idiopathic PD[205].

The bigger picture

VPS35 D620N may globally increase neurotransmitter release

In VKI mice, we observe early increases to presynaptic neurotransmitter release ahead of reduced release in old age. As this is a feature of both striatal glutamate and dopamine neurotransmission in VKIs, VPS35 D620N may alter the synaptic vesicle cycle in a non-cell type-specific manner. The drosophila variant of VPS35 has been shown affect synaptic vesicle endocytosis at drosophila neuromuscular junctions[81]. WT but not D620N VPS35 overexpression increases the localization of VPS35 onto synaptic boutons and overlap with the active zone (*ibid*). Knock-out of VPS35 leads to a reduction of synaptic vesicle number and an increase in synaptic vesicle size, which is rescued with WT but not D620N overexpression (*ibid*). The role of VPS35 in regulating synaptic vesicle number in mouse hippocampal neurons is contested, however, as knockdown of VSP35 does not seem to alter active-zone length or synaptic vesicle number[93]. It may be that the 30-80% reduction in VPS35 achieved with their shRNAs was not sufficient to affect the function of VPS35 at synapses, or that transient reduction in VPS35 can be compensated for.

VPS35 D620N may alter presynaptic release through impaired synaptic vesicle recycling

Presynaptic recycling of vesicular membranes through bulk endocytosis may implicate VPS35. While clathrin-mediated endocytosis (CME) directly from the postsynaptic membrane is well-recognized as a major process governing synaptic vesicle endocytosis (reviewed in Kaksonen and

Roux, 2018), ultra-fast bulk endocytosis followed by clathrin coating can also contribute to presynaptic vesicle recycling[217,218]. Bulk endocytosis can be triggered by the insertion of synaptic vesicle membrane to the postsynaptic membrane[219], or by high-frequency stimulation in a Rab11 dependent manner[220]. Previously, we found that the density of Rab11 clusters in primary cortical cultures is increased in VKIs, accompanied by a reduction in VPS35-Rab11 Pearson's coefficient[3]. This suggests that Rab11 may accumulate in recycling endosomes not localized with VPS35 D620N. Perhaps VPS35 D620N impairs recycling of synaptic membranes through bulk endocytosis, resulting in a compensatory shift towards the increased neurotransmitter content in 3- to 6-month-old VKIs. This theory is also supported by the observed increase in capacitance of VKI MSNs at 3 and 6 months, which may represent an accumulation of synaptic vesicle membrane on MSNs slowly increasing the surface area of MSN membranes. Impaired synaptic vesicle recycling may also contribute to the eventual reduction in dopamine and glutamate release in aged VKIs.

VPS35 D620N may impair retromer interactions

While we were not able to reverse changes in striatal neurotransmission in VKIs using acute MLi-2 treatment, a better understanding of how VPS35 interactions are altered with the D620N could lead to the development of alternative therapeutic interventions. For instance, if D620N is observed to be a non-selective loss-of-function mutation, chaperone proteins like TPT-172, which stabilizes VPS35-VPS29 interactions within the core retromer complex, could be used to increase levels of VPS35 and potentially ameliorate the cellular burden of the mutation[88]. It should be noted that affinity chromatography and gel filtration experiments show similar binding affinity of VPS35 D620N with both VPS26 and VPS29 to that of VPS35 WT[15]. While VPS35-VPS26 co-cluster intensity is similar across genotypes, the density of VPS26 clusters *in vitro* is reduced in VKI

cultures[3]. Therefore, D620N mutations may not destabilize the interaction of VPS35 within core retromer components but could still alter the localization of retromer components within the cell.

Another interactor, FAM21, binds to VPS35 to recruit the WASH-complex to endosomal membranes[123] to promote endosomal tubulation in an RME-8 dependent manner[127]. FAM21 not only co-IPs with VPS35 less in VKI mice but is increased in intensity of co-clustering with VPS35 in primary cortical neurons[3]. This suggests that VPS35 D620N may colocalize to a greater extent to compensate for the loss of binding to FAM21. FAM21 has also been shown to interact with SNX27 and retromer to direct endosomal cargo to the plasma membrane by suppressing the signaling cascade required to direct cargo to the golgi apparatus[221]. Therefore endosome-to-plasma membrane trafficking in VKI striata may be reduced. For example in PC-12 cells, VPS35 is shown to form a complex with FAM21 and DAT, and levels of this complex co-IP'ed with WT VPS35 are significantly higher than with VPS35 D620N[186]. Another WASH complex component, WASH-1 is shown to be selectively reduced in TH-positive nigral dopamine neurons of VKI mice[122]. Therefore, targeting the stability of interactions of VPS35 with the WASH complex in VKI mice may increase physiological trafficking of cargo from endosomal membranes.

VPS35 D620N may increase lysosomal stress while reducing lysosomal function

The sustained increase in neurotransmission we observe in young adult VKI mice may require increased synaptic protein turnover through lysosomal processes that further implicate VPS35 function. Patient-derived VPS35 D620N neurons show a reduction in lysosomal size and lysosomal LAMP1 and LAMP2 protein expression[129], suggesting an impairment of lysosomal function is a feature of VPS35 D620N-linked PD. Furthermore, endosome-to-golgi retrieval of LAMP2a proteins, which serve as receptors for α-synuclein during chaperone-mediated

autophagy, is reduced with VPS35 D620N expression[85]. In VPS35 D620N knock-in mice, total α-synuclein levels are reported to increase at 16 months[87], though there is no pathological pSer129-α-synuclein in whole brain lysates of 13-month-old VKI mice[122]. Together, this may reflect a failure to degrade accumulated proteins like α-synuclein, a key contributor to Lewy Body pathology in PD[222].

A failure to degrade misfolded protein is also more broadly, a feature of neurodegenerative disease. VKI mice show widespread neurite degeneration and dysregulation of tau protein[122]. Paired with the observation that VPS35 knock-down impairs the clearance of mutant MAPT proteins in HEK293T cells[223], these data suggest that VPS35 D620N may act as a loss-of-function mutation when it comes to lysosomal clearance of damaged proteins. It may be that the additional clearance of synaptic proteins required by the increased synaptic load coupled with the loss of autophagic capacity in neurons[224] results in the neurodegeneration and eventual loss of neurotransmission observed in aged VKI mice[73,122].

VPS35 D620N may increase mitochondrial stress while reducing mitochondrial turnover

The "final nail in the coffin" leading to a Parkinsonian state may be hammered by mitochondrial dysregulation and dysfunction in VKI brains. Mitochondrial respiration is reduced in patient-derived VPS35 D620N neurons[129]. This is also observed in VPS35 D620N knock-in mice, alongside a reduction in Complex I and IV activity, ATP generation, mitochondrial size, and expression of mitofusin 2, an outer membrane mitochondrial GTPase that regulates mitochondrial fusion, by 16 months[87].

VPS35 D620N expression in neuronal cultures also increases localization of mitochondrial E3 ubiquitin protein ligase 1 (MUL1 or MAPL) to mitochondria[85]. MAPL recruitment to

mitochondria and subsequent formation of MAPL-positive mitochondria derived vesicles (MDVs) is reduced in HeLa cells with VPS35 knock-down[225], implicating VPS35 in the turnover of mitochondrial proteins through MDVs. Furthermore, VSP35 D620N may also increase mitochondrial fragmentation through stabilizing the interaction of VPS35 with the dynamin-related GTPase, Dlp1/Drp1, which triggers trafficking of MDVs to lysosomes[101,226]. This would then promote the degradation, rather than recycling of mitochondrial proteins.

In young adult VKIs, which have increased glutamatergic and dopamine transmission in the striatum, proper calcium buffering and sufficient energy stores would be required support the increased demand on synaptic terminals[227–229]. This may necessitate additional ATP formation through mitochondrial oxidative respiration, leading to the generation and accumulation of mitochondrial reactive oxygen species[230] and ultimately adding another cellular stress to the roster of insults faced by VKI neurons. The accumulation of mitochondrial damage may drive the eventual reduction of mitochondrial activity, all while VPS35 D620N also impairs mitochondrial quality control through the recycling of mitochondrial proteins, and increases the mitochondrial fission:fusion ratio[85,129,226]. In turn, this could reduce the calcium buffering capacity and availability of energy to support presynaptic function, leading to the loss of neurotransmitter release in the STR of aged VKI mice.

Mitochondria are also important regulars of cell health and can respond to mitochondrial or cellular stress by triggering the protective unfolded protein response through retromer-dependent Wnt-signalling[89,231]. As the D620N mutation reduces pro-survival Wnt/β-catenin signalling and increases pro-apoptotic caspase 8 and caspase 9 activation[87], it could be that pro-survival signaling and adaptation after mitochondrial damage is also diminished in VKI mice. Altogether, multiple mitochondrial functions could be affected by the D620N mutation in VPS35,

and the combination of these effects may lead to an eventual loss of STR neurotransmission and promote neurodegeneration.

VPS35 D620N may lead to PD through changes to neuronal development, maturation, and aging

We know that VPS35 function is important for cellular and neuronal development as a knock-out of VPS35 is embryonic lethal[77]. VPS35 loss of function during neuronal development can reduce vascularization[83], cortical development[232], terminal differentiation[233], neurite outgrowth and complexity[82]. While there is no alteration in cell density or dendritic morphology in VKI primary cortical neurons[3], changes to membrane dynamics or plasticity, and neuronal function could serve to weaken the foundation from which neurons mature and age. Elevated neurotransmission could also point to impaired maturation or altered neurodevelopment, which many argue is inherently linked to the etiology of neurodegenerative disease[234–236]. Even if neurodevelopmental changes can be accommodated for during a significant portion of the animal's life – perhaps less so in humans than in mice – the weakened foundation may give way to a Parkinsonian state as additional insults, including aging, stress the system.

Towards a better understanding of PD

The objectives set out in this dissertation aimed to investigate the potential alterations to glutamatergic and dopaminergic transmission in the dorsolateral striatum of mice bearing PD-linked D620N mutations in VPS35, as well as the potential influence of acute LRRK2 kinase activity on observed phenotypes. We find that the striatal release of both neurotransmitters is increased in young adult VSP35 D620N knock-in mice and is conversely reduced in aged animals.

This biphasic deviation from WT striatal neurotransmission is not altered with acute treatment with LRRK2 kinase inhibitor, MLi-2, suggesting that VPS35 D620N-mediated changes to neurotransmission in the striatum not immediately dependent on LRRK2 kinase activity.

This biphasic transition from hyper-to-hypo-active striatal neurotransmission in VKI mice may be reflective of the progression into Parkinsonism. Initially, VPS35 D620N may increase neurotransmission in the striatum through a direct increase in presynaptic release of multiple neurotransmitters. This increase may intensify synaptic burden on striatal synapses and accelerate the age-related degradation of regulatory pathways including endo-lysosomal and mitochondrial function[212,213,224,228,230]. Dopaminergic neurons may be particularly vulnerable to the accumulation of such cellular stress by virtue of their increased metabolic demands, increased cellular ROS generation from dopamine synthesis, and extensive axonal networks that require more energy and resources to maintain[237,238].

Ultimately, the D620N mutation in VPS35 may overdrive the nigrostriatal pathway, in a manner not acutely dependent on LRRK2 kinase activity. This early hyperactivity could precipitate the eventual onset of PD-like loss of dopaminergic neurotransmission and motor dysfunction in aged animals[73,122]. Further, early elevations in striatal glutamate release may increase the activation of excitotoxic extra-synaptic NMDARs, potentially adding to the progression towards neurodegeneration[147,163]. An eventual loss of corticostriatal glutamate transmission could also impair alter striatal plasticity, which is important for the generation and maintenance of movement, and may be implicated in Levodopa-induced dyskinesia[239–242]. Glutamate transmission, and potentially other neurotransmitter systems affected by the VPS35 D620N mutation, may also drive non-motor symptom onset in PD including sleep disturbances, fatigue, gastrointestinal difficulties, cognitive impairment, anxiety and depression[10]. Altogether, the data presented in this dissertation

reveals progressive alterations to striatal neurotransmission in mice with VPS35 D620N mutations. We hope that this heightened understanding of the transition into a potentially Parkinsonian state will uncover novel targets and/or therapeutic windows for the development of disease-modifying treatments, especially in individuals carrying VPS35 D620N mutations.

Bibliography

1. Munsie, L.N., Milnerwood, A.J., Seibler, P., Beccano-Kelly, D.A., Tatarnikov, I., Khinda, J., Volta, M., Kadgien, C., Cao, L.P., Tapia, L., et al. (2015). Retromer-dependent neurotransmitter receptor trafficking to synapses is altered by the Parkinson's disease VPS35 mutation p.D620N. Hum. Mol. Genet. *24*, 1691–1703. 10.1093/hmg/ddu582.

2. Temkin, P., Morishita, W., Goswami, D., Arendt, K., Chen, L., and Malenka, R. (2017). The Retromer Supports AMPA Receptor Trafficking During LTP. Neuron *94*, 74-82.e5. 10.1016/j.neuron.2017.03.020.

3. Kadgien, C.A., Kamesh, A., and Milnerwood, A.J. (2021). Endosomal traffic and glutamate synapse activity are increased in VPS35 D620N mutant knock-in mouse neurons, and resistant to LRRK2 kinase inhibition. Mol Brain *14*, 1–20. 10.1186/s13041-021-00848-w.

4. Cataldi, S., Follett, J., Fox, J.D., Tatarnikov, I., Kadgien, C., Gustavsson, E.K., Khinda, J., Milnerwood, A.J., and Farrer, M.J. (2018). Altered dopamine release and monoamine transporters in Vps35 p.D620N knock-in mice. npj Parkinson's Disease *4*, 1–11. 10.1038/s41531-018-0063-3.

5. Mir, R., Tonelli, F., Lis, P., Macartney, T., Polinski, N.K., Martinez, T.N., Chou, M.-Y., Howden, A.J.M., König, T., Hotzy, C., et al. (2018). The Parkinson's disease VPS35[D620N] mutation enhances LRRK2-mediated Rab protein phosphorylation in mouse and human. Biochem. J. *475*, 1861–1883. 10.1042/BCJ20180248.

6. Kordower, J.H., Olanow, C.W., Dodiya, H.B., Chu, Y., Beach, T.G., Adler, C.H., Halliday, G.M., and Bartus, R.T. (2013). Disease duration and the integrity of the nigrostriatal system in Parkinson's disease. Brain *136*, 2419–2431. 10.1093/brain/awt192.

7. Fereshtehnejad, S.-M., Yao, C., Pelletier, A., Montplaisir, J.Y., Gagnon, J.-F., and Postuma, R.B. (2019). Evolution of prodromal Parkinson's disease and dementia with Lewy bodies: a prospective study. Brain *142*, 2051–2067. 10.1093/brain/awz111.

8. Foffani, G., and Obeso, J.A. (2018). A Cortical Pathogenic Theory of Parkinson's Disease. Neuron *99*, 1116–1128. 10.1016/j.neuron.2018.07.028.

9. Kalia, L.V., and Lang, A.E. (2015). Parkinson's disease. The Lancet *386*, 896–912. 10.1016/S0140-6736(14)61393-3.

10. Goldman, J.G., and Postuma, R. (2014). Premotor and nonmotor features of Parkinson's disease. Curr. Opin. Neurol. *27*, 434–441. 10.1097/WCO.0000000000000112.

11. Henderson, J.M., Carpenter, K., Cartwright, H., and Halliday, G.M. (2000). Loss of thalamic intralaminar nuclei in progressive supranuclear palsy and Parkinson's disease: clinical and therapeutic implications. Brain *123*, 1410–1421. 10.1093/brain/123.7.1410.

12. MacDonald, V., and Halliday, G.M. (2002). Selective loss of pyramidal neurons in the pre-supplementary motor cortex in Parkinson's disease. Mov. Disord. *17*, 1166–1173. 10.1002/mds.10258.

13. Diógenes, M.J., Dias, R.B., Rombo, D.M., Miranda, H.V., Maiolino, F., Guerreiro, P., Näsström, T., Franquelim, H.G., Oliveira, L.M.A., Castanho, M.A.R.B., et al. (2012). Extracellular Alpha-Synuclein Oligomers Modulate Synaptic Transmission and Impair LTP Via NMDA-Receptor Activation. J. Neurosci. *32*, 11750–11762. 10.1523/JNEUROSCI.0234-12.2012.

14. Matikainen-Ankney, B.A., Kezunovic, N., Mesias, R.E., Tian, Y., Williams, F.M., Huntley, G.W., and Benson, D.L. (2016). Altered Development of Synapse Structure and Function in Striatum Caused by Parkinson's Disease-Linked LRRK2–G2019S Mutation. J. Neurosci. *36*, 7128–7141. 10.1523/JNEUROSCI.3314-15.2016.

15. Follett, J., Norwood, S.J., Hamilton, N.A., Mohan, M., Kovtun, O., Tay, S., Zhe, Y., Wood, S.A., Mellick, G.D., Silburn, P.A., et al. (2014). The Vps35 D620N Mutation Linked to Parkinson's Disease Disrupts the Cargo Sorting Function of Retromer. Traffic *15*, 230–244. 10.1111/tra.12136.

16. Choy, R.W.-Y., Park, M., Temkin, P., Herring, B.E., Marley, A., Nicoll, R.A., and von Zastrow, M. (2014). Retromer Mediates a Discrete Route of Local Membrane Delivery to Dendrites. Neuron *82*, 55–62. 10.1016/j.neuron.2014.02.018.

17. Wang, C., Niu, M., Zhou, Z., Zheng, X., Zhang, L., Tian, Y., Yu, X., Bu, G., Xu, H., Ma, Q., et al. (2016). VPS35 regulates cell surface recycling and signaling of dopamine receptor D1. Neurobiol. Aging *46*, 22–31. 10.1016/j.neurobiolaging.2016.05.016.

18. Volta, M., Beccano-Kelly, D.A., Paschall, S.A., Cataldi, S., MacIsaac, S.E., Kuhlmann, N., Kadgien, C.A., Tatarnikov, I., Fox, J., Khinda, J., et al. (2017). Initial elevations in glutamate and dopamine neurotransmission decline with age, as does exploratory behavior, in LRRK2 G2019S knock-in mice. Elife *6*. 10.7554/eLife.28377.

19. Postuma, R.B., Berg, D., Stern, M., Poewe, W., Olanow, C.W., Oertel, W., Obeso, J., Marek, K., Litvan, I., Lang, A.E., et al. (2015). MDS clinical diagnostic criteria for Parkinson's disease. Movement Disorders *30*, 1591–1601. 10.1002/mds.26424.

20. Stern, M.B., Lang, A., and Poewe, W. (2012). Toward a redefinition of Parkinson's disease. Movement Disorders *27*, 54–60. 10.1002/mds.24051.

21. Weintraub, D., and Mamikonyan, E. (2019). The Neuropsychiatry of Parkinson Disease: A Perfect Storm. Am J Geriatr Psychiatry *27*, 998–1018. 10.1016/j.jagp.2019.03.002.

22. Ferrazzoli, D., Carter, A., Ustun, F.S., Palamara, G., Ortelli, P., Maestri, R., Yücel, M., and Frazzitta, G. (2016). Dopamine Replacement Therapy, Learning and Reward Prediction in Parkinson's Disease: Implications for Rehabilitation. Front Behav Neurosci *10*. 10.3389/fnbeh.2016.00121.

23. Oertel, W., and Schulz, J.B. (2016). Current and experimental treatments of Parkinson disease: A guide for neuroscientists. J. Neurochem. *139 Suppl 1*, 325–337. 10.1111/jnc.13750.

24. Marsden, C.D. (1994). Problems with long-term levodopa therapy for Parkinson's disease. Clin Neuropharmacol *17 Suppl 2*, S32-44.

25. Dorsey, E.R., Elbaz, A., Nichols, E., Abd-Allah, F., Abdelalim, A., Adsuar, J.C., Ansha, M.G., Brayne, C., Choi, J.-Y.J., Collado-Mateo, D., et al. (2018). Global, regional, and national burden of

Parkinson's disease, 1990–2016: a systematic analysis for the Global Burden of Disease Study 2016. The Lancet Neurology *17*, 939–953. 10.1016/S1474-4422(18)30295-3.

26. GBD 2015 Disease and Injury Incidence and Prevalence Collaborators (2016). Global, regional, and national incidence, prevalence, and years lived with disability for 310 diseases and injuries, 1990-2015: a systematic analysis for the Global Burden of Disease Study 2015. Lancet *388*, 1545–1602. 10.1016/S0140-6736(16)31678-6.

27. Kalinderi, K., Bostantjopoulou, S., and Fidani, L. (2016). The genetic background of Parkinson's disease: current progress and future prospects. Acta Neurol. Scand. *134*, 314–326. 10.1111/ane.12563.

28. Parkinsonism in Canada, including Parkinson's Disease (2018). (Public Health Agency of Canada).

29. Lesage, S., and Brice, A. (2009). Parkinson's disease: from monogenic forms to genetic susceptibility factors. Hum Mol Genet *18*, R48–R59. 10.1093/hmg/ddp012.

30. Volta, M., Milnerwood, A.J., and Farrer, M.J. (2015). Insights from late-onset familial parkinsonism on the pathogenesis of idiopathic Parkinson's disease. The Lancet Neurology *14*, 1054–1064. 10.1016/S1474-4422(15)00186-6.

31. Li, Y.I., Wong, G., Humphrey, J., and Raj, T. (2019). Prioritizing Parkinson's disease genes using population-scale transcriptomic data. Nature Communications *10*, 1–10. 10.1038/s41467-019-08912-9.

32. Huot, P., Levesque, M., and Parent, A. (2006). The fate of striatal dopaminergic neurons in Parkinson's disease and Huntington's chorea. Brain *130*, 222–232. 10.1093/brain/awl332.

33. Kreitzer, A.C., and Malenka, R.C. (2008). Striatal plasticity and basal ganglia circuit function. Neuron *60*, 543–554. 10.1016/j.neuron.2008.11.005.

34. Houk, J. c, Bastianen, C., Fansler, D., Fishbach, A., Fraser, D., Reber, P. j, Roy, S. a, and Simo, L. s (2007). Action selection and refinement in subcortical loops through basal ganglia and cerebellum. Philosophical Transactions of the Royal Society B: Biological Sciences *362*, 1573–1583. 10.1098/rstb.2007.2063.

35. Humphries, M.D., Stewart, R.D., and Gurney, K.N. (2006). A Physiologically Plausible Model of Action Selection and Oscillatory Activity in the Basal Ganglia. J. Neurosci. *26*, 12921–12942. 10.1523/JNEUROSCI.3486-06.2006.

36. Mink, J.W. (1996). The basal ganglia: focused selection and inhibition of competing motor programs. Prog. Neurobiol. *50*, 381–425. 10.1016/s0301-0082(96)00042-1.

37. Haber, S.N. (2011). Neuroanatomy of Reward: A View from the Ventral Striatum. In Neurobiology of Sensation and Reward Frontiers in Neuroscience., J. A. Gottfried, ed. (CRC Press/Taylor & Francis).

38. Balleine, B.W., Delgado, M.R., and Hikosaka, O. (2007). The Role of the Dorsal Striatum in Reward and Decision-Making. J. Neurosci. *27*, 8161–8165. 10.1523/JNEUROSCI.1554-07.2007.

39. Zhai, S., Tanimura, A., Graves, S.M., Shen, W., and Surmeier, D.J. (2018). Striatal synapses, circuits, and Parkinson's disease. Curr Opin Neurobiol *48*, 9–16. 10.1016/j.conb.2017.08.004.

40. Alloway, K.D., Smith, J.B., Mowery, T.M., and Watson, G.D.R. (2017). Sensory Processing in the Dorsolateral Striatum: The Contribution of Thalamostriatal Pathways. Front Syst Neurosci *11*. 10.3389/fnsys.2017.00053.

41. Surmeier, D.J., Graves, S.M., and Shen, W. (2014). Dopaminergic modulation of striatal networks in health and Parkinson's disease. Curr Opin Neurobiol *29*, 109–117. 10.1016/j.conb.2014.07.008.

42. Devan, B.D., Hong, N.S., and McDonald, R.J. (2011). Parallel associative processing in the dorsal striatum: Segregation of stimulus–response and cognitive control subregions. Neurobiology of Learning and Memory *96*, 95–120. 10.1016/j.nlm.2011.06.002.

43. Balleine, B.W., and O'Doherty, J.P. (2010). Human and Rodent Homologies in Action Control: Corticostriatal Determinants of Goal-Directed and Habitual Action. Neuropsychopharmacol *35*, 48–69. 10.1038/npp.2009.131.

44. Mi, T.-M., Zhang, W., Li, Y., Liu, A.-P., Ren, Z.-L., and Chan, P. (2021). Altered Functional Segregated Sensorimotor, Associative, and Limbic Cortical-Striatal Connections in Parkinson's Disease: An fMRI Investigation. Front. Neurol. *12*, 720293. 10.3389/fneur.2021.720293.

45. Kreitzer, A.C. (2009). Physiology and Pharmacology of Striatal Neurons. Annu. Rev. Neurosci. *32*, 127–147. 10.1146/annurev.neuro.051508.135422.

46. Smith, Y., Bevan, M.D., Shink, E., and Bolam, J.P. (1998). Microcircuitry of the direct and indirect pathways of the basal ganglia. Neuroscience *86*, 353–387. 10.1016/s0306-4522(98)00004-9.

47. Wichmann, T., and DeLong, M.R. (1998). Models of Basal Ganglia Function and Pathophysiology of Movement Disorders. Neurosurgery Clinics of North America *9*, 223–236. 10.1016/S1042-3680(18)30261-4.

48. Surmeier, D.J., Ding, J., Day, M., Wang, Z., and Shen, W. (2007). D1 and D2 dopamine-receptor modulation of striatal glutamatergic signaling in striatal medium spiny neurons. Trends Neurosci. *30*, 228–235. 10.1016/j.tins.2007.03.008.

49. Lee, F.J.S., Xue, S., Pei, L., Vukusic, B., Chéry, N., Wang, Y., Wang, Y.T., Niznik, H.B., Yu, X., and Liu, F. (2002). Dual regulation of NMDA receptor functions by direct protein-protein interactions with the dopamine D1 receptor. Cell *111*, 219–230. 10.1016/s0092-8674(02)00962-5.

50. Cepeda, C., Buchwald, N.A., and Levine, M.S. (1993). Neuromodulatory actions of dopamine in the neostriatum are dependent upon the excitatory amino acid receptor subtypes activated. Proc. Natl. Acad. Sci. U.S.A. *90*, 9576–9580. 10.1073/pnas.90.20.9576.

51. Gagnon, D., Petryszyn, S., Sanchez, M.G., Bories, C., Beaulieu, J.M., De Koninck, Y., Parent, A., and Parent, M. (2017). Striatal Neurons Expressing D1 and D2 Receptors are Morphologically Distinct and Differently Affected by Dopamine Denervation in Mice. Sci Rep *7*, 41432. 10.1038/srep41432.

52. Bertran-Gonzalez, J., Bosch, C., Maroteaux, M., Matamales, M., Hervé, D., Valjent, E., and Girault, J.-A. (2008). Opposing Patterns of Signaling Activation in Dopamine D_1 and D_2 Receptor-

Expressing Striatal Neurons in Response to Cocaine and Haloperidol. J. Neurosci. *28*, 5671–5685. 10.1523/JNEUROSCI.1039-08.2008.

53. Cui, Y., Carosi, J.M., Yang, Z., Ariotti, N., Kerr, M.C., Parton, R.G., Sargeant, T.J., and Teasdale, R.D. (2019). Retromer has a selective function in cargo sorting via endosome transport carriers. J Cell Biol *218*, 615–631. 10.1083/jcb.201806153.

54. Cazorla, M., Kang, U.J., and Kellendonk, C. (2015). Balancing the basal ganglia circuitry: A possible new role for dopamine D2 receptors in health and disease: Keeping the balance with bridging collaterals. Mov Disord. *30*, 895–903. 10.1002/mds.26282.

55. Smith, J.B., Klug, J.R., Ross, D.L., Howard, C.D., Hollon, N.G., Ko, V.I., Hoffman, H., Callaway, E.M., Gerfen, C.R., and Jin, X. (2016). Genetic-Based Dissection Unveils the Inputs and Outputs of Striatal Patch and Matrix Compartments. Neuron *91*, 1069–1084. 10.1016/j.neuron.2016.07.046.

56. Pert, C.B., Kuhar, M.J., and Snyder, S.H. (1976). Opiate receptor: autoradiographic localization in rat brain. Proc. Natl. Acad. Sci. U.S.A. *73*, 3729–3733. 10.1073/pnas.73.10.3729.

57. Graybiel, A.M., and Ragsdale, C.W. (1978). Histochemically distinct compartments in the striatum of human, monkeys, and cat demonstrated by acetylthiocholinesterase staining. Proc. Natl. Acad. Sci. U.S.A. *75*, 5723–5726. 10.1073/pnas.75.11.5723.

58. Brimblecombe, K.R., and Cragg, S.J. (2017). The Striosome and Matrix Compartments of the Striatum: A Path through the Labyrinth from Neurochemistry toward Function. ACS Chem. Neurosci. *8*, 235–242. 10.1021/acschemneuro.6b00333.

59. Bolam, J.P., and Pissadaki, E.K. (2012). Living on the edge with too many mouths to feed: why dopamine neurons die. Mov. Disord. *27*, 1478–1483. 10.1002/mds.25135.

60. Bernard, V., and Bolam, J.P. (1998). Subcellular and subsynaptic distribution of the NR1 subunit of the NMDA receptor in the neostriatum and globus pallidus of the rat: co-localization at synapses with the GluR2/3 subunit of the AMPA receptor. Eur. J. Neurosci. *10*, 3721–3736. 10.1046/j.1460-9568.1998.00380.x.

61. Fujiyama, F., Kuramoto, E., Okamoto, K., Hioki, H., Furuta, T., Zhou, L., Nomura, S., and Kaneko, T. (2004). Presynaptic localization of an AMPA-type glutamate receptor in corticostriatal and thalamostriatal axon terminals. Eur. J. Neurosci. *20*, 3322–3330. 10.1111/j.1460-9568.2004.03807.x.

62. Keeler, B.E., Lallemand, P., Patel, M.M., De Castro Brás, L.E., and Clemens, S. (2016). Opposing aging-related shift of excitatory dopamine D1 and inhibitory D3 receptor protein expression in striatum and spinal cord. Journal of Neurophysiology *115*, 363–369. 10.1152/jn.00390.2015.

63. Meador-Woodruff, J. (1996). Dopamine Receptor mRNA Expression in Human Striatum and Neocortex. Neuropsychopharmacology *15*, 17–29. 10.1016/0893-133X(95)00150-C.

64. Burke, D.A., Rotstein, H.G., and Alvarez, V.A. (2017). Striatal Local Circuitry: A New Framework for Lateral Inhibition. Neuron *96*, 267–284. 10.1016/j.neuron.2017.09.019.

65. Tepper, J.M., and Koós, T. (2016). GABAergic Interneurons of the Striatum. In Handbook of Behavioral Neuroscience (Elsevier), pp. 157–178. 10.1016/B978-0-12-802206-1.00008-8.

66. Poppi, L.A., Ho-Nguyen, K.T., Shi, A., Daut, C.T., and Tischfield, M.A. (2021). Recurrent Implication of Striatal Cholinergic Interneurons in a Range of Neurodevelopmental, Neurodegenerative, and Neuropsychiatric Disorders. Cells *10*, 907. 10.3390/cells10040907.

67. Sharma, M., Ioannidis, J.P.A., Aasly, J.O., Annesi, G., Brice, A., Bertram, L., Bozi, M., Barcikowska, M., Crosiers, D., Clarke, C.E., et al. (2012). A multi-centre clinico-genetic analysis of the VPS35 gene in Parkinson disease indicates reduced penetrance for disease-associated variants. J Med Genet *49*, 721–726. 10.1136/jmedgenet-2012-101155.

68. Zimprich, A., Benet-Pagès, A., Struhal, W., Graf, E., Eck, S.H., Offman, M.N., Haubenberger, D., Spielberger, S., Schulte, E.C., Lichtner, P., et al. (2011). A Mutation in VPS35, Encoding a Subunit of the Retromer Complex, Causes Late-Onset Parkinson Disease. The American Journal of Human Genetics *89*, 168–175. 10.1016/j.ajhg.2011.06.008.

69. Vilariño-Güell, C., Wider, C., Ross, O.A., Dachsel, J.C., Kachergus, J.M., Lincoln, S.J., Soto-Ortolaza, A.I., Cobb, S.A., Wilhoite, G.J., Bacon, J.A., et al. (2011). VPS35 mutations in Parkinson disease. Am. J. Hum. Genet. *89*, 162–167. 10.1016/j.ajhg.2011.06.001.

70. Wider, C., Skipper, L., Solida, A., Brown, L., Farrer, M., Dickson, D., Wszolek, Z.K., and Vingerhoets, F.J.G. (2008). Autosomal dominant dopa-responsive parkinsonism in a multigenerational Swiss family. Parkinsonism & Related Disorders *14*, 465–470. 10.1016/j.parkreldis.2007.11.013.

71. Sjöstedt, E., Zhong, W., Fagerberg, L., Karlsson, M., Mitsios, N., Adori, C., Oksvold, P., Edfors, F., Limiszewska, A., Hikmet, F., et al. (2020). An atlas of the protein-coding genes in the human, pig, and mouse brain. Science *367*, eaay5947. 10.1126/science.aay5947.

72. Sargent, D., Cunningham, L.A., Dues, D.J., Ma, Y., Kordich, J.J., Mercado, G., Brundin, P., Cowell, R.M., and Moore, D.J. (2021). Neuronal *VPS35* deletion induces spinal cord motor neuron degeneration and early post-natal lethality. Brain Communications *3*, fcab208. 10.1093/braincomms/fcab208.

73. Niu, M., Zhao, F., Bondelid, K., Siedlak, S.L., Torres, S., Fujioka, H., Wang, W., Liu, J., and Zhu, X. (2021). VPS35 D620N knockin mice recapitulate cardinal features of Parkinson's disease. Aging Cell, e13347. 10.1111/acel.13347.

74. Yin, J., Liu, X., He, Q., Zhou, L., Yuan, Z., and Zhao, S. (2016). Vps35-dependent recycling of Trem2 regulates microglial function. Traffic *17*, 1286–1296. 10.1111/tra.12451.

75. Tremblay, M.-E., Cookson, M.R., and Civiero, L. (2019). Glial phagocytic clearance in Parkinson's disease. Mol Neurodegeneration *14*, 16. 10.1186/s13024-019-0314-8.

76. Tsika, E., Glauser, L., Moser, R., Fiser, A., Daniel, G., Sheerin, U.-M., Lees, A., Troncoso, J.C., Lewis, P.A., Bandopadhyay, R., et al. (2014). Parkinson's disease-linked mutations in VPS35 induce dopaminergic neurodegeneration. Hum Mol Genet *23*, 4621–4638. 10.1093/hmg/ddu178.

77. Wen, L., Tang, F.-L., Hong, Y., Luo, S.-W., Wang, C.-L., He, W., Shen, C., Jung, J.-U., Xiong, F., Lee, D., et al. (2011). VPS35 haploinsufficiency increases Alzheimer's disease neuropathology. Journal of Cell Biology *195*, 765–779. 10.1083/jcb.201105109.

78. Ishizu, N., Yui, D., Hebisawa, A., Aizawa, H., Cui, W., Fujita, Y., Hashimoto, K., Ajioka, I., Mizusawa, H., Yokota, T., et al. (2016). Impaired striatal dopamine release in homozygous Vps35 D620N knock-in mice. Human Molecular Genetics *25*, 4507–4517. 10.1093/hmg/ddw279.

79. Liu, W., Tang, F.-L., Erion, J., Xiao, H., Ye, J., and Xiong, W.-C. (2014). Vps35 haploinsufficiency results in degenerative-like deficit in mouse retinal ganglion neurons and impairment of optic nerve injury-induced gliosis. Mol Brain *7*, 10. 10.1186/1756-6606-7-10.

80. Jiang, M., Tu, H.-T., Zhang, K., Zhang, W., Yu, W.-P., Xu, J., Tan, E.-K., Guo, K.-H., and Zeng, L. (2021). Impaired neurogenesis in the hippocampus of an adult VPS35 mutant mouse model of Parkinson's disease through interaction with APP. Neurobiology of Disease *153*, 105313. 10.1016/j.nbd.2021.105313.

81. Inoshita, T., Arano, T., Hosaka, Y., Meng, H., Umezaki, Y., Kosugi, S., Morimoto, T., Koike, M., Chang, H.-Y., Imai, Y., et al. (2017). Vps35 in cooperation with LRRK2 regulates synaptic vesicle endocytosis through the endosomal pathway in Drosophila. Hum. Mol. Genet. *26*, 2933–2948. 10.1093/hmg/ddx179.

82. Wang, C.-L., Tang, F.-L., Peng, Y., Shen, C.-Y., Mei, L., and Xiong, W.-C. (2012). VPS35 regulates developing mouse hippocampal neuronal morphogenesis by promoting retrograde trafficking of BACE1. Biology Open *1*, 1248–1257. 10.1242/bio.20122451.

83. Zhao, Y., Lee, D., Zhu, X.-J., and Xiong, W.-C. (2022). Critical Role of Neuronal Vps35 in Blood Vessel Branching and Maturation in Developing Mouse Brain. Biomedicines *10*, 1653. 10.3390/biomedicines10071653.

84. Tang, F.-L., Zhao, L., Zhao, Y., Sun, D., Zhu, X.-J., Mei, L., and Xiong, W.-C. (2020). Coupling of terminal differentiation deficit with neurodegenerative pathology in Vps35-deficient pyramidal neurons. Cell Death & Differentiation *27*, 2099–2116. 10.1038/s41418-019-0487-2.

85. Tang, F.-L., Liu, W., Hu, J.-X., Erion, J.R., Ye, J., Mei, L., and Xiong, W.-C. (2015). VPS35 Deficiency or Mutation Causes Dopaminergic Neuronal Loss by Impairing Mitochondrial Fusion and Function. Cell Rep *12*, 1631–1643. 10.1016/j.celrep.2015.08.001.

86. Belenkaya, T.Y., Wu, Y., Tang, X., Zhou, B., Cheng, L., Sharma, Y.V., Yan, D., Selva, E.M., and Lin, X. (2008). The Retromer Complex Influences Wnt Secretion by Recycling Wntless from Endosomes to the Trans-Golgi Network. Developmental Cell *14*, 120–131. 10.1016/j.devcel.2007.12.003.

87. Chiu, C.-C., Weng, Y.-H., Huang, Y.-Z., Chen, R.-S., Liu, Y.-C., Yeh, T.-H., Lu, C.-S., Lin, Y.-W., Chen, Y.-J., Hsu, C.-C., et al. (2020). (D620N) VPS35 causes the impairment of Wnt/β-catenin signaling cascade and mitochondrial dysfunction in a PARK17 knockin mouse model. Cell Death & Disease *11*, 1–14. 10.1038/s41419-020-03228-9.

88. Li, J.-G., Chiu, J., Ramanjulu, M., Blass, B.E., and Praticò, D. (2020). A pharmacological chaperone improves memory by reducing Aβ and tau neuropathology in a mouse model with plaques and tangles. Mol Neurodegeneration *15*, 1. 10.1186/s13024-019-0350-4.

89. Zhang, Q., Wu, X., Chen, P., Liu, L., Xin, N., Tian, Y., and Dillin, A. (2018). The mitochondrial unfolded protein response is mediated cell-non-autonomously by retromer-dependent Wnt signaling. Cell *174*, 870-883.e17. 10.1016/j.cell.2018.06.029.

90. Serafino, A., Giovannini, D., Rossi, S., and Cozzolino, M. (2020). Targeting the Wnt/β-catenin pathway in neurodegenerative diseases: recent approaches and current challenges. Expert Opinion on Drug Discovery *15*, 803–822. 10.1080/17460441.2020.1746266.

91. Prasad, B.C., and Clark, S.G. (2006). Wnt signaling establishes anteroposterior neuronal polarity and requires retromer in *C. elegans*. Development *133*, 1757–1766. 10.1242/dev.02357.

92. Bhalla, A., Vetanovetz, C.P., Morel, E., Chamoun, Z., Di Paolo, G., and Small, S.A. (2012). The location and trafficking routes of the neuronal retromer and its role in amyloid precursor protein transport. Neurobiol. Dis. *47*, 126–134. 10.1016/j.nbd.2012.03.030.

93. Vazquez-Sanchez, S., Bobeldijk, S., Dekker, M.P., Van Keimpema, L., and Van Weering, J.R.T. (2018). VPS35 depletion does not impair presynaptic structure and function. Sci Rep *8*, 2996. 10.1038/s41598-018-20448-4.

94. Wu, S., Fagan, R.R., Uttamapinant, C., Lifshitz, L.M., Fogarty, K.E., Ting, A.Y., and Melikian, H.E. (2017). The Dopamine Transporter Recycles via a Retromer-Dependent Postendocytic Mechanism: Tracking Studies Using a Novel Fluorophore-Coupling Approach. J. Neurosci. *37*, 9438–9452. 10.1523/JNEUROSCI.3885-16.2017.

95. Wu, Q., Xu, H., Wang, W., Chang, F., Jiang, Y., and Liu, Y. (2016). Retrograde trafficking of VMAT2 and its role in protein stability in non-neuronal cells. J Biomed Res *30*, 502–509. 10.7555/JBR.30.20160061.

96. Tan, W., Zhang, J., Liu, L., Liang, M., Li, J., Deng, Z., Zheng, Z., Deng, Y., Liu, C., Li, Y., et al. (2022). Hsp90 Inhibitor STA9090 induced VPS35 related extracellular vesicle release and metastasis in hepatocellular carcinoma. Translational Oncology *26*, 101502. 10.1016/j.tranon.2022.101502.

97. Walsh, R.B., Dresselhaus, E.C., Becalska, A.N., Zunitch, M.J., Blanchette, C.R., Scalera, A.L., Lemos, T., Lee, S.M., Apiki, J., Wang, S., et al. (2021). Opposing functions for retromer and Rab11 in extracellular vesicle traffic at presynaptic terminals. J Cell Biol *220*. 10.1083/jcb.202012034.

98. Winklhofer, K.F., and Haass, C. (2010). Mitochondrial dysfunction in Parkinson's disease. Biochimica et Biophysica Acta (BBA) - Molecular Basis of Disease *1802*, 29–44. 10.1016/j.bbadis.2009.08.013.

99. Chan, D.C. (2006). Mitochondrial fusion and fission in mammals. Annu. Rev. Cell Dev. Biol. *22*, 79–99. 10.1146/annurev.cellbio.22.010305.104638.

100. Wang, W., Wang, X., Fujioka, H., Hoppel, C., Whone, A.L., Caldwell, M.A., Cullen, P.J., Liu, J., and Zhu, X. (2016). Parkinson's disease-associated mutant VPS35 causes mitochondrial dysfunction by recycling DLP1 complexes. Nat Med *22*, 54–63. 10.1038/nm.3983.

101. Wang, W., Ma, X., Zhou, L., Liu, J., and Zhu, X. (2017). A conserved retromer sorting motif is essential for mitochondrial DLP1 recycling by VPS35 in Parkinson's disease model. Hum. Mol. Genet. *26*, 781–789. 10.1093/hmg/ddw430.

102. Jimenez-Orgaz, A., Kvainickas, A., Nägele, H., Denner, J., Eimer, S., Dengjel, J., and Steinberg, F. (2018). Control of RAB7 activity and localization through the retromer-TBC1D5 complex enables RAB7-dependent mitophagy. The EMBO Journal *37*, 235–254. 10.15252/embj.201797128.

103. Bellomo, G., Paciotti, S., Gatticchi, L., and Parnetti, L. (2020). The vicious cycle between α-synuclein aggregation and autophagic-lysosomal dysfunction. Mov Disord *35*, 34–44. 10.1002/mds.27895.

104. MacLeod, D.A., Rhinn, H., Kuwahara, T., Zolin, A., Di Paolo, G., McCabe, B.D., MacCabe, B.D., Marder, K.S., Honig, L.S., Clark, L.N., et al. (2013). RAB7L1 interacts with LRRK2 to modify intraneuronal protein sorting and Parkinson's disease risk. Neuron *77*, 425–439. 10.1016/j.neuron.2012.11.033.

105. Maruzs, T., Lőrincz, P., Szatmári, Z., Széplaki, S., Sándor, Z., Lakatos, Z., Puska, G., Juhász, G., and Sass, M. (2015). Retromer Ensures the Degradation of Autophagic Cargo by Maintaining Lysosome Function in Drosophila. Traffic *16*, 1088–1107. 10.1111/tra.12309.

106. Huang, Y., Chen, X., He, X., Guo, C., Sun, X., Liang, F., Long, S., Lu, X., Feng, L., Guo, W., et al. (2017). High expression levels of the D686N Parkinson's disease mutation in VPS35 induces α-synuclein-dependent toxicity in yeast. Mol Med Rep *16*, 254–262. 10.3892/mmr.2017.6551.

107. Gao, L., Xiao, H., Ai, L.-Q.-Y., Chen, C., Lin, S., Zhou, Y., Ye, J., and Liu, W. (2020). Vps35 Deficiency Impairs Cdk5/p35 Degradation and Promotes the Hyperphosphorylation of Tau Protein in Retinal Ganglion Cells. Invest Ophthalmol Vis Sci *61*, 1. 10.1167/iovs.61.1.1.

108. Tofaris, G.K. (2012). Lysosome-dependent pathways as a unifying theme in Parkinson's disease. Movement Disorders *27*, 1364–1369. 10.1002/mds.25136.

109. Vogiatzi, T., Xilouri, M., Vekrellis, K., and Stefanis, L. (2008). Wild type alpha-synuclein is degraded by chaperone-mediated autophagy and macroautophagy in neuronal cells. J. Biol. Chem. *283*, 23542–23556. 10.1074/jbc.M801992200.

110. Tang, F.-L., Erion, J.R., Tian, Y., Liu, W., Yin, D.-M., Ye, J., Tang, B., Mei, L., and Xiong, W.-C. (2015). VPS35 in Dopamine Neurons Is Required for Endosome-to-Golgi Retrieval of Lamp2a, a Receptor of Chaperone-Mediated Autophagy That Is Critical for α-Synuclein Degradation and Prevention of Pathogenesis of Parkinson's Disease. J. Neurosci. *35*, 10613–10628. 10.1523/JNEUROSCI.0042-15.2015.

111. Miura, E., Hasegawa, T., Konno, M., Suzuki, M., Sugeno, N., Fujikake, N., Geisler, S., Tabuchi, M., Oshima, R., Kikuchi, A., et al. (2014). VPS35 dysfunction impairs lysosomal degradation of α-synuclein and exacerbates neurotoxicity in a Drosophila model of Parkinson's disease. Neurobiol Dis *71*, 1–13. 10.1016/j.nbd.2014.07.014.

112. Ravussin, A., Brech, A., Tooze, S.A., and Stenmark, H. (2021). The phosphatidylinositol 3-phosphate-binding protein SNX4 controls ATG9A recycling and autophagy. J Cell Sci *134*. 10.1242/jcs.250670.

113. Zavodszky, E., Seaman, M.N.J., Moreau, K., Jimenez-Sanchez, M., Breusegem, S.Y., Harbour, M.E., and Rubinsztein, D.C. (2014). Mutation in VPS35 associated with Parkinson's disease impairs WASH complex association and inhibits autophagy. Nat Commun *5*, 3828. 10.1038/ncomms4828.

114. Ibata, K., and Yuzaki, M. (2021). Destroy the old to build the new: Activity-dependent lysosomal exocytosis in neurons. Neuroscience Research *167*, 38–46. 10.1016/j.neures.2021.03.011.

115. Steger, M., Tonelli, F., Ito, G., Davies, P., Trost, M., Vetter, M., Wachter, S., Lorentzen, E., Duddy, G., Wilson, S., et al. (2016). Phosphoproteomics reveals that Parkinson's disease kinase LRRK2 regulates a subset of Rab GTPases. Elife *5*. 10.7554/eLife.12813.

116. Reczek, D., Schwake, M., Schröder, J., Hughes, H., Blanz, J., Jin, X., Brondyk, W., Van Patten, S., Edmunds, T., and Saftig, P. (2007). LIMP-2 Is a Receptor for Lysosomal Mannose-6-Phosphate-Independent Targeting of β-Glucocerebrosidase. Cell *131*, 770–783. 10.1016/j.cell.2007.10.018.

117. Zhao, Y., Perera, G., Takahashi-Fujigasaki, J., Mash, D.C., Vonsattel, J.P.G., Uchino, A., Hasegawa, K., Jeremy Nichols, R., Holton, J.L., Murayama, S., et al. (2018). Reduced LRRK2 in association with retromer dysfunction in post-mortem brain tissue from LRRK2 mutation carriers. Brain *141*, 486–495. 10.1093/brain/awx344.

118. Kuo, S.-H., Tasset, I., Cuervo, A.M., and Sulzer, D. (2022). Misfolded GBA/β-glucocerebrosidase impairs ER-quality control by chaperone-mediated autophagy in Parkinson disease. Autophagy *18*, 3050–3052. 10.1080/15548627.2022.2071383.

119. Leneva, N., Kovtun, O., Morado, D.R., Briggs, J.A.G., and Owen, D.J. (2021). Architecture and mechanism of metazoan retromer:SNX3 tubular coat assembly. Sci. Adv. *7*, eabf8598. 10.1126/sciadv.abf8598.

120. Kovtun, O., Leneva, N., Bykov, Y.S., Ariotti, N., Teasdale, R.D., Schaffer, M., Engel, B.D., Owen, David.J., Briggs, J.A.G., and Collins, B.M. (2018). Structure of the membrane-assembled retromer coat determined by cryo-electron tomography. Nature *561*, 561–564. 10.1038/s41586-018-0526-z.

121. Hierro, A., Rojas, A.L., Rojas, R., Murthy, N., Effantin, G., Kajava, A.V., Steven, A.C., Bonifacino, J.S., and Hurley, J.H. (2007). Functional architecture of the retromer cargo-recognition complex. Nature *449*, 1063–1067. 10.1038/nature06216.

122. Chen, X., Kordich, J.K., Williams, E.T., Levine, N., Cole-Strauss, A., Marshall, L., Labrie, V., Ma, J., Lipton, J.W., and Moore, D.J. (2019). Parkinson's disease-linked D620N VPS35 knockin mice manifest tau neuropathology and dopaminergic neurodegeneration. PNAS *116*, 5765–5774. 10.1073/pnas.1814909116.

123. McGough, I.J., Steinberg, F., Jia, D., Barbuti, P.A., McMillan, K.J., Heesom, K.J., Whone, A.L., Caldwell, M.A., Billadeau, D.D., Rosen, M.K., et al. (2014). Retromer Binding to FAM21 and the WASH Complex Is Perturbed by the Parkinson Disease-Linked VPS35(D620N) Mutation. Current Biology *24*, 1670–1676. 10.1016/j.cub.2014.06.024.

124. Kvainickas, A., Jimenez-Orgaz, A., Nägele, H., Hu, Z., Dengjel, J., and Steinberg, F. (2017). Cargo-selective SNX-BAR proteins mediate retromer trimer independent retrograde transport. Journal of Cell Biology *216*, 3677–3693. 10.1083/jcb.201702137.

125. Derivery, E., Sousa, C., Gautier, J.J., Lombard, B., Loew, D., and Gautreau, A. (2009). The Arp2/3 Activator WASH Controls the Fission of Endosomes through a Large Multiprotein Complex. Developmental Cell *17*, 712–723. 10.1016/j.devcel.2009.09.010.

126. Wang, F., Zhang, L., Zhang, G.-L., Wang, Z.-B., Cui, X.-S., Kim, N.-H., and Sun, S.-C. (2014). WASH complex regulates Arp2/3 complex for actin-based polar body extrusion in mouse oocytes. Sci Rep *4*, 5596. 10.1038/srep05596.

127. Freeman, C.L., Hesketh, G., and Seaman, M.N.J. (2014). RME-8 coordinates the WASH complex with the retromer SNX-BAR dimer to control endosomal tubulation. Journal of Cell Science, jcs.144659. 10.1242/jcs.144659.

128. Seaman, M.N.J., Gautreau, A., and Billadeau, D.D. (2013). Retromer-mediated endosomal protein sorting: all WASHed up! Trends in Cell Biology *23*, 522–528. 10.1016/j.tcb.2013.04.010.

129. Hanss, Z., Larsen, S.B., Antony, P., Mencke, P., Massart, F., Jarazo, J., Schwamborn, J.C., Barbuti, P.A., Mellick, G.D., and Krüger, R. (2021). Mitochondrial and Clearance Impairment in p.D620N VPS35 Patient-Derived Neurons. Movement Disorders *36*, 704–715. https://doi.org/10.1002/mds.28365.

130. Vanan, S., Zeng, X., Chia, S.Y., Varnäs, K., Jiang, M., Zhang, K., Saw, W.T., Padmanabhan, P., Yu, W.-P., Zhou, Z.-D., et al. (2020). Altered striatal dopamine levels in Parkinson's disease VPS35 D620N mutant transgenic aged mice. Mol Brain *13*, 164. 10.1186/s13041-020-00704-3.

131. Jensen, T.P., Zheng, K., Cole, N., Marvin, J.S., Looger, L.L., and Rusakov, D.A. (2019). Multiplex imaging relates quantal glutamate release to presynaptic Ca2+ homeostasis at multiple synapses in situ. Nat Commun *10*, 1414. 10.1038/s41467-019-09216-8.

132. Giansante, G., Marte, A., Romei, A., Prestigio, C., Onofri, F., Benfenati, F., Baldelli, P., and Valente, P. (2020). Presynaptic L-Type Ca $^{2+}$ Channels Increase Glutamate Release Probability and Excitatory Strength in the Hippocampus during Chronic Neuroinflammation. J. Neurosci. *40*, 6825–6841. 10.1523/JNEUROSCI.2981-19.2020.

133. Sun, X.-D., Chen, W.-B., Sun, D., Huang, J., Li, Y.-Q., Pan, J.-X., Wang, Y.-N., Zhao, K., Dong, Z.-Q., Wang, H.-S., et al. (2018). Neogenin in Amygdala for Neuronal Activity and Information Processing. J. Neurosci. *38*, 9600–9613. 10.1523/JNEUROSCI.0433-18.2018.

134. Lin, P.-Y., Chen, L.Y., Zhou, P., Lee, S.-J., Trotter, J.H., and Südhof, T.C. (2023). Neurexin-2 restricts synapse numbers and restrains the presynaptic release probability by an alternative splicing-dependent mechanism. Proc. Natl. Acad. Sci. U.S.A. *120*, e2300363120. 10.1073/pnas.2300363120.

135. Lisman, J.E., Raghavachari, S., and Tsien, R.W. (2007). The sequence of events that underlie quantal transmission at central glutamatergic synapses. Nat Rev Neurosci *8*, 597–609. 10.1038/nrn2191.

136. Wilson, N.R., Kang, J., Hueske, E.V., Leung, T., Varoqui, H., Murnick, J.G., Erickson, J.D., and Liu, G. (2005). Presynaptic Regulation of Quantal Size by the Vesicular Glutamate Transporter VGLUT1. J. Neurosci. *25*, 6221–6234. 10.1523/JNEUROSCI.3003-04.2005.

137. Wadiche, J.I., and Jahr, C.E. (2001). Multivesicular Release at Climbing Fiber-Purkinje Cell Synapses. Neuron *32*, 301–313. 10.1016/S0896-6273(01)00488-3.

138. Oertner, T.G., Sabatini, B.L., Nimchinsky, E.A., and Svoboda, K. (2002). Facilitation at single synapses probed with optical quantal analysis. Nat Neurosci *5*, 657–664. 10.1038/nn867.

139. Serrano-Saiz, E., Vogt, M.C., Levy, S., Wang, Y., Kaczmarczyk, K.K., Mei, X., Bai, G., Singson, A., Grant, B.D., and Hobert, O. (2020). SLC17A6/7/8 Vesicular Glutamate Transporter Homologs in Nematodes. Genetics *214*, 163–178. 10.1534/genetics.119.302855.

140. Kavalali, E.T. (2015). The mechanisms and functions of spontaneous neurotransmitter release. Nat Rev Neurosci *16*, 5–16. 10.1038/nrn3875.

141. Peled, E.S., Newman, Z.L., and Isacoff, E.Y. (2014). Evoked and Spontaneous Transmission Favored by Distinct Sets of Synapses. Current Biology *24*, 484–493. 10.1016/j.cub.2014.01.022.

142. Peng, A., Rotman, Z., Deng, P.-Y., and Klyachko, V.A. (2012). Differential Motion Dynamics of Synaptic Vesicles Undergoing Spontaneous and Activity-Evoked Endocytosis. Neuron *73*, 1108–1115. 10.1016/j.neuron.2012.01.023.

143. Kim, Y., Lee, U., Choi, C., and Chang, S. (2020). Release Mode Dynamically Regulates the RRP Refilling Mechanism at Individual Hippocampal Synapses. J. Neurosci. *40*, 8426–8437. 10.1523/JNEUROSCI.3029-19.2020.

144. Tran, V., Miki, T., and Marty, A. (2022). Three small vesicular pools in sequence govern synaptic response dynamics during action potential trains. Proc. Natl. Acad. Sci. U.S.A. *119*, e2114469119. 10.1073/pnas.2114469119.

145. Logsdon, S., Johnstone, A.F.M., Viele, K., and Cooper, R.L. (2006). Regulation of synaptic vesicles pools within motor nerve terminals during short-term facilitation and neuromodulation. Journal of Applied Physiology *100*, 662–671. 10.1152/japplphysiol.00580.2005.

146. Wu, W.-H., and Cooper, R.L. (2012). The regulation and packaging of synaptic vesicles as related to recruitment within glutamatergic synapses. Neuroscience *225*, 185–198. 10.1016/j.neuroscience.2012.08.037.

147. Rothstein, J.D., Dykes-Hoberg, M., Pardo, C.A., Bristol, L.A., Jin, L., Kuncl, R.W., Kanai, Y., Hediger, M.A., Wang, Y., Schielke, J.P., et al. (1996). Knockout of Glutamate Transporters Reveals a Major Role for Astroglial Transport in Excitotoxicity and Clearance of Glutamate. Neuron *16*, 675–686. 10.1016/S0896-6273(00)80086-0.

148. Armbruster, M., Hanson, E., and Dulla, C.G. (2016). Glutamate Clearance Is Locally Modulated by Presynaptic Neuronal Activity in the Cerebral Cortex. J. Neurosci. *36*, 10404–10415. 10.1523/JNEUROSCI.2066-16.2016.

149. Swanson, G.T., Kamboj, S.K., and Cull-Candy, S.G. (1997). Single-Channel Properties of Recombinant AMPA Receptors Depend on RNA Editing, Splice Variation, and Subunit Composition. J. Neurosci. *17*, 58–69. 10.1523/JNEUROSCI.17-01-00058.1997.

150. Bowie, D., and Mayer, M.L. (1995). Inward rectification of both AMPA and kainate subtype glutamate receptors generated by polyamine-mediated ion channel block. Neuron *15*, 453–462. 10.1016/0896-6273(95)90049-7.

151. Bowie, D. (2012). Redefining the classification of AMPA-selective ionotropic glutamate receptors: Counting the number of AMPA receptor subtypes. The Journal of Physiology *590*, 49–61. 10.1113/jphysiol.2011.221689.

152. Cathala, L., Holderith, N.B., Nusser, Z., DiGregorio, D.A., and Cull-Candy, S.G. (2005). Changes in synaptic structure underlie the developmental speeding of AMPA receptor–mediated EPSCs. Nat Neurosci *8*, 1310–1318. 10.1038/nn1534.

153. Rall, W. (1977). Core Conductor Theory and Cable Properties of Neurons. In Comprehensive Physiology, R. Terjung, ed. (Wiley), pp. 39–97. 10.1002/cphy.cp010103.

154. Kandel, E.R. (2013). Membrane Potential and the Passive Electrical Properties of the Neuron. In Principles of Neural Science (McGraw-Hill), pp. 126–147.

155. Holmes, W.R. (2015). Time Constant, Tau, in Neuronal Signaling. In Encyclopedia of Computational Neuroscience, D. Jaeger and R. Jung, eds. (Springer New York), pp. 2965–2966. 10.1007/978-1-4614-6675-8_37.

156. Flurkey, K., Mcurrer, J., and Harrison, D. (2007). Mouse Models in Aging Research. In The Mouse in Biomedical Research (Elsevier), pp. 637–672. 10.1016/B978-012369454-6/50074-1.

157. Hill, M.P., and Brotchie, J.M. (1995). Modulation of glutamate release by a κ-opioid receptor agonist in rodent and primate striatum. European Journal of Pharmacology *281*, R1–R2. 10.1016/0014-2999(95)00385-X.

158. Ferré, S., Sarasola, L.I., Quiroz, C., and Ciruela, F. (2023). Presynaptic adenosine receptor heteromers as key modulators of glutamatergic and dopaminergic neurotransmission in the striatum. Neuropharmacology *223*, 109329. 10.1016/j.neuropharm.2022.109329.

159. Köfalvi, A., Moreno, E., Cordomí, A., Cai, N.-S., Fernández-Dueñas, V., Ferreira, S.G., Guixà-González, R., Sánchez-Soto, M., Yano, H., Casadó-Anguera, V., et al. (2020). Control of glutamate release by complexes of adenosine and cannabinoid receptors. BMC Biol *18*, 9. 10.1186/s12915-020-0739-0.

160. Howe, W.M., Young, D.A., Bekheet, G., and Kozak, R. (2016). Nicotinic receptor subtypes differentially modulate glutamate release in the dorsal medial striatum. Neurochemistry International *100*, 30–34. 10.1016/j.neuint.2016.08.009.

161. Zhou, F.-M. (2020). The striatal medium spiny neurons: what they are and how they link with Parkinson's disease. In Genetics, Neurology, Behavior, and Diet in Parkinson's Disease (Elsevier), pp. 395–412. 10.1016/B978-0-12-815950-7.00025-4.

162. Plenz, D., and Wickens, J.R. (2016). The Striatal Skeleton: Medium Spiny Projection Neurons and Their Lateral Connections. In Handbook of Behavioral Neuroscience (Elsevier), pp. 121–136. 10.1016/B978-0-12-802206-1.00006-4.

163. Milnerwood, A.J., Gladding, C.M., Pouladi, M.A., Kaufman, A.M., Hines, R.M., Boyd, J.D., Ko, R.W.Y., Vasuta, O.C., Graham, R.K., Hayden, M.R., et al. (2010). Early increase in extrasynaptic NMDA receptor signaling and expression contributes to phenotype onset in Huntington's disease mice. Neuron *65*, 178–190. 10.1016/j.neuron.2010.01.008.

164. Milnerwood, A.J., and Raymond, L.A. (2007). Corticostriatal synaptic function in mouse models of Huntington's disease: early effects of huntingtin repeat length and protein load: Corticostriatal synaptic function in Huntington's disease. The Journal of Physiology *585*, 817–831. 10.1113/jphysiol.2007.142448.

165. Ding, J., Peterson, J.D., and Surmeier, D.J. (2008). Corticostriatal and Thalamostriatal Synapses Have Distinctive Properties. Journal of Neuroscience *28*, 6483–6492. 10.1523/JNEUROSCI.0435-08.2008.

166. Smeal, R.M., Gaspar, R.C., Keefe, K.A., and Wilcox, K.S. (2007). A rat brain slice preparation for characterizing both thalamostriatal and corticostriatal afferents. Journal of Neuroscience Methods *159*, 224–235. 10.1016/j.jneumeth.2006.07.007.

167. Kolodziejczyk, K., and Raymond, L.A. (2016). Differential changes in thalamic and cortical excitatory synapses onto striatal spiny projection neurons in a Huntington disease mouse model. Neurobiology of Disease *86*, 62–74. 10.1016/j.nbd.2015.11.020.

168. Jackman, S.L., Beneduce, B.M., Drew, I.R., and Regehr, W.G. (2014). Achieving High-Frequency Optical Control of Synaptic Transmission. J. Neurosci. *34*, 7704–7714. 10.1523/JNEUROSCI.4694-13.2014.

169. Meng, X., Murali, S., Cheng, Y.-F., Lu, J., Hight, A.E., Kanumuri, V.V., Brown, M.C., Holt, J.R., Lee, D.J., and Edge, A.S.B. (2019). Increasing the expression level of ChR2 enhances the optogenetic excitability of cochlear neurons. Journal of Neurophysiology *122*, 1962–1974. 10.1152/jn.00828.2018.

170. He, T., Itano, M.S., Earley, L.F., Hall, N.E., Riddick, N., Samulski, R.J., and Li, C. (2019). The Influence of Murine Genetic Background in Adeno-Associated Virus Transduction of the Mouse Brain. Human Gene Therapy Clinical Development *30*, 169–181. 10.1089/humc.2019.030.

171. Tanimura, A., Shen, W., Wokosin, D., and Surmeier, D.J. (2022). Pathway-Specific Remodeling of Thalamostriatal Synapses in a Mouse Model of Parkinson's Disease. Movement Disorders *37*, 1164–1174. 10.1002/mds.29030.

172. Liévens, J.-C., Salin, P., Had-Aissouni, L., Mahy, N., and Goff, L.K.-L. (2000). Differential Effects of Corticostriatal and Thalamostriatal Deafferentation on Expression of the Glutamate Transporter GLT1 in the Rat Striatum. Journal of Neurochemistry *74*, 909–919. 10.1046/j.1471-4159.2000.0740909.x.

173. Cai, Y., and Ford, C.P. (2018). Dopamine Cells Differentially Regulate Striatal Cholinergic Transmission across Regions through Corelease of Dopamine and Glutamate. Cell Reports *25*, 3148-3157.e3. 10.1016/j.celrep.2018.11.053.

174. Stuber, G.D., Hnasko, T.S., Britt, J.P., Edwards, R.H., and Bonci, A. (2010). Dopaminergic Terminals in the Nucleus Accumbens But Not the Dorsal Striatum Corelease Glutamate. Journal of Neuroscience *30*, 8229–8233. 10.1523/JNEUROSCI.1754-10.2010.

175. Lee, H.J., Weitz, A.J., Bernal-Casas, D., Duffy, B.A., Choy, M., Kravitz, A.V., Kreitzer, A.C., and Lee, J.H. (2016). Activation of Direct and Indirect Pathway Medium Spiny Neurons Drives Distinct Brain-wide Responses. Neuron *91*, 412–424. 10.1016/j.neuron.2016.06.010.

176. Burkhardt, J.M. (2009). Dissociable effects of dopamine on neuronal firing rate and synchrony in the dorsal striatum. Front. Integr. Neurosci. *3*. 10.3389/neuro.07.028.2009.

177. Cui, G., Jun, S.B., Jin, X., Pham, M.D., Vogel, S.S., Lovinger, D.M., and Costa, R.M. (2013). Concurrent activation of striatal direct and indirect pathways during action initiation. Nature *494*, 238–242. 10.1038/nature11846.

178. Shen, W., Flajolet, M., Greengard, P., and Surmeier, D.J. (2008). Dichotomous Dopaminergic Control of Striatal Synaptic Plasticity. Science *321*, 848–851. 10.1126/science.1160575.

179. Kravitz, A.V., Freeze, B.S., Parker, P.R.L., Kay, K., Thwin, M.T., Deisseroth, K., and Kreitzer, A.C. (2010). Regulation of parkinsonian motor behaviours by optogenetic control of basal ganglia circuitry. Nature *466*, 622–626. 10.1038/nature09159.

180. Cerri, S., Mus, L., and Blandini, F. (2019). Parkinson's Disease in Women and Men: What's the Difference? JPD *9*, 501–515. 10.3233/JPD-191683.

181. Gillies, G.E., Pienaar, I.S., Vohra, S., and Qamhawi, Z. (2014). Sex differences in Parkinson's disease. Frontiers in Neuroendocrinology *35*, 370–384. 10.1016/j.yfrne.2014.02.002.

182. Pitts, E.G., Stowe, T.A., Christensen, B.A., and Ferris, M.J. (2020). Comparing dopamine release, uptake, and D2 autoreceptor function across the ventromedial to dorsolateral striatum in adolescent and adult male and female rats. Neuropharmacology *175*, 108163. 10.1016/j.neuropharm.2020.108163.

183. Logrip, M.L., and Gainey, S.C. (2020). Sex differences in the long-term effects of past stress on alcohol self-administration, glucocorticoid sensitivity and phosphodiesterase 10A expression. Neuropharmacology *164*, 107857. 10.1016/j.neuropharm.2019.107857.

184. Quigley, J.A., and Becker, J.B. (2021). Activation of G-protein coupled estradiol receptor 1 in the dorsolateral striatum attenuates preference for cocaine and saccharin in male but not female rats. Hormones and Behavior *130*, 104949. 10.1016/j.yhbeh.2021.104949.

185. Rangel-Barajas, C., Boehm, S.L., and Logrip, M.L. (2021). Altered excitatory transmission in striatal neurons after chronic ethanol consumption in selectively bred crossed high alcohol-preferring mice. Neuropharmacology *190*, 108564. 10.1016/j.neuropharm.2021.108564.

186. Huang, Y., Huang, H., Zhou, L., Li, J., Chen, X., Thomas, J., He, X., Guo, W., Zeng, Y., Low, B.C., et al. (2022). Mutant VPS35-D620N induces motor dysfunction and impairs DAT-mediated dopamine recycling pathway. Hum Mol Genet *31*, 3886–3896. 10.1093/hmg/ddac142.

187. Venton, B.J., and Cao, Q. (2020). Fundamentals of fast-scan cyclic voltammetry for dopamine detection. Analyst *145*, 1158–1168. 10.1039/C9AN01586H.

188. Bath, B.D., Michael, D.J., Trafton, B.J., Joseph, J.D., Runnels, P.L., and Wightman, R.M. (2000). Subsecond Adsorption and Desorption of Dopamine at Carbon-Fiber Microelectrodes. Anal. Chem. *72*, 5994–6002. 10.1021/ac000849y.

189. Salinas, A.G., Lee, J.O., Augustin, S.M., Zhang, S., Patriarchi, T., Tian, L., Morales, M., Mateo, Y., and Lovinger, D.M. (2023). Distinct sub-second dopamine signaling in dorsolateral striatum measured by a genetically-encoded fluorescent sensor. Nat Commun *14*, 5915. 10.1038/s41467-023-41581-3.

190. Mamaligas, A.A., Barcomb, K., and Ford, C.P. (2019). Cholinergic Transmission at Muscarinic Synapses in the Striatum Is Driven Equally by Cortical and Thalamic Inputs. Cell Reports *28*, 1003-1014.e3. 10.1016/j.celrep.2019.06.077.

191. Threlfell, S., Lalic, T., Platt, N.J., Jennings, K.A., Deisseroth, K., and Cragg, S.J. (2012). Striatal dopamine release is triggered by synchronized activity in cholinergic interneurons. Neuron *75*, 58–64. 10.1016/j.neuron.2012.04.038.

192. Kramer, P.F., Brill-Weil, S.G., Cummins, A.C., Zhang, R., Camacho-Hernandez, G.A., Newman, A.H., Eldridge, M.A.G., Averbeck, B.B., and Khaliq, Z.M. (2022). Synaptic-like axo-axonal transmission from striatal cholinergic interneurons onto dopaminergic fibers. Neuron *110*, 2949-2960.e4. 10.1016/j.neuron.2022.07.011.

193. Liu, C., Cai, X., Ritzau-Jost, A., Kramer, P.F., Li, Y., Khaliq, Z.M., Hallermann, S., and Kaeser, P.S. (2022). An action potential initiation mechanism in distal axons for the control of dopamine release. Science *375*, 1378–1385. 10.1126/science.abn0532.

194. Stella, V.J., and Rajewski, R.A. (2020). Sulfobutylether-β-cyclodextrin. International Journal of Pharmaceutics *583*, 119396. 10.1016/j.ijpharm.2020.119396.

195. Pardeshi, C.V., Kothawade, R.V., Markad, A.R., Pardeshi, S.R., Kulkarni, A.D., Chaudhari, P.J., Longhi, M.R., Dhas, N., Naik, J.B., Surana, S.J., et al. (2023). Sulfobutylether-β-cyclodextrin: A functional biopolymer for drug delivery applications. Carbohydrate Polymers *301*, 120347. 10.1016/j.carbpol.2022.120347.

196. Wasser, C.R., Ertunc, M., Liu, X., and Kavalali, E.T. (2007). Cholesterol-dependent balance between evoked and spontaneous synaptic vesicle recycling: Synaptic cholesterol and vesicle recycling. The Journal of Physiology *579*, 413–429. 10.1113/jphysiol.2006.123133.

197. Yue, H.-Y., and Xu, J. (2015). Cholesterol regulates multiple forms of vesicle endocytosis at a mammalian central synapse. J. Neurochem. *134*, 247–260. 10.1111/jnc.13129.

198. Choi, T.-Y., Jung, S., Nah, J., Ko, H.-Y., Jo, S.-H., Chung, G., Park, K., Jung, Y.-K., and Choi, S.-Y. (2015). Low levels of methyl β-cyclodextrin disrupt GluA1-dependent synaptic potentiation but not synaptic depression. J. Neurochem. *132*, 276–285. 10.1111/jnc.12995.

199. Frech, M.J., Rabenstein, M., Bovensiepen, K., Rost, S., and Rolfs, A. (2015). Cyclodextrin Alters GABAergic Input to CA1 Pyramidal Cells in Wild-Type But Not in NPC1-Deficient Mice. BioResearch Open Access *4*, 358–362. 10.1089/biores.2015.0023.

200. Geda, O., Tábi, T., Lakatos, P.P., and Szökő, É. (2022). Differential Ganglioside and Cholesterol Depletion by Various Cyclodextrin Derivatives and Their Effect on Synaptosomal Glutamate Release. IJMS *23*, 9460. 10.3390/ijms23169460.

201. Qiuzi, W., Hongfei, X., Wei, W., Fei, C., Yu, J., and Yongjian, L. (2016). Retrograde trafficking of VMAT2 and its role in protein stabilityin non-neuronal cells. J Biomed Res *30*, 502. 10.7555/JBR.30.20160061.

202. Stansley, B.J., and Yamamoto, B.K. (2013). l-dopa-induced dopamine synthesis and oxidative stress in serotonergic cells. Neuropharmacology *67*, 243–251. 10.1016/j.neuropharm.2012.11.010.

203. Smith, W.W., Pei, Z., Jiang, H., Dawson, V.L., Dawson, T.M., and Ross, C.A. (2006). Kinase activity of mutant LRRK2 mediates neuronal toxicity. Nat Neurosci *9*, 1231–1233. 10.1038/nn1776.

204. Di Maio, R., Hoffman, E.K., Rocha, E.M., Keeney, M.T., Sanders, L.H., De Miranda, B.R., Zharikov, A., Van Laar, A., Stepan, A.F., Lanz, T.A., et al. (2018). LRRK2 activation in idiopathic Parkinson's disease. Sci Transl Med *10*. 10.1126/scitranslmed.aar5429.

205. Zhao, Y., and Dzamko, N. (2019). Recent Developments in LRRK2-Targeted Therapy for Parkinson's Disease. Drugs *79*, 1037–1051. 10.1007/s40265-019-01139-4.

206. Fell, M.J., Mirescu, C., Basu, K., Cheewatrakoolpong, B., DeMong, D.E., Ellis, J.M., Hyde, L.A., Lin, Y., Markgraf, C.G., Mei, H., et al. (2015). MLi-2, a Potent, Selective, and Centrally Active Compound for Exploring the Therapeutic Potential and Safety of LRRK2 Kinase Inhibition. J Pharmacol Exp Ther *355*, 397–409. 10.1124/jpet.115.227587.

207. Mercatelli, D., Bolognesi, P., Frassineti, M., Pisanò, C.A., Longo, F., Shimshek, D.R., and Morari, M. (2019). Leucine-rich repeat kinase 2 (LRRK 2) inhibitors differentially modulate glutamate release and Serine935 LRRK 2 phosphorylation in striatal and cerebrocortical synaptosomes. Pharmacol Res Perspect *7*, e00484. 10.1002/prp2.484.

208. Bu, M., Follett, J., Tatarnikov, I., Wall, S., Guenther, D., Deng, I., Wimsatt, G., Milnerwood, A., Moehle, M.S., Khoshbouei, H., et al. (2023). Inhibition of LRRK2 kinase activity rescues deficits in striatal dopamine dynamics in VPS35 p.D620N knock-in mice. Preprint in BioRxiv. 10.1101/2023.05.14.540654.

209. Pal, P., Taylor, M., Lam, P.Y., Tonelli, F., Hecht, C.A., Lis, P., Nirujogi, R.S., Phung, T.K., Dickie, E.A., Wightman, M., et al. (2023). Parkinson's VP535[D620N] mutation induces LRRK2 mediated lysosomal association of RILPL1 and TMEM55B. Preprint in BioRxiv 10.1101/2023.06.07.544051.

210. Steger, M., Diez, F., Dhekne, H.S., Lis, P., Nirujogi, R.S., Karayel, O., Tonelli, F., Martinez, T.N., Lorentzen, E., Pfeffer, S.R., et al. (2017). Systematic proteomic analysis of LRRK2-mediated Rab GTPase phosphorylation establishes a connection to ciliogenesis. eLife Sciences *6*, e31012. 10.7554/eLife.31012.

211. Bonet-Ponce, L., Beilina, A., Williamson, C.D., Lindberg, E., Kluss, J.H., Saez-Atienzar, S., Landeck, N., Kumaran, R., Mamais, A., Bleck, C.K.E., et al. (2020). LRRK2 mediates tubulation and vesicle sorting from lysosomes. Sci. Adv. *6*, eabb2454. 10.1126/sciadv.abb2454.

212. Bondy, S. (1989). Increased fragility of neuronal membranes with aging. Experimental Neurology *103*, 61–63. 10.1016/0014-4886(89)90185-4.

213. Colin, J., Thomas, M.H., Gregory-Pauron, L., Pinçon, A., Lanhers, M.-C., Corbier, C., Claudepierre, T., Yen, F.T., Oster, T., and Malaplate-Armand, C. (2017). Maintenance of membrane organization in the aging mouse brain as the determining factor for preventing receptor dysfunction and for improving response to anti-Alzheimer treatments. Neurobiology of Aging *54*, 84–93. 10.1016/j.neurobiolaging.2017.02.015.

214. Eguchi, T., Kuwahara, T., Sakurai, M., Komori, T., Fujimoto, T., Ito, G., Yoshimura, S., Harada, A., Fukuda, M., Koike, M., et al. (2018). LRRK2 and its substrate Rab GTPases are sequentially targeted onto stressed lysosomes and maintain their homeostasis. Proc. Natl. Acad. Sci. U.S.A. *115*. 10.1073/pnas.1812196115.

215. Komori, T., Kuwahara, T., Fujimoto, T., Sakurai, M., Koyama-Honda, I., Fukuda, M., and Iwatsubo, T. (2023). Phosphorylation of Rab29 at Ser185 regulates its localization and role in the lysosomal stress response in concert with LRRK2. Journal of Cell Science *136*, jcs261003. 10.1242/jcs.261003.

216. Kaksonen, M., and Roux, A. (2018). Mechanisms of clathrin-mediated endocytosis. Nat Rev Mol Cell Biol *19*, 313–326. 10.1038/nrm.2017.132.

217. Watanabe, S., Trimbuch, T., Camacho-Pérez, M., Rost, B.R., Brokowski, B., Söhl-Kielczynski, B., Felies, A., Davis, M.W., Rosenmund, C., and Jorgensen, E.M. (2014). Clathrin regenerates synaptic vesicles from endosomes. Nature *515*, 228–233. 10.1038/nature13846.

218. Arpino, G., Somasundaram, A., Shin, W., Ge, L., Villareal, S., Chan, C.Y., Ashery, U., Shupliakov, O., Taraska, J.W., and Wu, L.-G. (2022). Clathrin-mediated endocytosis cooperates with bulk endocytosis to generate vesicles. iScience *25*, 103809. 10.1016/j.isci.2022.103809.

219. Gad, H., Löw, P., Zotova, E., Brodin, L., and Shupliakov, O. (1998). Dissociation between Ca2+-Triggered Synaptic Vesicle Exocytosis and Clathrin-Mediated Endocytosis at a Central Synapse. Neuron *21*, 607–616. 10.1016/S0896-6273(00)80570-X.

220. Kokotos, A.C., Peltier, J., Davenport, E.C., Trost, M., and Cousin, M.A. (2018). Activity-dependent bulk endocytosis proteome reveals a key presynaptic role for the monomeric GTPase Rab11. Proc. Natl. Acad. Sci. U.S.A. *115*. 10.1073/pnas.1809189115.

221. Lee, S., Chang, J., and Blackstone, C. (2016). FAM21 directs SNX27–retromer cargoes to the plasma membrane by preventing transport to the Golgi apparatus. Nat Commun *7*, 10939. 10.1038/ncomms10939.

222. Kim, W.S., Kågedal, K., and Halliday, G.M. (2014). Alpha-synuclein biology in Lewy body diseases. Alz Res Therapy *6*, 73. 10.1186/s13195-014-0073-2.

223. Carosi, J.M., Hein, L.K., van den Hurk, M., Adams, R., Milky, B., Singh, S., Bardy, C., Denton, D., Kumar, S., and Sargeant, T.J. (2020). Retromer regulates the lysosomal clearance of MAPT/tau. Autophagy, 1–21. 10.1080/15548627.2020.1821545.

224. Kaushik, S., Tasset, I., Arias, E., Pampliega, O., Wong, E., Martinez-Vicente, M., and Cuervo, A.M. (2021). Autophagy and the hallmarks of aging. Ageing Research Reviews *72*, 101468. 10.1016/j.arr.2021.101468.

225. Braschi, E., Goyon, V., Zunino, R., Mohanty, A., Xu, L., and McBride, H.M. (2010). Vps35 Mediates Vesicle Transport between the Mitochondria and Peroxisomes. Current Biology *20*, 1310–1315. 10.1016/j.cub.2010.05.066.

226. Wang, W., Wang, X., Fujioka, H., Hoppel, C., Whone, A.L., Caldwell, M.A., Cullen, P.J., Liu, J., and Zhu, X. (2016). Parkinson's disease-associated mutant VPS35 causes mitochondrial dysfunction by recycling DLP1 complexes. Nat. Med. *22*, 54–63. 10.1038/nm.3983.

227. Devine, M.J., and Kittler, J.T. (2018). Mitochondria at the neuronal presynapse in health and disease. Nat Rev Neurosci *19*, 63–80. 10.1038/nrn.2017.170.

228. Todorova, V., and Blokland, A. (2017). Mitochondria and Synaptic Plasticity in the Mature and Aging Nervous System. CN *15*, 166–173. 10.2174/1570159X14666160414111821.

229. Thomas, C.I., Keine, C., Okayama, S., Satterfield, R., Musgrove, M., Guerrero-Given, D., Kamasawa, N., and Young, S.M. (2019). Presynaptic Mitochondria Volume and Abundance

Increase during Development of a High-Fidelity Synapse. J Neurosci *39*, 7994–8012. 10.1523/JNEUROSCI.0363-19.2019.

230. Giorgi, C., Marchi, S., Simoes, I.C.M., Ren, Z., Morciano, G., Perrone, M., Patalas-Krawczyk, P., Borchard, S., Jędrak, P., Pierzynowska, K., et al. (2018). Mitochondria and Reactive Oxygen Species in Aging and Age-Related Diseases. In International Review of Cell and Molecular Biology (Elsevier), pp. 209–344. 10.1016/bs.ircmb.2018.05.006.

231. Shpilka, T., and Haynes, C.M. (2018). The mitochondrial UPR: mechanisms, physiological functions and implications in ageing. Nat Rev Mol Cell Biol *19*, 109–120. 10.1038/nrm.2017.110.

232. Roque, M., Alves Rodrigues De Souza, D., Rangel-Sosa, M.M., Altounian, M., Hocine, M., Deloulme, J.-C., Barbier, E.L., Mann, F., and Chauvet, S. (2022). VPS35 deficiency in the embryonic cortex leads to prenatal cell loss and abnormal development of axonal connectivity. Molecular and Cellular Neuroscience *120*, 103726. 10.1016/j.mcn.2022.103726.

233. Zhao, Y., Tang, F., Lee, D., and Xiong, W.-C. (2021). Expression of Low Level of VPS35-mCherry Fusion Protein Diminishes Vps35 Depletion Induced Neuron Terminal Differentiation Deficits and Neurodegenerative Pathology, and Prevents Neonatal Death. IJMS *22*, 8394. 10.3390/ijms22168394.

234. Grice, S., and Liu, J.-L. (2023). Neurodevelopmental defects as a primer of neurodegeneration: lessons from spinal muscular atrophy and Huntington's disease. Neural Regen Res *0*, 0. 10.4103/1673-5374.367844.

235. Hickman, R.A., O'Shea, S.A., Mehler, M.F., and Chung, W.K. (2022). Neurogenetic disorders across the lifespan: from aberrant development to degeneration. Nat Rev Neurol *18*, 117–124. 10.1038/s41582-021-00595-5.

236. Ouellette, J., and Lacoste, B. (2021). From Neurodevelopmental to Neurodegenerative Disorders: The Vascular Continuum. Front. Aging Neurosci. *13*, 749026. 10.3389/fnagi.2021.749026.

237. Nguyen, M., Wong, Y.C., Ysselstein, D., Severino, A., and Krainc, D. (2019). Synaptic, Mitochondrial, and Lysosomal Dysfunction in Parkinson's Disease. Trends in Neurosciences *42*, 140–149. 10.1016/j.tins.2018.11.001.

238. Pacelli, C., Giguère, N., Bourque, M.-J., Lévesque, M., Slack, R.S., and Trudeau, L.-É. (2015). Elevated Mitochondrial Bioenergetics and Axonal Arborization Size Are Key Contributors to the Vulnerability of Dopamine Neurons. Current Biology *25*, 2349–2360. 10.1016/j.cub.2015.07.050.

239. Calabresi, P., Maj, R., Pisani, A., Mercuri, N.B., and Bernardi, G. (1992). Long-term synaptic depression in the striatum: physiological and pharmacological characterization. J. Neurosci. *12*, 4224–4233.

240. Calabresi, P., Saiardi, A., Pisani, A., Baik, J.H., Centonze, D., Mercuri, N.B., Bernardi, G., and Borrelli, E. (1997). Abnormal synaptic plasticity in the striatum of mice lacking dopamine D2 receptors. J. Neurosci. *17*, 4536–4544.

241. Calabresi, P., Pisani, A., Mercuri, N.B., and Bernardi, G. (1996). The corticostriatal projection: from synaptic plasticity to dysfunctions of the basal ganglia. Trends in Neurosciences *19*, 19–24. 10.1016/0166-2236(96)81862-5.

242. Calabresi, P., Giacomini, P., Centonze, D., and Bernardi, G. (2000). Levodopa-induced dyskinesia: a pathological form of striatal synaptic plasticity? Ann Neurol *47*, S60-68; discussion S68-69.

Appendix

Vehicle effects in WT and VKI mice

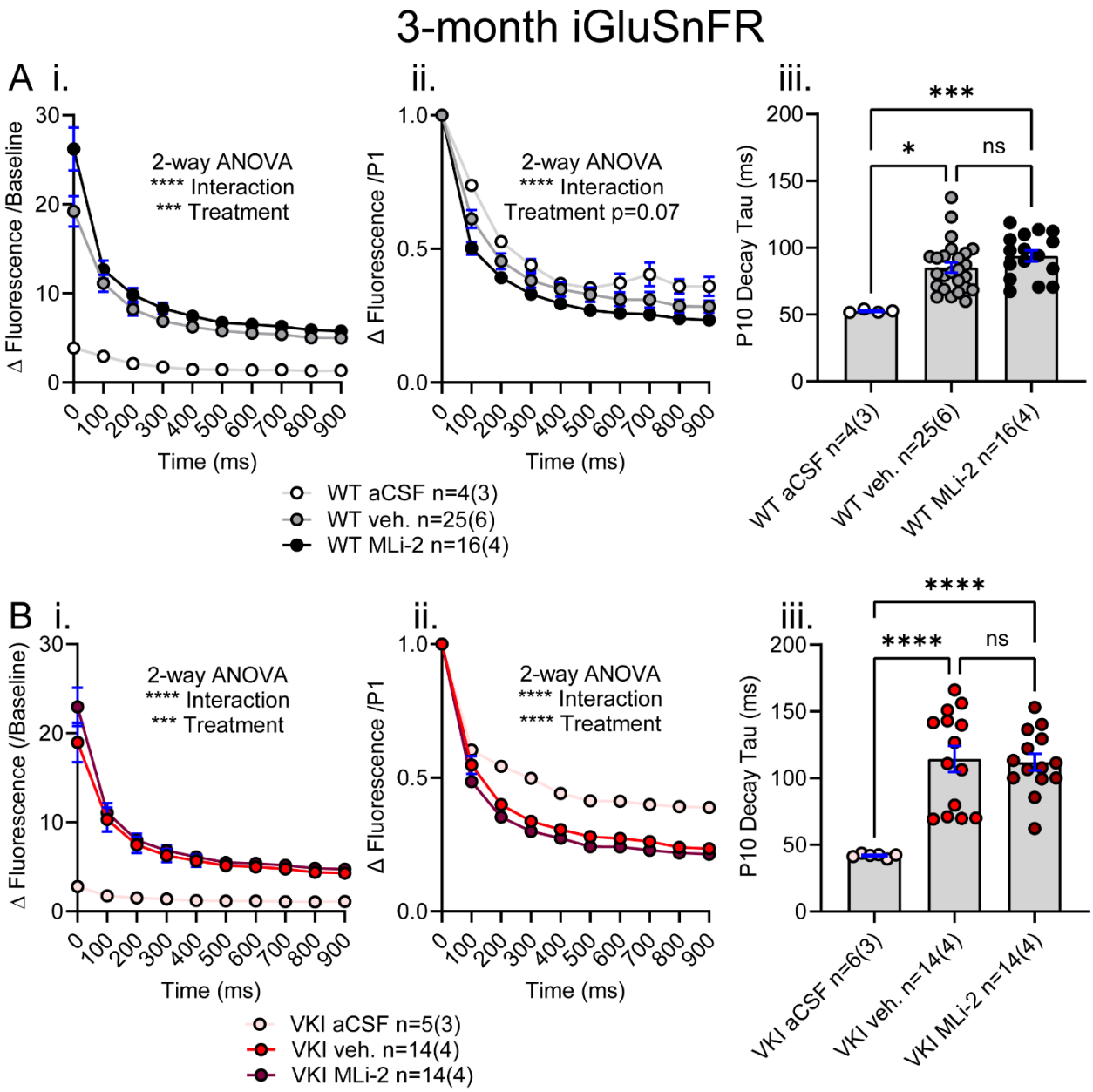

Figure S1. Vehicle treatment increases striatal glutamate release in both WT and VKI 3-month-old mice.

A) At 3 months, **i)** iGluSnFR fluorescent change in WT mice is significantly higher with Captisol® vehicle alone or MLi-2 treatment (in Captisol® vehicle) compared to aCSF alone (2-way ANOVA interaction $p<0.0001$, treatment $p=0.0003$, Holm-Šídák's multiple comparisons test WT aCSF vs WT veh. $p<0.0001$ for all pulses; WT aCSF vs WT MLi-2 $p<0.0001$ for all pulses). There is no significant difference between Captisol® vehicle treated responses and MLi-2 treatment (Holm-Šídák's multiple comparisons test WT veh. vs WT MLi-2 @0ms $p=0.57$, @100-900ms $p>0.97$). **ii)** 1st pulse-normalized iGluSnFR responses in WT striata are significantly altered by vehicle and by MLi-2 treatment when compared to aCSF alone (2-way ANOVA interaction $p<0.0001$, treatment $p=0.07$, Holm-Šídák's

(Figure S1 cont'd) multiple comparisons test WT aCSF vs WT veh. @100ms p=0.07, @200ms p=0.52, @300-900ms p>0.90; WT aCSF vs WT MLi-2 @100-200ms p<0.0001, @300ms p=0.19, @400ms p=0.12, @500ms p=0.06, @600ms p=0.75, @700ms p=0.68, @800ms p=0.36, @900ms p=0.65). Treatment with MLi-2 does not alter iGluSnFR normalized responses when compared to vehicle alone (Holm-Šídák's multiple comparisons test WT veh. vs WT MLi-2 @100ms p=0.27, @200-900ms p>0.83). **iii)** WT iGluSnFR responses in aCSF alone have significantly lower 10th pulse decay tau when compared to vehicle or MLi-2 treated responses, (Kruskal-Wallis test p=0.0013, Dunn's multiple comparisons test WT aCSF vs WT veh. p=0.02, WT aCSF vs WT MLi-2 p=0.0009). There is no difference in decay tau with MLi-2 treatment when compared with vehicle alone (Dunn's multiple comparisons test WT veh. vs WT MLi-2 p=0.32). **B)** At 3 months, **i)** iGluSnFR fluorescent change in VKI mice is significantly higher with Captisol® vehicle or MLi-2 treatment (in Captisol® vehicle) compared to aCSF alone (2-way ANOVA interaction p<0.0001, treatment p=0.0002, Holm-Šídák's multiple comparisons test VKI aCSF vs VKI veh. 0.0002>p>0.0008 for all pulses; VKI aCSF vs VKI MLi-2 p<0.0001 for all pulse train). There is no significant difference between Captisol® vehicle-treated responses and MLi-2 treatment (Holm-Šídák's multiple comparisons test VKI veh. vs VKI MLi-2 p>0.99 for all pulses). **ii)** 1st pulse-normalized iGluSnFR responses in VKI mice are significantly altered by vehicle and by MLi-2 treatment when compared to aCSF alone (2-way ANOVA interaction p<0.0001, treatment p<0.0001, Holm-Šídák's multiple comparisons test VKI aCSF vs VKI veh. @100ms p=0.98, @200ms p=0.0003, @300-900ms p<0.0001; VKI aCSF vs VKI MLi-2 p<0.0001 for all pulses). Treatment with MLi-2 does not alter iGluSnFR normalized responses when compared to vehicle alone (Holm-Šídák's multiple comparisons test VKI veh. vs VKI MLi-2 @100ms p=0.27, @200-900ms p>0.83). **iii)** VKI iGluSnFR responses in aCSF alone have significantly lower 10th pulse decay taus when compared to vehicle or MLi-2 treated responses, (1-way ANOVA p<0.0001, Tukey's multiple comparisons test VKI aCSF vs VKI veh. p<0.0001, VKI aCSF vs VKI MLi-2 p<0.0001). There wis no difference in decay tau with MLi-2 treatment when compared with vehicle alone (Tukey's multiple comparisons test VKI veh. vs VKI MLi-2 p=0.97).

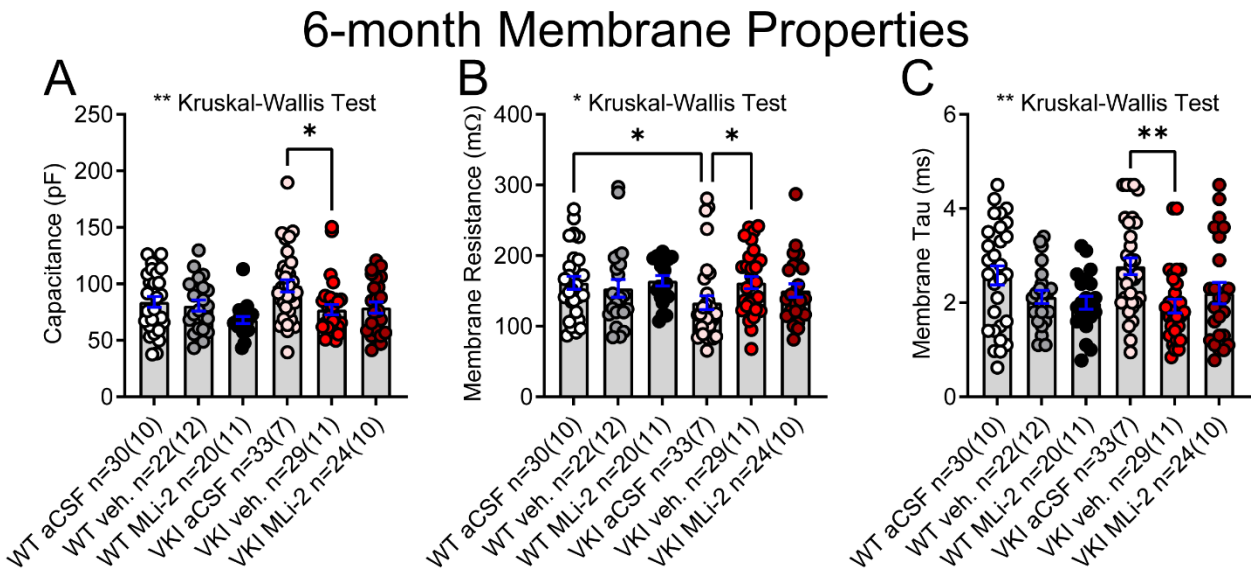

Figure S2. Captisol® vehicle treatment selectively alters passive membrane properties of 6-month-old dorsolateral STR MSNs in VKI mice.

A) At 6 months, membrane capacitance is significantly reduced in VKI MSNs with Captisol® vehicle treatment (Kruskal-Wallis test p=0.003, Dunn's multiple comparisons test VKI aCSF vs VKI veh. p=0.02). There is no significant change in WT MSNs with Captisol® vehicle treatment (Dunn's multiple comparisons test WT aCSF vs WT veh. p>0.99). There is no significant difference with MLi-2 treatment in either genotype, when compared to either aCSF or vehicle conditions (Dunn's multiple comparisons test WT aCSF vs WT MLi-2. p=0.22, WT veh. vs WT MLi-2 p=0.78, VKI aCSF vs VKI MLi-2 p=0.13, VKI veh. vs VKI MLi-2 p>0.99). No significant difference is observed between genotypes when comparing within treatment conditions (Dunn's multiple comparisons test WT aCSF vs VKI aCSF p=0.81, WT veh. vs VKI veh. p>0.99, WT MLi-2 vs VKI MLi-2 p>0.99). **B)** Membrane resistance is significantly increased with vehicle treatment in VKI, but not WT MSNs (Kruskal-Wallis test p=0.01, Dunn's multiple comparisons test VKI aCSF vs VKI veh. p=0.03, WT aCSF vs WT veh. p>0.99). There is no significant difference **(Figure S6 cont'd)** with MLi-2 treatment when compared to aCSF or vehicle condition in either genotype (Dunn's multiple comparisons test WT aCSF vs WT MLi-2. p>0.99, WT veh. vs WT MLi-2 p>0.99, VKI aCSF vs VKI MLi-2 p=0.53, VKI veh. vs VKI MLi-2 p>0.99. There is a significant reduction in membrane resistance when comparing WT vs VKI MSNs perfused with aCSF (Dunn's multiple comparisons test WT aCSF vs VKI aCSF p=0.05). No significant difference is observed between genotypes within vehicle or MLI-2 treatment conditions (Dunn's multiple comparisons test WT veh. vs VKI veh p>0.99, WT MLi-2 vs VKI MLi-2). **C)** MSN membrane tau is significantly reduced with captisol treatment in VKI but not WT mice (Kruskal-Wallis test p=0.007, Dunn's multiple comparisons test VKI aCSF vs VKI veh. p=0.007, WT aCSF vs WT veh. p>0.99). Membrane tau is not significantly altered by MLi-2 treatment in either genotype when compared to aCSF or vehicle conditions (WT aCSF vs WT MLi-2 p=0.63, WT veh. vs WT MLi-2 p>0.99, VKI aCSF vs VKI MLi-2 p=0.18, VKI veh. vs VKI MLi-2 p>0.99). There is no significant difference when comparing membrane either aCSF perfusion, captisol treatment, or MLi-2 treatment effects between genotypes (WT aCSF vs VKI aCSF p>0.99, WT veh. vs VKI veh. p>0.99, WT MLi-2 vs VKI MLi-2 p>0.99).

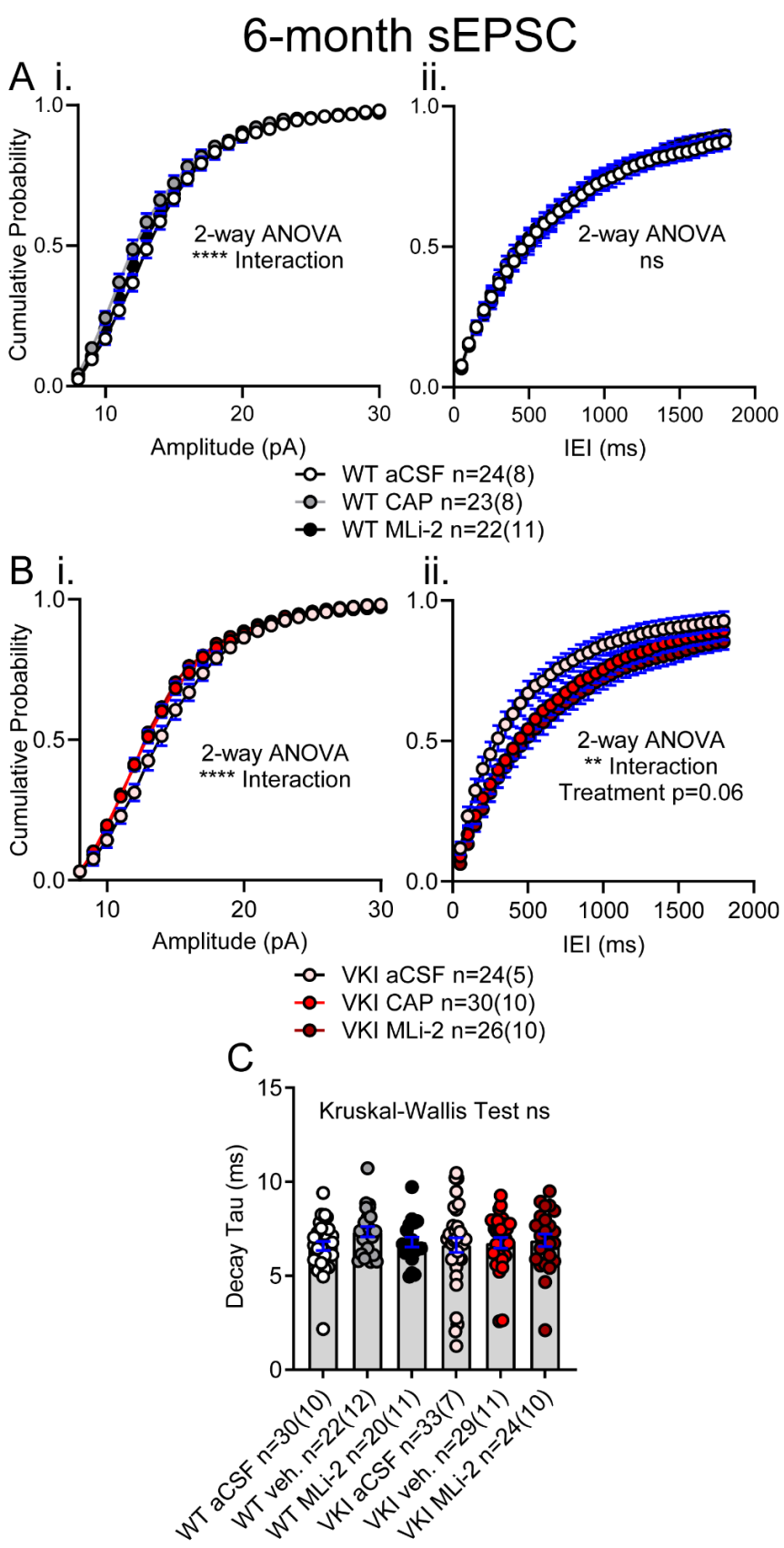

Figure S3. sEPSCs in 6-month-old MSNs are differentially altered in the presence of Captisol® vehicle in WT and VKI mice.

A) At 6 months, **i)** cumulative distribution of sEPSC amplitude in WT MSNs is significantly altered by treatment condition (2-way ANOVA interaction $p<0.0001$, treatment $p=0.59$). There is a significant increase in the number of lower amplitude events in WT MSNs with vehicle, but not MLi-2 treatment relative to aCSF alone (Holm-Šídák's multiple comparisons test WT aCSF vs WT veh. @8-9pA $p>0.99$, @10pA $p=0.07$, @11pA $p=0.0006$, @12pA $p<0.0001$, @13pA $p=0.001$, @14pA $p=0.06$, @15pA $p=0.77$, @>16pA $p>0.99$; WT aCSF vs WT MLi-2 @8-11pA $p>0.99$, @12pA $p=0.49$, @ >13pA $p>0.99$). MLi-2 treatment in WT mice does not significantly alter the number of lower amplitude events when compared to vehicle alone (WT veh. vs WT MLi-2 @8-10pA $p>0.99$, @11pA $p=0.71$, @12pA $p=0.70$, @13pA $p=0.92$, @14pA $p=0.83$, @>15pA $p>0.99$. **ii)** Cumulative distribution of sEPSC inter-event interval in WT MSNs is not significantly different when comparing across treatments (2-way ANOVA interaction $p=0.97$, treatment $p=0.97$). **B)** At 6 months, **i)** in VKI MSNs, cumulative distribution of sEPSC amplitude is significantly altered by treatment condition (2-way ANOVA interaction $p<0.0001$, treatment $p=0.22$). Vehicle and MLi-2 treatment significantly increase the number of lower-amplitude sEPSC events in VKI MSNs when compared to aCSF alone (Holm-Šídák's multiple comparisons test VKI aCSF vs VKI veh. @8-9pA $p>0.99$, @10pA $p=0.37$, @11pA $p=0.02$, @12pA $p<0.0001$, @13pA

(Figure S3 cont'd) p=0.0003, @14pA p=0.0001, @15pA p=0.003, @16pA p=0.01, @17pA p=0.16, @ >18pA p>0.99; VKI aCSF vs VKI MLi-2 @8-10pA p>0.99, @11pA p=0.005, @12-16pA p<0.0001, @17pA p=0.09, @18pA p=0.50, @ >19pA p>0.99). VKI brain slices treated with MLi-2 do not significantly differ in the number of lower amplitude events when compared to vehicle alone (VKI veh. vs VKI MLi-2 @ all amplitudes p>0.99). **ii)** Cumulative distribution of sEPSC inter-event interval in VKI MSNs is significantly different when comparing across all treatments (2-way ANOVA interaction p=0.003, treatment p=0.06). Vehicle and MLi-2 treatment does not significantly increase the sEPSC inter-event interval in VKI MSNs when compared to aCSF alone by post-hoc comparison (Holm-Šídák's multiple comparisons test VKI aCSF vs VKI veh.@5-500ms p>0.84, @600ms p>0.68, @700ms p=0.74, @800ms p=0.71, @900ms p=0.68, @ >1000ms p>0.82; VKI aCSF vs VKI MLi-2 @50-200ms p>0.81, @300ms p=0.46, @400ms p=0.55, @500ms p=0.50, @600ms p=0.31, @700ms p=0.29, @800ms p=0.27, @900ms p=0.30, @1000ms p=0.40, @1100ms p=0.44, @ >1200ms p>0.47). VKI MSNs are not altered in sEPSC inter-event interval with MLi-2 treatment when compared to vehicle alone (Holm-Šídák's multiple comparisons test VKI veh. vs VKI MLi-2 @ all intervals p>0.99) **C)** At 6 months, average sEPSC decay tau is not significantly different with vehicle or MLi-2 treatment in either genotype when compared to aCSF perfused MSNs (Kruskal-Wallis test p=0.66 Dunn's multiple comparisons test WT aCSF vs WT veh. p>0.99, WT aCSF vs WT MLi-2 p>0.99, VKI aCSF vs VKI veh. p>0.99, VKI aCSF vs VKI MLi-2 p>0.99). There is no difference between MLi-2 and captisol treated sEPSC decay taus in either genotype (Dunn's multiple comparisons test WT veh. vs WT MLi-2 p>0.99, VKI veh. vs VKI MLI-2 p>0.99). No significant difference is observed when comparing between WT and VKI sEPSC decay tau within treatment conditions (Dunn's multiple comparisons test WT aCSF vs VKI aCSF p>0.99, WT veh. vs VKI veh. p>0.99, WT MLi-2 vs VKI MLi-2 p>0.99).

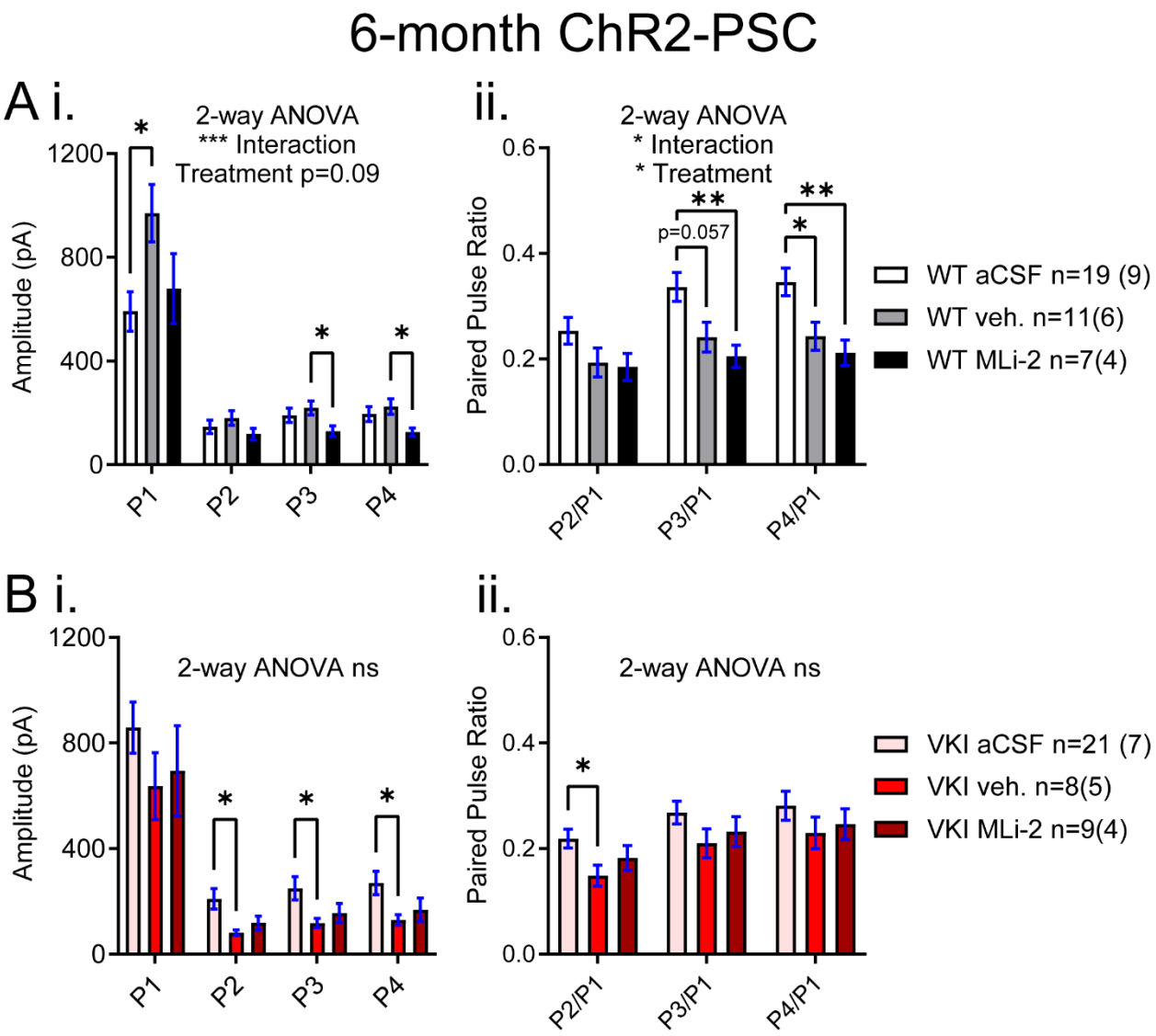

Figure S4. Captisol® vehicle treatment increases ChR2-evoked cortico-striatal glutamate release probability onto MSNs in both WT and VKI 6-month-old brain slices.

A) At 6 months, **i)** WT ChR2-evoked PSC 1st pulse (P1) amplitude is increased with Captisol® vehicle treatment when compared to aCSF alone (2-way ANOVA WT aCSF vs WT veh. vs WT MLi-2 interaction p=0.0001, treatment p=0.09; Tukey's multiple comparisons test WT aCSF vs WT veh. @ P1 p=0.03, @ P2 p=0.65, @ P3 p=0.74, @ P4=0.77). WT ChR2-PSCs are not affected by MLi-2 treatment when comparing with aCSF perfusion (Tukey's multiple comparisons test WT aCSF vs WT MLi-2 @ P1 p=0.84, @ P2 p=0.69**,** @ P3 p=0.21, @ P4 p=0.11). MLi-2 treatment significantly reduces P3 and P4, but not P1 and P2 amplitudes relative to vehicle treatment in WT MSNs (Tukey's multiple comparisons test WT veh. vs WT MLi-2 @ P1 p=0.25, @ P2 p=0.22, @ P3 p=0.05, @ P4 p=0.03). **ii)** Paired-pulse ratios of ChR2-PSCs in WT brain slices are significantly reduced with vehicle and MLi-2 treatment when compared to aCSF alone, but only at P3/P1 and P4/P1 ratios (2-way ANOVA WT aCSF vs WT veh. vs WT MLi-2 interaction p=0.03, treatment p=0.01; Tukey's multiple comparisons test WT aCSF vs WT veh. @ P2/P1 p=0.26, @ P3/P1 p=0.06, @ P4/P1 p=0.03; WT aCSF vs WT MLi-2 @ P2/P1 p=0.17, @ P3/P1 p=0.003, @ P4/P1 p=0.003). Paired pulse ratios are not different in WT MSNs when comparing MLi-2 to vehicle treatment (Tukey's multiple comparisons test WT veh. vs WT MLi-2 @ P2/P1 p=0.97, @ P3/P1 p=0.57, @ P4/P1 p=0.66). **B)** At 6 months, **i)** VKI MSNs treated with vehicle show reduced ChR2-PSC amplitudes during P2-P4, but not P1 ChR2 stimulation (2-way ANOVA VKI aCSF vs VKI veh. vs VKI MLi-2 interaction p=0.95, treatment p=0.18; Tukey's multiple comparisons test VKI aCSF vs VKI veh. @ P1 p=0.37, @ P2 p=0.02, @ P3 p=0.03, @ P4=0.02). VKI MSNs treated with MLi-2

(Figure S4 cont'd) are no different in ChR2-PSC amplitudes compared to either aCSF or vehicle conditions (Tukey's multiple comparisons test VKI aCSF vs VKI MLi-2 @ P1 p=0.69, @ P2 p=0.15**,** @ P3 p=0.26, @ P4 p=0.26; VKI veh. vs VKI MLi-2 @ P1 p=0.96, @ P2 p=0.43, @ P3 p=0.64, @ P4 p=0.72). **ii)** VKI MSNs have a significant reduction in paired-pulse ratio at P2/P1 only with vehicle, not MLi-2 treatment (2-way ANOVA VKI aCSF vs VKI veh vs VKI MLi-2 interaction p=0.94, treatment p=0.24; Tukey's multiple comparisons test VKI aCSF vs VKI veh. @ P2/P1 p=0.04**,** @ P3/P1 p=0.25, @ P4/P1 p=0.43; VKI aCSF vs VKI MLi-2 @ P2/P1 p=0.45**,** @ P3/P1 p=0.57, @ P4/P1 p=0.66). MLi-2 treatment in VKIs does not alter paired-pulse ratio when compared to vehicle alone (Tukey's multiple comparisons test VKI veh. vs VKI MLi-2 @ P2/P1 p=0.54**,** @ P3/P1 p=0.84, @ P4/P1 p=0.92).

Striatal neurotransmitter release in aged animals by sex

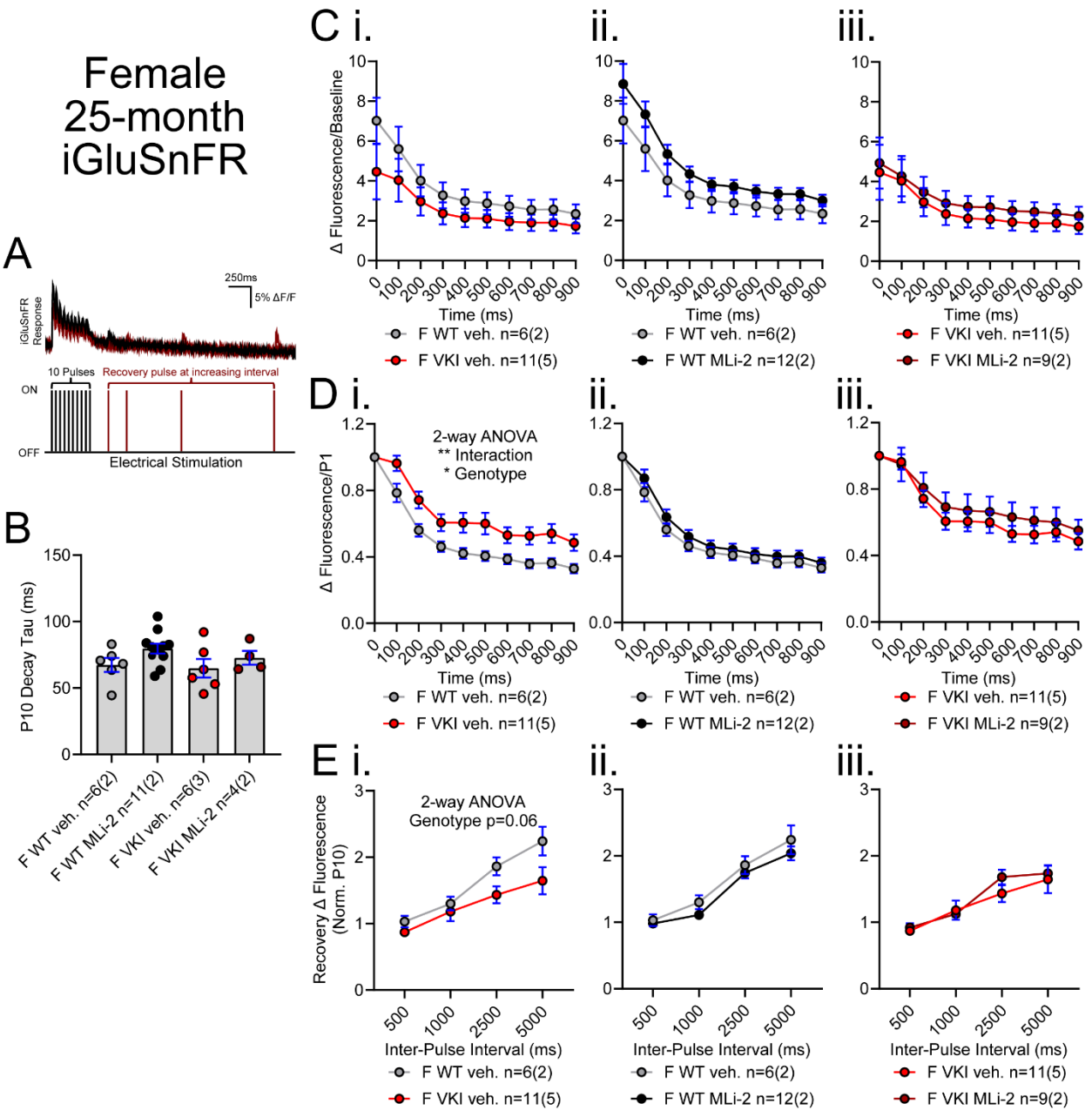

Figure S5. Striatal glutamate release is reduced in aged female VKI vs WT brain slices.

A) Representative iGluSnFR response in dorsolateral STR corresponding to train of 10x10Hz pulses of electrical stimulation followed by 11th pulse at increasing interval with each repetition of the protocol. **B)** P10 decay tau of iGluSnFR responses are not significantly different across genotype with MLi-2 treatment (1-way ANOVA p=0.15). **C** At ~25 months, **i)** vehicle-treated WT responses are not significantly different in Δfluorescence/baseline measures compared to VKIs (2-way ANOVA interaction p=0.26, genotype p=0.30). **ii)** WT iGluSnFR responses are not altered with MLi-2 treatment (2-way ANOVA interaction p=0.36, treatment p=0.19). **iii)** VKI iGluSnFR responses are not significantly altered with MLi-2 treatment (2-way ANOVA interaction p>0.99, treatment p=0.58). **D** At 25 months, **i)**

(Figure S5 cont'd) iGluSnFR responses normalized to P1 response are significantly lower in vehicle-treated VKI vs WT brain slices (2-way ANOVA interaction p=0.0056, genotype p=0.03) **ii)** WT responses normalized to P1 peak are not significantly altered with MLi-2 treatment (2-way ANOVA interaction p=0.32, treatment p=0.44). **iii)** VKI responses normalized to P1 peak are not significantly altered with MLi-2 treatment (2-way ANOVA interaction p=0.60, treatment p=0.52). **E** At 25 months, **i)** iGluSnFR response following 10x10Hz pulse stimulation, when normalized to P10 peak, trends towards significantly lower values in vehicle-treated VKI vs WT striata (2-way ANOVA interaction p=0.19, genotype p=0.06). **ii)** P10-normalized iGluSnFR responses following pulse train stimulation are not significantly different in WT brain slices treated with MLi-2 vs vehicle (2-way ANOVA interaction p=0.57, treatment p=0.25). **iii)** P10-normalized iGluSnFR responses following pulse train stimulation are not significantly different in VKI brain slices treated with MLi-2 vs vehicle (2-way ANOVA interaction p=0.60, treatment p=0.47).

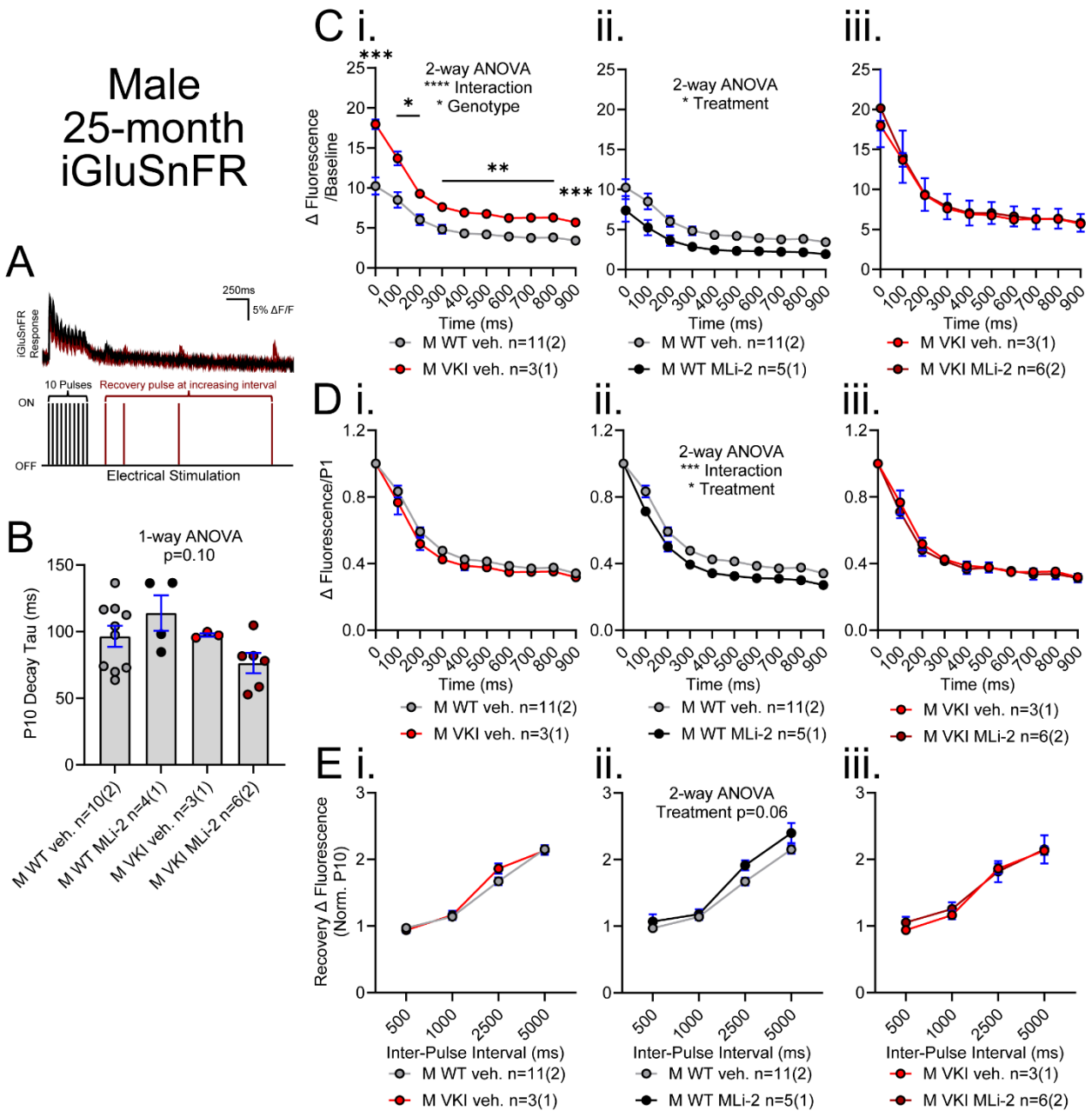

Figure S6. Striatal glutamate release is reduced in aged male VKI vs WT brain slices.

A) Representative iGluSnFR response in dorsolateral STR corresponding to train of 10x10Hz pulses of electrical stimulation followed by 11th pulse at increasing interval with each repetition of the protocol. **B)** P10 decay tau of iGluSnFR responses trend towards significant differences when comparing WT and VKI responses to MLi-2 treatment (1-way ANOVA p=0.10). **C** At ~25 months, **i)** vehicle-treated WT responses are significantly larger in Δ fluorescence/baseline measures compared to VKI responses (2-way ANOVA interaction p<0.0001, genotype p=0.01, Holm-Šídák's multiple comparisons test WT veh. vs VKI veh. @ 0ms p=0.0005, @100ms, p=0.04, @200ms p=0.01, @300ms p=0.0047, @400ms p=0.0069, @500ms p=0.0032, @600ms p=0.0056, @700ms p=0.0010, @800ms**)** p=0.0017, @900ms p=0.0010). **ii)** WT iGluSnFR responses are significantly reduced with MLi-2 treatment (2-way ANOVA interaction p=0.14, treatment p=0.04). **iii)** VKI iGluSnFR responses are not significantly altered with MLi-2 treatment (2-way ANOVA interaction p>0.99, treatment p=0.90). **D** At 25 months, **i)** iGluSnFR responses normalized to P1 peak Δ fluorescence/baseline are not significantly different in vehicle-treated VKI vs WT brain slices (2-way ANOVA interaction p=0.39, genotype p=0.37) **ii)** WT responses normalized to P1 peak are significantly reduced with

(Figure S6 cont'd) MLi-2 treatment (2-way ANOVA interaction p=0.0006, treatment p=0.03). **iii)** VKI responses normalized to P1 peak are not significantly altered with MLi-2 treatment (2-way ANOVA interaction p=0.81, treatment p=0.71). **E** At 25 months, **i)** iGluSnFR response following 10x10Hz pulse stimulation, when normalized to P10 peak, is not significantly different between vehicle-treated VKI and WT striata (2-way ANOVA interaction p=0.19, genotype p=0.63). **ii)** P10-normalized iGluSnFR responses following pulse train stimulation in WT brain slices trend towards increased responses with MLi-2 treatment vs vehicle (2-way ANOVA interaction p=0.18, treatment p=0.06). **iii)** P10-normalized iGluSnFR responses following pulse train stimulation are not significantly different in VKI brain slices treated with MLi-2 vs vehicle (2-way ANOVA interaction p=0.94, treatment p=0.15).

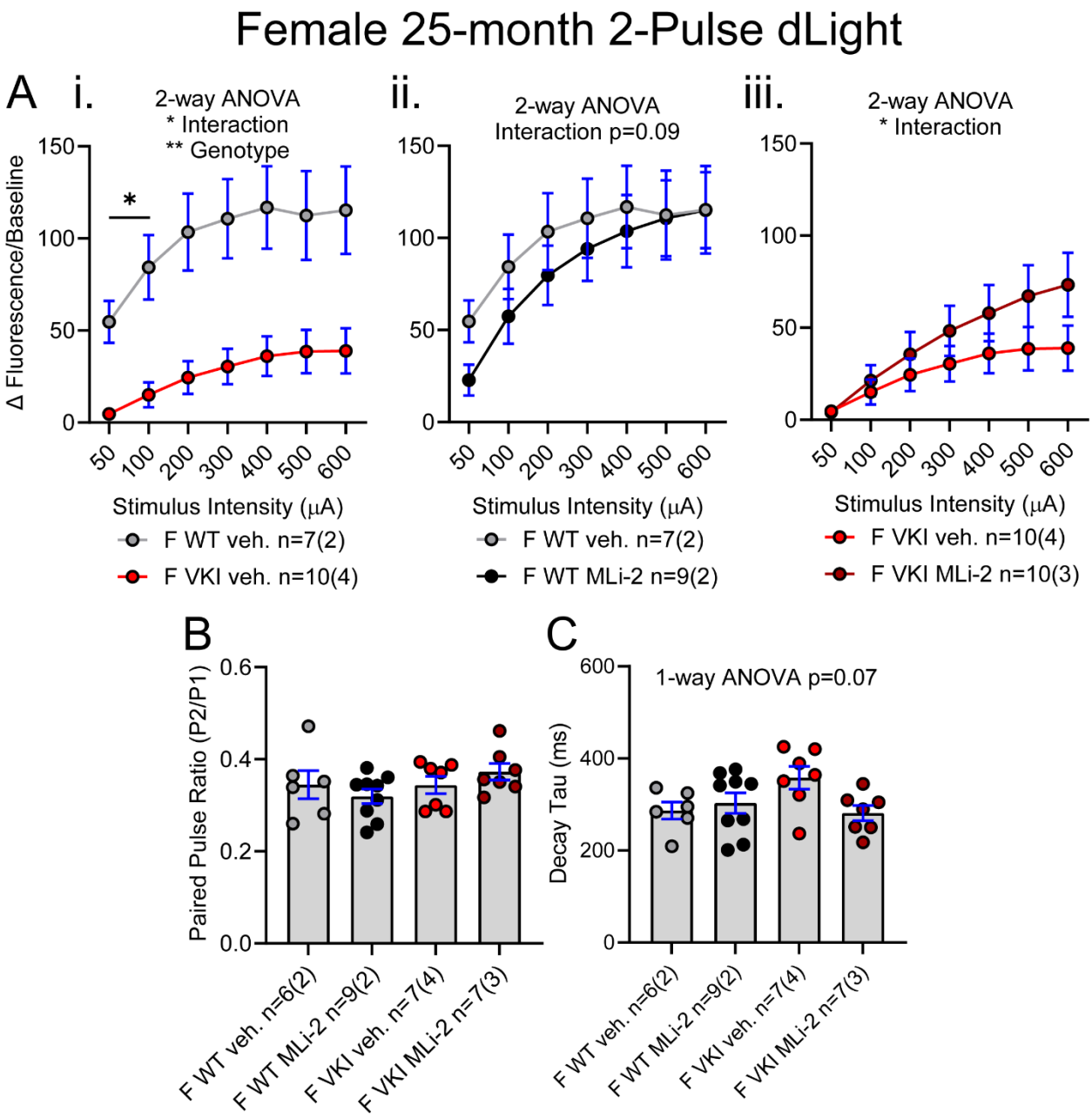

Figure S7. Striatal dopamine release is reduced in aged female VKI vs WT brain slices.

A) At 25 months, **i)** P1 peaks across increasing stimulation intensity are significantly reduced in vehicle-treated VKI brain slices vs WT (2-way ANOVA interaction p=0.04, genotype p=0.0019, Holm-Šídák's multiple comparisons test WT veh. vs VKI veh. @50μA p=0.03, and @100μA p=0.04). **ii)** WT P1 peak with increasing stimulation intensity trends towards significant difference with MLi-2 treatment (2-way ANOVA interaction p=0.09, treatment p=0.53). **iii)** VKI P1 peak with increasing stimulation intensity is significantly altered with MLi-2 treatment (2-way ANOVA interaction p=0.04, treatment p=0.25). **B)** Ratio of P2:P1 peaks are not significantly different across genotype or treatment condition (1-way ANOVA p=0.31). **D)** P1 decay tau trends towards significant difference when comparing WT and VKI vehicle- and MLi-2 treated decays (1-way ANOVA p=0.08).

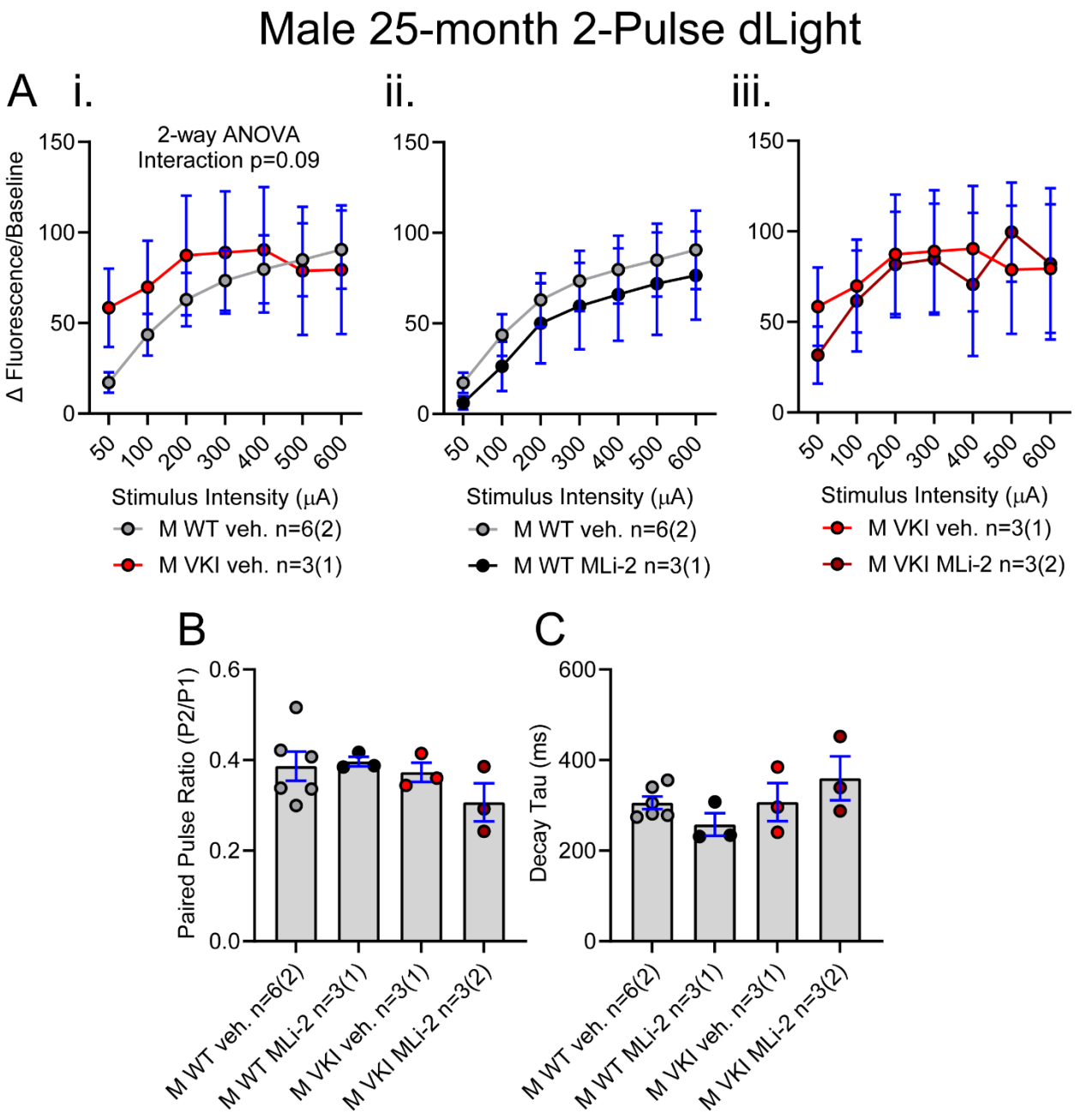

Figure S8. Striatal dopamine release is reduced in aged male VKI vs WT brain slices.

A) At 25 months, **i)** P1 peaks across increasing stimulation intensity trend towards significant difference in vehicle-treated VKI brain slices vs WT (2-way ANOVA interaction p=0.10, genotype p=0.64). **ii)** WT P1 peak with increasing stimulation intensity is not significantly different with MLi-2 treatment (2-way ANOVA interaction p>0.99, treatment p=0.60). **iii)** VKI P1 peak with increasing stimulation intensity is not significantly altered with MLi-2 treatment (2-way ANOVA interaction p=0.25, treatment p=0.90). **B)** Ratio of P2:P1 peaks are not significantly different across genotype or treatment condition (1-way ANOVA p=0.33). **D)** P1 decay tau trends towards significant difference when comparing WT and VKI vehicle- and MLi-2 treated decays (1-way ANOVA p=0.23).